

AN INVESTIGATION OF SOLIDIFICATION
MICROSTRUCTURE AND COPPER OXIDE FORMATION ON
MELTED MARK OF COPPER WIRE FOR FIRE
INVESTIGATION

スパットラ, サチャナー

<https://hdl.handle.net/2324/6787568>

出版情報 : Kyushu University, 2022, 博士 (工学), 課程博士
バージョン :
権利関係 :

**AN INVESTIGATION OF SOLIDIFICATION MICROSTRUCTURE
AND COPPER OXIDE FORMATION ON MELTED MARK OF
COPPER WIRE FOR FIRE INVESTIGATION**

SUPHATTRA SACHANA



**An investigation of solidification microstructure and
copper oxide formation on melted mark of copper wire
for fire investigation**

By

Suphattra Sachana

A thesis submitted to Kyushu University
for the degree of Doctor of Engineering

Department of Materials Process Engineering
Graduate School of Engineering
Kyushu University
Fukuoka, Japan

CONTENTS

Chapter 1 Introduction	1
1.1 Introduction	1
1.2 Copper properties	2
1.3 Copper wire manufacturing process	6
1.4 Short circuit	7
1.5 Cu-O phase diagram	9
1.6 Solidification interface	11
1.7 Solidification Structures	14
1.8 Solid solutions and precipitation	16
1.9 Heat treatment	18
1.9.1 Solution Heat Treating	19
1.9.2 Precipitation Heat Treating	19
1.10 Effect of oxygen and hydrogen	21
1.10.1 Oxygen effect	21
1.10.2 Hydrogen sickness	22
1.11 Thermal expansion and thermal conduction	23
1.12 Oxidation mechanism	25
1.13 Manual for fire investigation by NITE	28
1.14 Objectives of this thesis	29
References	32
Chapter 2 Investigation of solidification microstructure at various cooling rates before and after heat treatments on the melted mark of copper wire	35
2.1 Introduction	35
2.2 Materials and methods	39
2.3 Results and discussions	41
2.3.1 Cooling rate effect on solidification of unannealed melted marks	41

2.3.1.1 Dendrite growth	42
2.3.1.2 Heat conduction	44
2.3.1.3 Microstructure characterization	48
2.3.1.4. Oxygen concentration	50
2.3.2 Cooling rate effect on microstructure formation of annealed melted marks	54
2.3.2.1 Surface morphology	54
2.3.2.2 Phase identification of oxide layer	57
2.3.2.3 Crystallite size of oxide layer	58
2.3.2.4 Microstructure characterization	60
2.4 Conclusions	67
References	68

Chapter 3 Investigation of microstructure and oxide formations under various annealing temperatures and times on the melted mark of copper wire.....72

3.1 Introduction	72
3.1.1 Presence of CuO	72
3.1.2 Presence of Cu ₂ O	75
3.1.3 Activation energy	76
3.1.4 Objective of the study	80
3.2 Materials and methods	81
3.3 Results and discussions	83
3.3.1 Temperature dependence	83
3.3.1.1 Evolution of surface morphology	83
3.3.1.2 Phase transformation of oxide layer	87
3.3.1.3 Temperature effect on Cu ₂ O crystallite size	90
3.3.2 Change in oxide layer thickness	91
3.3.3 Calculation of activation energy	96
3.3.4 Observation on microstructure characterization	98
3.4 Conclusions	103
References	104

Chapter 4 Establishing the metallurgical examination method and method validating by using the melted mark from real fire scenes	108
4.1 Introduction	108
4.2 Objectives of this chapter	111
4.3 Establishing the metallurgical examination method	112
4.4 Method validation on melted marks of copper wire collected from real fire scenes	120
4.4.1 Materials and Methods	120
4.4.2 Examination of typical appearance	123
4.4.3 Examination of surface morphology	123
4.4.4 Examination of oxide layer	128
4.4.4.1 Evaluation of fire temperature from copper oxide	128
4.4.4.2 Investigation of Cu ₂ O crystallite size	130
4.4.4.3 Evaluation of fire temperature from copper oxide layer thickness	132
4.4.5 Describing melted mark forming from microstructure	134
4.4.6 Explaining fire behaviors and identifying fire's origin	139
4.5 Conclusions	143
References	145
Chapter 5 Conclusions	148
Acknowledgments	152

Chapter 1 Introduction

1.1 Introduction

A commercial 99.95% pure copper wire has been extensively used for building wirings and electrical application because of their excellent electrical conductivity.^{1,2} However, the solidification structure of a “melted mark” on copper wire caused by short-circuiting in a fire accident is still inadequate to explain fire behaviors and determine the cause of the fire accident. The vital evidence used to determine the source of fire for the fire investigator is the melted mark on the copper wire because it is not destroyed and left after the fire. However, various melted marks are sometimes discovered in the fire: fire melted mark (FMM) and electrical melted mark (EMM).³ The FMM is a mark resulting from heat damage by flames along a conductor wire. The EMM can be further classified into primary melted mark (PMM) and secondary melted mark (SMM). The distinguishing between primary melted mark (PMM) and secondary melted mark (SMM) can be difficult. The electrical melted mark from the first short-circuiting that caused the fire generated before the fire is referred to as PMM. It should be exposed to a longer period of fire and a higher fire temperature than other melted marks. SMM is the electrical melted mark by the second short-circuiting caused by the burning of PVC insulating after a fire.^{4,5}

According to Lee et al.⁶, PMM was produced in an atmosphere at or near room temperature and rapidly cooled, whereas SMM was produced in a high fire temperature. As a result, the cooling rate of PMM should be much higher than that of SMM. Then, they proposed that measuring the oxygen concentration and dendrite arm spacing of melted marks on copper wire can distinguish between PMM and SMM. Liu et al.⁷ studied the solidification

structure of melted mark on copper simulated by short-circuiting in the atmosphere. They presented that the Cu-dendrites and (Cu+Cu₂O) eutectic structure beneath the cuprous oxide (Cu₂O) surface layer are the typical microstructure of PMM.

Not only the microstructure of the melted mark on the copper wire but also the oxide layer plays a role in the fire investigation. Generally, copper has two major types of oxide: cuprous oxide (Cu₂O, cuprite) and cupric oxide (CuO, tenorite). When copper is oxidized in oxygen or air at high temperatures, multiphase scales such as Cu₂O and CuO form.^{8,9} In particular, the oxide on the melted mark's surface of copper wire from short-circuiting formed in the fire ambient during fire accidents is important to describe the fire behaviors. This scientific explanation provides significant evidence that substantially impacts the reliability of fire judgments.

1.2 Copper properties

Copper (Cu) has a face-centered cubic (FCC) crystal structure (Fig. 1.1), which results in high ductility, toughness, and formability. The density of copper is 8.96 (g/cm³). It has a high room temperature electrical conductivity of 0.5800×10^5 (Ω cm)⁻¹. Copper conductivity decreases as temperature rises due to cold work and alloy content. The thermal conductivity of copper is 398 (W/mK). Copper has good corrosion resistance. This is because there is a surface reaction between copper and the oxygen in the air which results in the formation of a thin protective oxide layer.

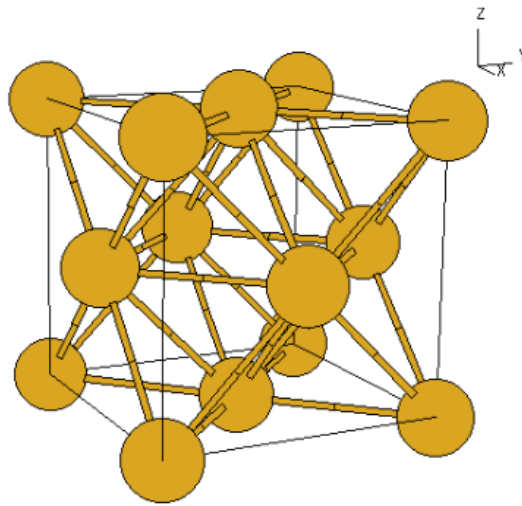


Fig. 1.1 FCC lattice of copper ¹⁰

Crystallographic of copper

As mentioned, the crystal structure of copper is FCC. Fig. 1.2 depicts four main directions in the FCC unit cell: along the cube edge $\langle 100 \rangle$, the face diagonal $\langle 110 \rangle$, the cube diagonal $\langle 111 \rangle$, and the corner to the face center $\langle 112 \rangle$. The atomic packing density differs in each direction and many physical properties change corresponding to these directions.

However, wire drawing deformation produces a texture or preferred grain orientations. The properties of wire vary with direction and because the textures vary in direction or a non-random manner. Therefore, properties in the axial direction (along the length of the wire) are different.¹¹

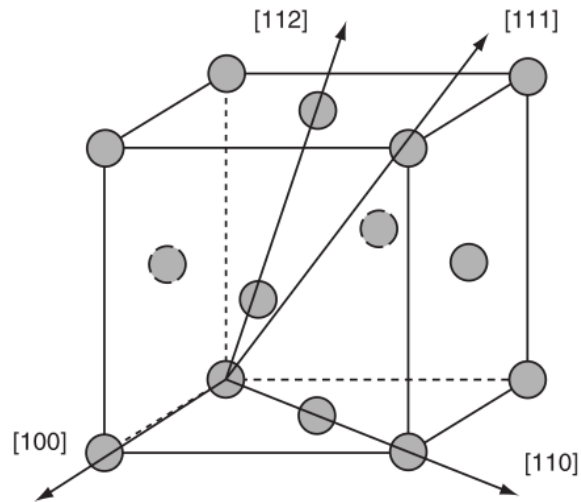


Fig. 1.2 Four important directions in the FCC unit cell ¹¹

A significant crystalline growth occurs when the liquid-solid interface moves ahead of the interface into a supercooled liquid that has a lower temperature. The crystallographic growth direction of these cells is called the dendritic growth direction. The growth direction of dendrites depends on the crystal structure of the material. For copper that has FCC crystal structure, the dendrite growth is in $\langle 100 \rangle$ direction.¹²

Classification of copper

Copper and its alloys can be classified into three types.¹³

1. Oxygen-free copper: Oxygen-free copper is typically produced at high purity levels through electrolytic refining. Because it contains almost no oxygen, certified oxygen-free copper has a minimum copper content of 99.99 wt%. So pure copper is a superb electrical conductor.

2. Phosphorous deoxidized copper: The oxygen level in phosphorous deoxidized copper has been significantly reduced by addition of phosphorous. Deoxidized copper alloys are suitable for welding all coppers because they do not result from hydrogen sickness. Hydrogen sickness takes place when the copper oxide is exposed to reducing hydrogen gas at high temperatures.

3. Electrolytic tough pitch (ETP) copper: ETP copper contains an oxygen of approximately 0.03 - 0.04 wt%. Higher oxygen content may cause defects like cracks, laps, seams. ETP copper grades has an alloy number C11000 which are extensively used in almost applications which require high conductivity such as electrical power transmission, electronic appliances and building wire.^{3,4} Because the copper wire used in this work is in this type, so following contexts are related to ETP copper.¹²

Oxygen in ETP copper is presented in form of Cu_2O . When copper is heated, such as during welding, oxygen is released in the following order:



The rapid solidification that occurs after welding entraps the oxygen in the metal, resulting in porosity. Furthermore, the oxygen reacts with hydrogen in the furnace atmosphere, forming steam, which causes micropores.^{1,2}

1.3 Copper wire manufacturing process

Wire manufactured from copper and its alloys has been in use since approximately 3000-2000 BC. It is widely used in electronic appliances and wiring buildings. Copper is a metal used mainly for the formation of copper wire. It needs to take many following steps to produce copper wire.^{1,15}

1. Wire drawing

The initial stage of the manufacturing process is to gradually reduce the diameter of the copper wire until it reaches its final diameter. Usually, a continuous cast copper rod of 8 mm diameter is used in this process. The copper rod is reduced to 2 mm by using several dyes. Then, this 2 mm wire is drawn further to minimize the diameter of the wire to the size required for each kind of conductor. After copper wire drawing, the wire turns to extremely thin and malleable.¹⁵⁻¹⁷

2. Annealing

Following the wire drawing process, all wires are subjected to a heat treatment known as "annealing" to increase the conductivity and ductility of the copper and remove internal stresses. The drawn wire is placed in an Electric Furnace in a pot. The temperature of the furnace is set to up to 1000 °F. This process is a highly precise and controlled procedure. Water is used in the annealing process to ensure that no oxidation occurs. This procedure is carried out in order to soften the copper wire.¹⁵⁻¹⁷

3. Stranding

Many wires are available as solid or stranded wires. For the stranded wire, after the wires are annealed, copper wires are stranded together by wire-stranding machines to create

conductors with a wide range of stranded wire sizes. Then, to achieve a smoother surface, these are subjected to a nozzling process.¹⁵⁻¹⁷

4. Insulation

The insulation process is the final step in the production of copper wire. It entails covering the conductor with an insulating cover to prevent current leakage. The insulating material is added through an extrusion process at high temperatures. There are several insulating materials that can be used: Polyvinyl chloride (PVC), Ethylene propylene rubber (EPR), Cross linked polyethylene (XLPE), etc. The maximum voltage of the wire depends on its thickness and insulating capacity.¹⁶

Because wire drawing causes metal wires to harden and lose mechanical and electrical properties. These degradations are the result of microstructural defects caused by the plastic deformation. When the strain degree of wire-drawing becomes significant, the microstructure will exhibit morphological texture. The grains are elongated and needle-shaped, running parallel to the direction of wire-drawing.¹⁸

1.4 Short circuit

A short circuit occurs when an energized conductor (Line) in the circuit makes contact with a grounded conductor (Neutral) or a metal material that is grounded with almost zero resistance, the two conductor wires will be melted by the high energy of short-circuiting at the point of contact. Some defects in PVC insulation may cause this event, such as failure to protect wire insulation appropriately or burning by fire. The high current flow generates heat, which has the potential to melt the conductor wires, as shown in Fig. 1.3. The mark on the

conductor from melting by electrical current is called an “electrical melted mark” (EMM).¹⁹ The electrical melted mark can mainly divide into two types; primary melted mark (PMM) and secondary melted mark (SMM).²⁰ PMM is a melted mark created from the first short circuit that caused the fire. SMM is a melted mark from a second or another short circuit that happens on conductor wire after PMM due to PVC insulation has been damaged by the flame^{3,6,21}, as depicted in Fig. 1.4.

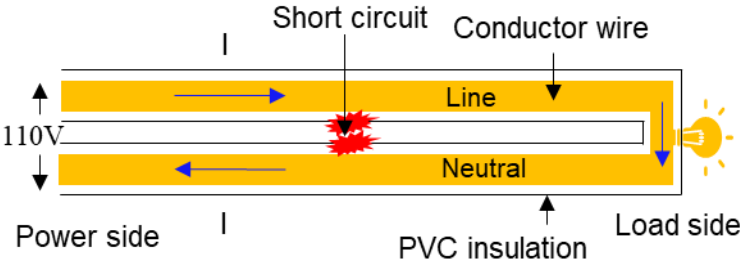


Fig. 1.3 Schematic diagram of short circuit

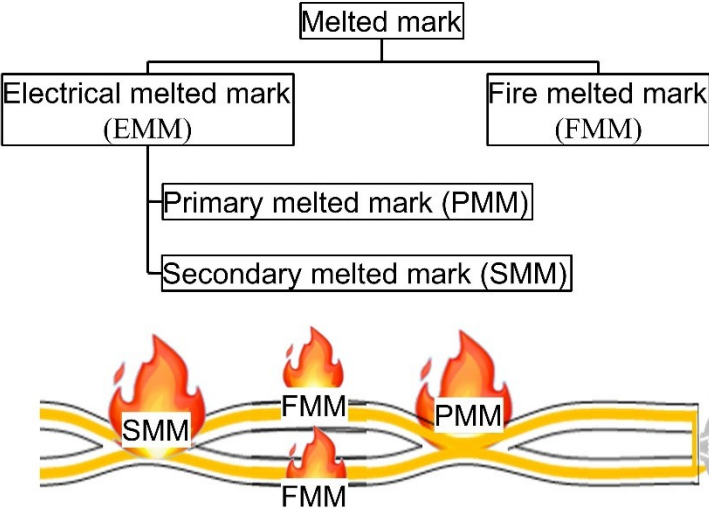


Fig. 1.4 Schematic diagram of melted mark types

In addition to the electrical melted mark, there is also the “fire melted mark” (FMM). FMM is thermal damage along a conductor wire resulting from a fire. It has more widespread damage with no distinction between the non-melting/melting interface.¹⁹

1.5 Cu-O phase diagram

Understanding phase diagrams for copper-oxygen systems is extremely substantial because the phase diagram characteristics have a strong relationship with the microstructure. Furthermore, the phase diagram contains important information about crystallization, melting, and other phenomena. For an equilibrium binary system of known composition and temperature, there are at least three types of information available: (1) the phases present, (2) their compositions, and (3) the percentages or proportions of the phases.²² The copper-oxygen system is a simple eutectic system. In Fig. 1.5, the phase diagram can be divided into two partial systems following.

The partial system Cu-Cu₂O: The solubility of oxygen in copper is extremely small. The solubility is the highest at the eutectic temperature, with 0.008 wt. (0.03 at.) % oxygen. The eutectic temperature is 1065 °C, and the eutectic composition is 0.39 wt. (1.54 at.) %oxygen.^{23,24}

The partial system Cu₂O-CuO: Cu₂O and CuO at 20.12 wt.% oxygen is indicated as phases of fixed composition. With 14 wt. (39.2 at.) % oxygen , the two compounds form a eutectic with 68 wt. % Cu₂O, 32 wt. %CuO. The eutectic temperature is 1075 °C.²³

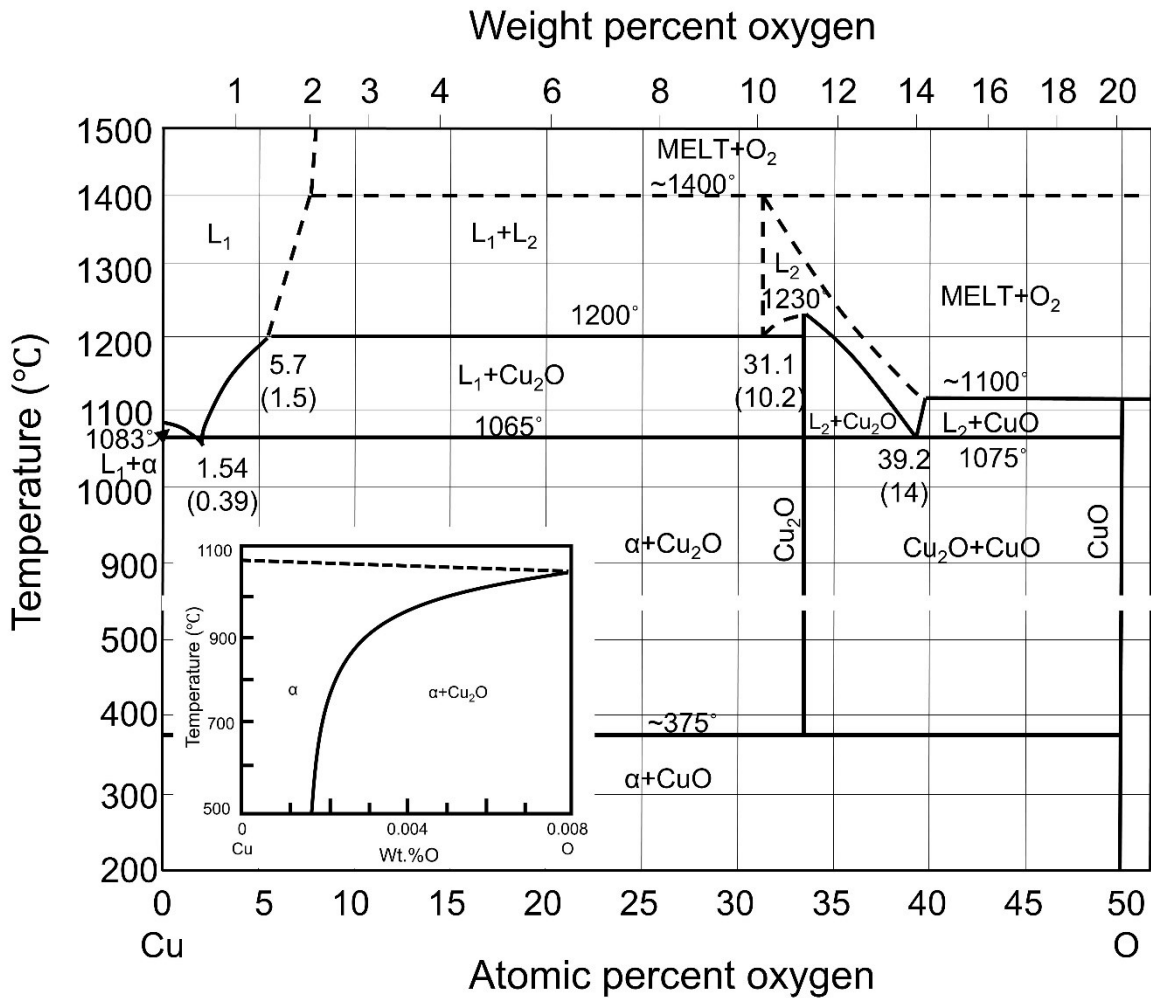
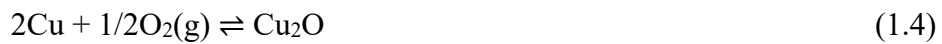


Fig. 1.5 Copper-oxygen phase diagram ²³

The oxygen content of high-conductivity copper used in the majority of electrical applications ranges from 0.01 to 0.05 wt.% oxygen, but can reach 0.1%. Solidification begins with the formation of nuclei when it cools below the liquidus temperature. As the temperature drops, pure copper formed by the nuclei grows in size, causing the liquid to become more oxygen-rich. The liquid composition follows the liquidus line until at eutectic point. The residual liquid between the primary grains solidifies at eutectic temperature to form the

eutectic structure composed of α and Cu_2O . It can be seen from the diagram that the proportion of residual liquid solidifying with eutectic composition is controlled by the oxygen level of the melt. Therefore, the relative amount of primary and eutectic constituents provides a good indication of the alloy composition.²

The copper-oxygen system has two stable oxides, CuO and Cu_2O .²⁵ The solid-state thermodynamic equilibria of Cu , Cu_2O and CuO are well established, as shown below.²⁴



1.6 Solidification interface

There are three types of interfacial growth in liquid at the solid-liquid interface: planar, cellular, and dendritic. The growth type is under control by removing the heat from the system.

1. Planar growth

When the liquid in advance at the solid-liquid interface has a positive temperature gradient, heat transfers from the liquid through the growing solid by heat conduction. Because the temperature gradient is uniform perpendicular to the interface and linear, a smooth interface is kept and growth into the liquid is planar. (Fig. 1.6(a))

When there is an inversion of temperature due to the decrease in temperature ahead of the solid-liquid interface, cellular or dendritic growth occurs (Fig. 1.6(b,c)). The difference between the two growths is the degree of undercooling; small undercooling generally produces cellular growth, whereas large undercooling creates dendritic growth. In pure

metals, undercooling can be caused by thermal supercooling, whereas in alloys, it can be caused by a combination of constitutional and thermal supercooling.

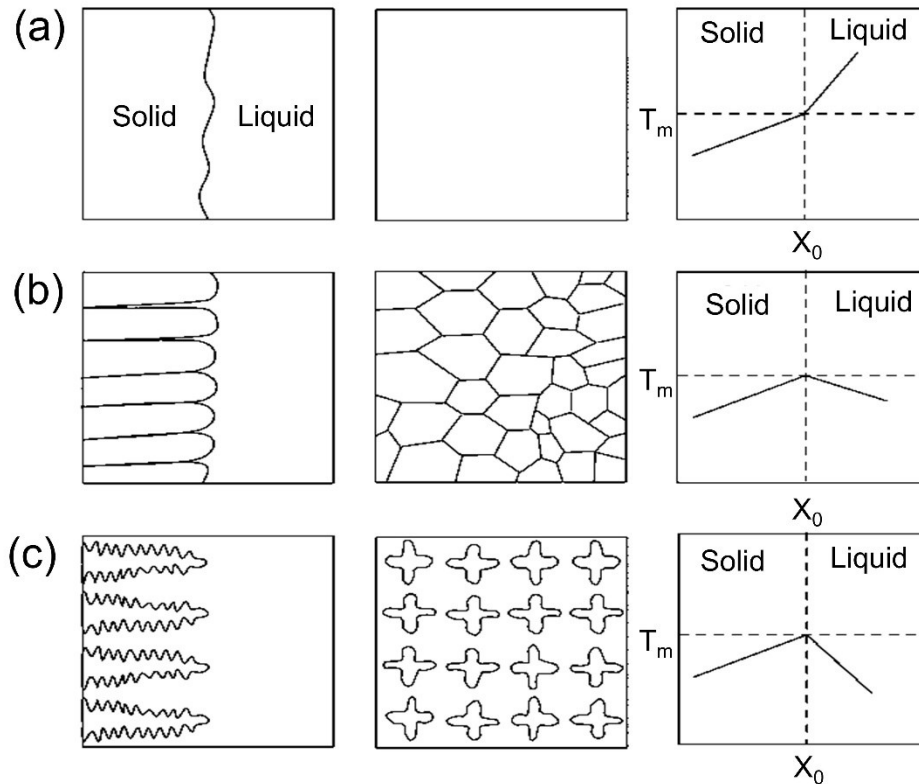


Fig. 1.6 Growth interface; (a) Planar growth (b) Cell growth (c) Dendritic growth ²⁶

2. Cellular growth

As displayed in Fig. 1.7, cellular growth occurs when the heading planar solid-liquid interface becomes unstable, and a small spike arises on the interface that then develops into a cellular-type structure. The planar surface is unstable because any part of the interface that grows ahead of the rest enters a liquid region that has a lower temperature. The initial spikes formed are isolated because as they solidify, the latent heat of fusion is released from the

spike tips into the adjacent liquid, resulting in a regional temperature increase. As a result, parallel spikes with a nearly similar spacing advance into the liquid.

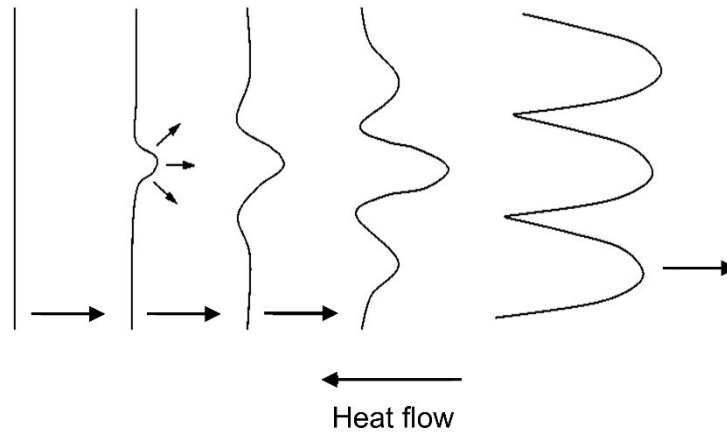


Fig. 1.7 Transition from planer to cellular growth ²⁶

3. Dendritic growth

Dendritic growth is a further representation of cellular growth in which the spikes grow side protrusions. The cells grow progressively at still higher growth velocities and higher undercooling. Their tree-like forms have given them the name "dendrites", which come from the Greek word "dendros" which means "tree." When the primary arms solidify and release latent heat, the temperature adjacent to the primary arm increases immediately, resulting in the secondary arms of dendrites growing perpendicular to the primary arms. This produces temperature inversion between the primary arms in the liquid, so secondary arms develop in that direction. A similar situation can be made to form the tertiary arms. The secondary arm spacing is proportional to the heat rate removed during solidification. The faster cooling rates create smaller dendrite arm spacings.

Although dendrites can form in pure metals to a limited extent due to temperature inversions, they are more dominant in alloys because of the extra undercooling caused by constitutional supercooling. Constitutional supercooling occurs due to the segregation of alloying elements advancing the solid-liquid front. The additional concentration of alloying elements causes the melting point of the liquid to be reduced below the actual temperature then the liquid is declared to be locally constitutionally supercooled. That is efficiently undercooled due to a change in the constitution of the liquid.

1.7 Solidification Structures

The solidification structure of cast metal in a mold has two or three different zones, including a chill zone, columnar grains zone, and a center-equiaxed grain zone (Fig. 1.8). In contrast, not all three zones are always present in pure metals. It can have a chill zone and a columnar zone but no center-equiaxed zone.^{26,27}

1. Chill zone

Since the mold wall is much cooler than the liquid metal, nucleation will occur on the inner surface of the mold wall, and the nucleation rate is high, resulting in a small average grain size. Each nucleation event results in forming a single crystal or grain to grow in a dendritic manner perpendicular to the mold wall until it impinges with other grains. The solidifying grains release the latent heat of fusion into the liquid, then superheat from liquid dissipate, leading to a slow growth rate. Each grain in the chill zone has a random orientation with respect to the mold wall, which is the major axis for grain orientation.

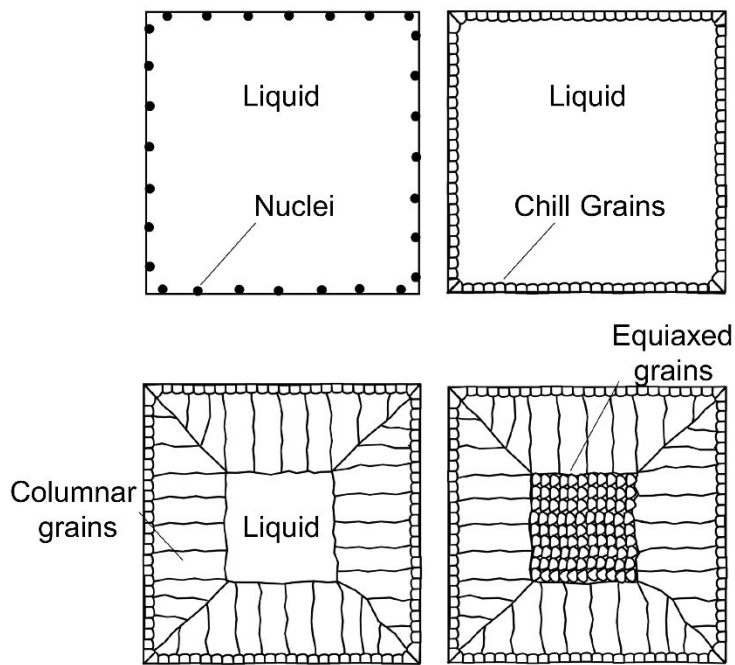


Fig. 1.8 Solidification structure in each zone for cast metal ²⁶

2. Columnar Zone

Column-shaped grains are located next to the chill zone and are oriented nearly parallel to the direction of heat flow. However, most grain prefers the growth in one principal crystallographic direction; only grains with a growth direction nearly perpendicular to the mold wall will grow quickly into the casting center. Columnar grains have axis parallel to the heat flow direction and grow along particular crystalline planes. When they grow, perfectly aligned grains will develop progressively ahead of imperfectly arranged grains. Because the grains grow quickly from the mold wall to the casting center, the parallel growth of the dendrites and the gradually lateral growth result in the final shape of grains being columnar.

3. Center-Equiaxed Zone

Smaller grains are randomly oriented and nearly equiaxed at the center of the casting. The thermal gradient decreases during solidification, causing the dendrites to grow very long. Long dendrite grains may break down due to convection currents in the melt. Then these broken dendrite arms can act as nuclei for new grains. In addition, new grains form due to segregation and a low thermal gradient during solidification. The entire casting may solidify with an equiaxed structure at low casting temperatures.^{26,27}

1.8 Solid solutions and precipitation

In general, alloying elements may occupy some positions in the copper lattice. If these elements replace a copper atom, this case is called substitutional, or they may fill normally the void among copper atoms, in which case they may be called interstitial. These elements are called to be soluble in copper, and copper containing this kind of solute is named a solid solution. The composition of these solid solutions is known as the solubility limit, in which the solute atoms are no longer dissolved but instead participate in the formation of new phases. The stable relationship between temperature, composition, and phases is presented in a phase diagram.

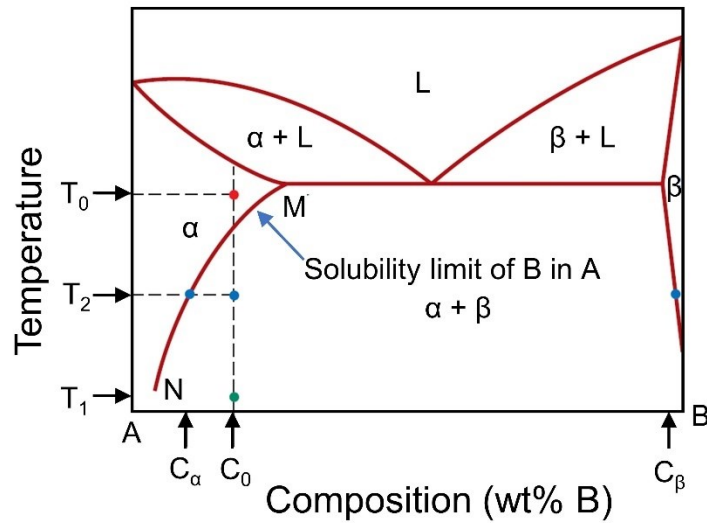


Fig. 1.9 Hypothetical phase diagram ²²

Fig.1.9 depicts a hypothetical phase diagram related to the presence of B in A. The left-hand portion of the diagram contains a region where an A solid solution, labeled (α), is present. This phase exists all the path to the melting range but has small width at low temperatures. The line labeled “Solubility limit of B in A” shows the compositions in which increasing B content will not dissolve in A, but will form a second phase with a very high B content. On the other hand, at point M, the maximum solubility of B can be presented in a solid solution of A and B. As this solution is slowly cooled, a B-rich phase will precipitate, creating a two-phase, B-rich structure distributed in the otherwise A-rich matrix phase. If the solution is rapidly cooled, there may not be adequate time for forming a stable amount of the precipitate phase. Therefore, the matrix or solvent phase contains solute that exceeds the limit of stable solubility and is called a supersaturated solid solution.¹¹

1.9 Heat treatment

The hardness and strength of some metal alloys are enhanced by forming secondary phase particles uniformly distributed in the original matrix. These particles are generated by appropriate “heat treatment”. It is called “precipitation hardening” because the small particles of this new phase are known as precipitates. Precipitation hardening results from small particle formation of a new phase (or second phase). An explanation of the heat treatment procedure can be easily described using a phase diagram. Although many precipitation-hardenable alloys consist of two or more alloying elements in practice, the discussions are simplified by using the binary system. The phase diagram must be the same as the hypothetical A-B system shown in Fig. 1.9.

Two characteristics that must be presented in the phase diagram of materials for precipitation hardening: the maximum solubility of the solute in the solvent is very high. The solubility limit (in several percent) and the solubility limit of solute decreases sharply when the temperature is reduced. The hypothetical phase diagram shown in Fig. 1.9 has these two characteristics. The point M indicates the maximum solubility. The solubility limit is represented by the boundary line between the phase regions α and $\alpha+\beta$ decreasing with temperature. It shows that the solubility limit of B in A (at the N point) is very low. The composition of the precipitation-hardenable alloys should be less than the highest solubility. All of the above characteristics are required for precipitation hardening.

1.9.1 Solution Heat Treating

Precipitation hardening consists of two different heat treatments. The first one is a solution heat treatment in which the solute atoms are dissolved into a solution and form a single-phase solid solution. When consider alloys at composition C_0 in Fig. 1.9. Heat treatment begins by heating the alloy to a temperature in the phase α region, assume T_0 , and waiting until β phase is completely dissolved. At this point, the alloy has an α phase with only composition C_0 only. A rapid cooling is followed to prevent diffusion and formation of β phase by quenching to T_1 , which may be room temperature for many alloys. A rapid cooling produces a nonequilibrium situation; that is, α phase solid solution is supersaturated with B atoms at T_1 . The alloy is relatively soft, and most alloys diffuse so slowly that the α phase can be preserved at this temperature for long periods.

1.9.2 Precipitation Heat Treating

For the second process is precipitation heat treating. It is a heating the supersaturated α solid solution to a temperature T_2 within $\alpha+\beta$ two-phase region (Fig. 1.9). At this temperature, the rate of diffusion occurs extremely fast causing β phase to begin to precipitate into fine particles containing C_β , sometimes referred to as aging. After proper aging time at temperature T_2 , the alloy is cooled to room temperature. Normally, the cooling rate at this stage is negligible. Fig. 1.10 depicts the temperature versus time plot for both solution and precipitation heat treatments. The character of β particles affects the strength and hardness of alloys. The aging time and the precipitation temperature T_2 are important parameters affecting β particle characteristics.

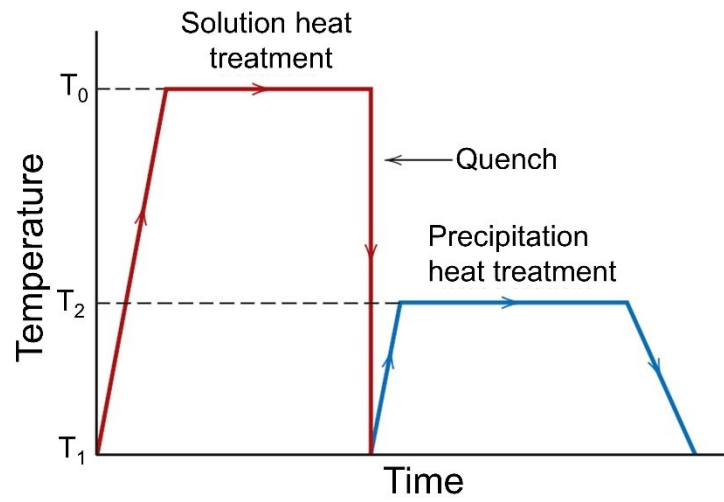


Fig. 1.10 Schematic temperature-versus-time plot showing both solution and precipitation heat treatments for precipitation hardening²²

The aging of some alloys may occur at room temperature if there is a sufficiently long duration. As the time increases, the strength or hardness increases to the maximum, and when the time is reached, a certain value leads to a decreased hardness. The reduction in strength and hardness that occurs when the aging time is too long is called “overaging”, the effect of temperature has no clear tendency.²²

1.10 Effect of oxygen and hydrogen

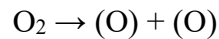
1.10.1 Oxygen effect

In copper melting, oxygen is a significant hazard. It is a cause of porosity and decreases the strength of copper alloys if lack of sufficient phosphorous contains or other deoxidizers. Most copper alloys contain deoxidizing elements, which are typically phosphorous, silicon, manganese, aluminum, or iron. These elements will commonly combine with oxygen to eliminate the possibility of porosity. The cuprous oxide content affects the soundness and strength of commercial coppers; as the oxide content decreases, the soundness increases.

In electrical Cu, the oxygen impurity causes particular problems. Although liquid Cu can dissolve several percent O, only an extremely small amount of oxygen can dissolve into solid copper, as shown in the copper-oxygen phase diagram. (Fig. 1.5) The oxygen solubility is highest (0.008 wt%) at 1065°C and near-zero at 20°C. At an oxygen content of 0.39 wt%, the solid solution α with Cu_2O forms as an eutectic structure. The Cu_2O proportion in the eutectic is approximately 3.5 wt% when the oxygen amount of Cu_2O is 11.2 wt%. This relatively small content of Cu_2O -oxides distributes in the copper matrix formed by the solid solution α . The eutectic has no effect on copper ductility if the eutectic content does not reach 10% in copper. Nevertheless, the eutectic structure can be destroyed from hot forming. When the eutectic at the grain boundaries dissolves above the eutectic temperature (1065 °C), The oxygen-containing copper is sensitive to hot cracking.

ETP copper contains about 0.06 wt % oxygen. Oxygen can also be found in the form of a free gas. When the solid copper is heated, e.g., during melting, Cu_2O -oxides release the

oxygen. The released oxygen is entrapped in the metal during rapid solidification, causing porosity of the melt, the oxygen is released in the following manner:



During rapid solidification, dissolved oxygen is redistributed as a small quantity of oxygen in a solid solution with Cu_2O precipitate particles. The dissolved oxygen and Cu_2O precipitates both cause problems. Even small contents of dissolved oxygen reduce electrical conductivity. Cu_2O precipitates have a slight effect on conductivity, but they degrade ductility for hot and cold work.^{13,28}

1.10.2 Hydrogen sickness

The existence of oxygen in the material makes copper sensitive to hydrogen sickness. If a copper material has oxygen, it tends to have hydrogen sickness. When oxygen and hydrogen are simultaneous in the molten solution or heated solid copper. Hydrogen from atmospheric humidity or the combustion products of furnace fuel used to melt the metal can enter hot copper. The Cu_2O precipitates can then react with hydrogen to generate steam bubbles inside the copper by the following reaction.



Raising the temperature of the copper leads more oxygen to react with hydrogen, resulting in water bubbles are formed both inside the grains and the grain boundaries. Because the molecules of H_2O are excessively large to diffuse in the metal, small steam

bubbles gather, producing high enough internal pressures to crack the metal. Water presents as small droplets retained in closed holes. When they form particularly at the grain boundaries, the strength of copper is significantly reduced. This phenomenon is referred to as hydrogen sickness.^{13,28}

1.11 Thermal expansion and thermal conduction

Thermal expansion

Many solid materials expand when heated and contract when it is cooled. Changes in the temperature and length of the solid material may be displayed as follows.

$$\frac{l_f - l_0}{l_0} = \alpha_l (T_f - T_0) \quad (1.7)$$

or

$$\frac{\Delta l}{l_0} = \alpha_l \Delta T \quad (1.8)$$

Where l_0 and l_f are the original length and final length at temperature T_0 and T_f , respectively. The parameter α_l represents linear coefficient of thermal expansion. It is a material property that indicates thermal expansion of materials when heated. Its unit is $(^\circ\text{C})^{-1}$ or $(^\circ\text{F})^{-1}$. The linear coefficient of thermal expansion for copper is $17 (\text{C})^{-1}$.

Moreover, heating or cooling has an effect on the dimensions of material, resulting in a change in volume. Volume changes with temperature can be calculated using

$$\frac{\Delta V}{V_0} = \alpha_v \Delta T \quad (1.9)$$

Where ΔV and V_0 represent, respectively, the volume change and the initial volume. The parameter α_v is the volume coefficient of thermal expansion. In most materials, the value of α_v is anisotropic; In other words, it depends on the direction of crystallography as it is

measured. For materials with isotropic thermal expansion, α_v is about $3\alpha_l$. When consider in atom, the thermal expansion is the result of an increase in average distance between atoms.²²

Thermal conduction

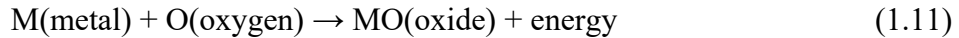
Thermal conduction is a phenomenon in which heat in a substance is transported from high-temperature to low-temperature regions. The material property that defines the ability to transfer heat is thermal conductivity. It is well described by the Fourier's law expression

$$q = -k \frac{dT}{dx} \quad (1.10)$$

Where q is heat flux or the heat flow, per unit time per unit area. k denotes the thermal conductivity; 398 W/mK for copper, and dT/dx is the temperature gradient across a conductive medium. Equation 1.10 is applicable only for steady-state heat flow— in this case, the heat flux does not change over time. The minus sign in Eq. 1.10 represents heat flow from high to low temperature. Fourier's law for heat flow in Eq.1.10 is identical in form to Fick's first law for steady-state diffusion. This means that the solutions to heat flow problems are the similar as those to matter flow problems when k is replaced by the diffusion coefficient D , and temperature gradient dT/dx is replaced by concentration gradient dc/dx .^{22,29}

1.12 Oxidation mechanism

Most elements are most stable in their oxide state. When any metal is exposed to the atmosphere, a thin oxide film forms immediately following the reaction.



The free energy of oxidation released when a material reacts with oxygen is the driving force for a material to oxidize. At room temperature, most metals oxidize at too slow a rate. The rate of oxidation increases when they are heated.

The gain or loss in weight, Δm , can be measured after the metal is held at temperature T for an increasing time t . If the oxide bonds to the metal, the gain weight increases in time t in either a linear ($\Delta m \propto t$) or a parabolic ($\Delta m \propto t^{1/2}$) manner. On the other hand, when the oxide is volatile, the metal loses weight linearly with time ($\Delta m \rightarrow -t$).

Therefore, there are two different types of weight gain behavior. Some metals exhibit linear weight gain, implying that oxidation is occurring at a constant rate:

$$\frac{dm}{dt} = k_l \quad \text{giving} \quad \Delta m = k_l t \quad (1.12)$$

where k_l is the linear rate constant. This is caused by the oxide film cracking or spalling off when it becomes too thick and fails to cover the underlying metal. The oxide film of some metals firmly adhered to the metal. It is coherent and compact. Thus, the weight gain for these is parabolic, slowing with time, implying the rate of oxidation rate with the form

$$\frac{d\Delta m}{dt} = \frac{k_p}{\Delta m} \quad \text{giving} \quad \Delta m^2 = k_p t \quad (1.13)$$

where k_p is the parabolic rate constant. Once the oxide film is formed, the metal is separated from the oxygen by oxide film. To continue the reaction, oxygen atoms must either

diffuse through the film to encounter the metal or metal atoms must get outward through the film to react with the oxygen. For this reason, if the film is thicker, it takes a longer to diffuse to reach each other so the oxidation is restrained by the diffusion rate.

The oxidation mechanisms occur on both sides of the oxide film, as described below.

1. Cu forms an ion by releasing electrons:



2. The electron is absorbed by oxygen to give an oxygen ion:



3. Copper ion combines with oxygen ion to form Cu_2O :

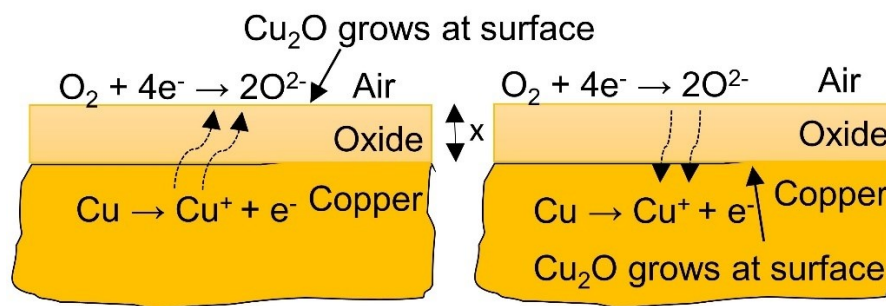


Fig. 1.11 Oxidation mechanisms of copper (a) Growth by copper diffusion (b) Growth by oxygen diffusion

In Fig. 1.11(a), the copper ion gets out through oxide film to react with oxygen from the air, Cu_2O growth by copper diffusion appears at oxide and air interface. At the same time,

Cu_2O grows at the interface between copper and oxide when oxygen ion diffuses inward to meet copper ion, as shown in Fig. 1.11(b). If there are many oxides because of thickness increases, the oxide behaves an insulator, electrons cannot diffuse through. Thus, oxygen must diffuse inward. The gradient of oxygen concentration is C_0 divided by the thickness of oxide film, x . The growth rate of oxide film is proportional to the flux of atomic diffusion through it, giving

$$\frac{dx}{dt} \propto D \frac{C_0}{x} = K_0 \left(e^{-\frac{Q}{RT}} \right) \frac{C_0}{x} \quad (1.17)$$

Where D is the diffusion coefficient, K_0 is a kinetic constant and Q is the activation energy of oxygen diffusion. Integrating gives

$$x^2 = k_p t \quad (1.18)$$

The equation (1.18) is identical as equation (1.13)

Where
$$k_p = A e^{-\frac{Q}{RT}} \quad (1.19)$$

The equation (1.19) is commonly referred to as the "Arrhenius expression." The oxidation rate rises rapidly with increasing temperature and the growth rate obeys the parabolic rate law.

Where k_p is the parabolic rate constant, A is the pre-exponential constant, and R is the gas constant.²⁹

1.13 Manual for fire investigation by NITE

In Japan, the National Institute of Technology and Evaluation (NITE) was disclosed the Manual for investigating the cause of fire accidents in home appliances 2010.² They discriminated PMM and SMM by estimating the surrounding temperature during short-circuiting from the “dendrite arm spacing” (DAS) method and the “cell size” (CS) method, as presented in Fig. 1.12.

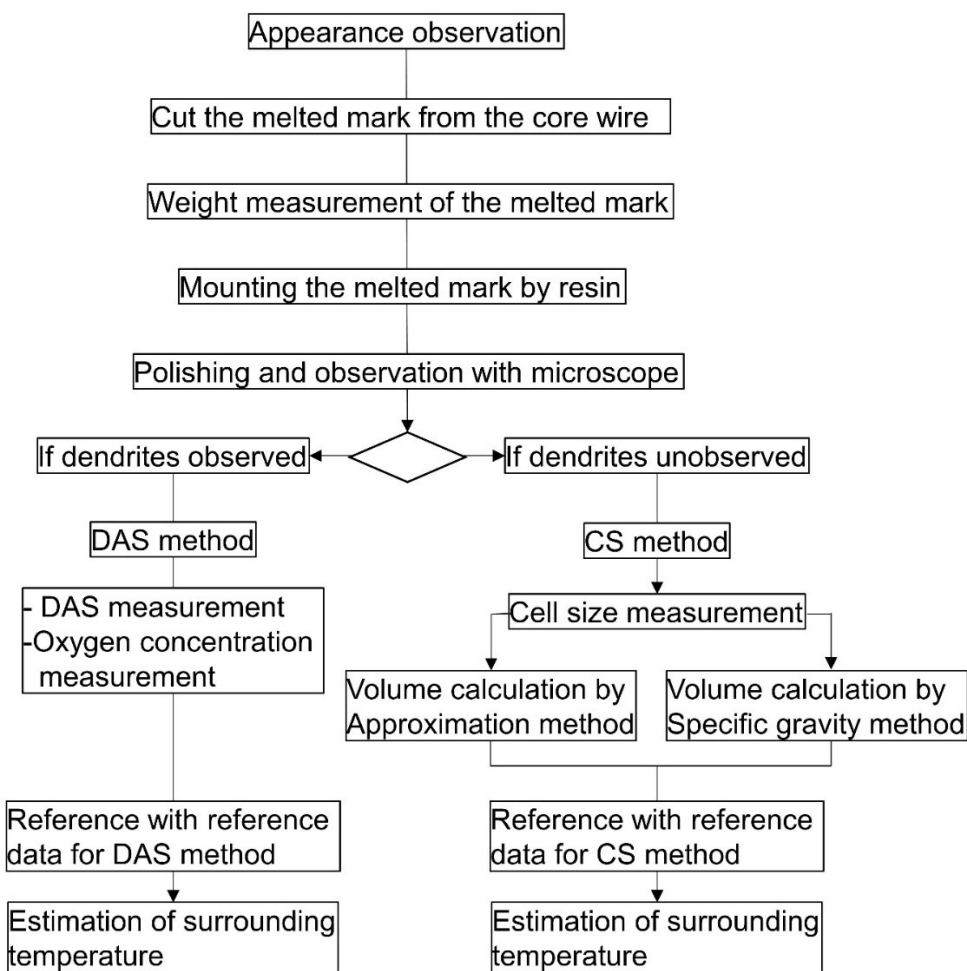


Fig. 1.12 Flow chart of the metallurgical examination method on melted of copper wire by DAS method and CS method²

DAS method is used to estimate the surrounding temperature by measuring DAS and oxygen concentration and comparing it to reference data.

CS method is used to estimate the surrounding temperature by measuring cell size and melted mark volume and comparing it to reference data.

From method validation by Lee et al.⁶, the PMM can be formed at about 400 °C or less, the oxygen concentration in the oxidized structure ranges from 0.05 wt% to 0.16 wt%, while the SMM can be made at about 600 °C or more, and the oxygen concentration of 0.05 wt% to 0.26 wt% contains in the oxidized structure. If the estimated surrounding temperature is between 400 °C and 600 °C, this flow chart is insufficient to classify PMM and SMM. Therefore, the estimated surrounding temperature from this flow chart cannot identify PMM and SMM at intermediate surrounding temperatures.

1.14 Objectives of this thesis

1. To collect the characteristic microstructures and copper oxide formation of the primary melted mark on copper wire formed and annealed under various fire environments
2. To establish the metallurgical examination method for fire investigation by using the collected characteristic microstructures and copper oxide of PMM to describe the fire behaviors and identify the PMM leading to pointing out the origin of the fire.

The fire investigation from the copper oxide and the microstructure of melted mark on the copper wire has received little attention. Moreover, the complexity and diversity of fire behaviors have been found in fire accidents. Additionally, the fire investigation method

on the melted mark of copper wire by metallurgical technique remains unclear. Thus, the objectives of the research presented in this thesis are:

In **chapter 1**, to indicate the background and significance of the investigation of solidification microstructure and copper oxide formation on the melted mark of copper wire for fire investigation. Furthermore, to point out that the present fire investigation methods are still insufficient to identify the PMM. Thus, we have to fulfill them by establishing the metallurgical examination method for the melted mark on copper wire.

In **chapter 2**, the first goal of this chapter is to investigate the characteristics of PMM solidified in the air and water before heat treatment by observing microstructure and dendrite growth direction, as well as examining the cooling rate impact on oxygen concentration for each zone of the melted mark on copper wire. The second purpose is to investigate the effect of cooling rate on the melted mark on copper wire after heat treatment in order to describe the fire behaviors by observation of surface morphology and microstructure evaluation, phase identification of the oxide layer using XRD, and investigation of the cooling rate influence on crystallite size of the oxide layer.

In **chapter 3**, because of the variety of fire behaviors discovered in the fire event, the evolution of the microstructure and oxide layer on the melted mark of copper wire in various fire environments is important in fire investigation. In particular, the effect of annealing temperature and annealing time on the microstructure and oxide layer of the melted mark on the copper wire after heat treatment has not been extensively researched. Therefore, this study investigated the microstructure and typical oxide layer of PMM after annealing at different annealing temperatures and times.

In **chapter 4**, the first aim is to establish a metallurgical examination method for melted marks on the copper wire formed in a fire accident by referring to the solidification microstructure and oxide evolution in chapters 2 and 3 to describe the fire behavior and identify the origin of the fire. The second objective is to validate the method by examining real melted marks on copper wires collected from actual fire accident sites in Thailand using our established metallurgical examination method.

References

1. D. Agakidou V, Kanakoudi-Tsakalidou F, Sarafidis K, et al. Properties and Selection: Nonferrous Alloys and Special-Purpose Materials. *Eur J Pediatr* 1998; 157: 583–588.
2. Association CD. *Equilibrium Diagrams Selected copper alloy diagrams illustrating the major types of phase transformation*, www.cda.org.uk (1992).
3. Liu KH, Shih YH, Chen GJ, et al. Microstructural Study on Molten Marks of Fire-Causing Copper Wires. *Materials (Basel)* 2015; 8: 3776–3790.
4. Lee EP, Ohtani H, Matsubara Y, et al. Study on discrimination between primary and secondary molten marks using carbonized residue. *Fire Saf J* 2002; 37: 353–368.
5. Howitt DG. The Surface Analysis of Copper Arc Beads—A Critical Review. *J Forensic Sci* 1997; 42: 14172J.
6. LEE EP, OHTANI H, SEKI T, et al. Study on discrimination between primary and secondary molten marks by DAS. *Bull Japan Assoc Fire Sci Eng* 2000; 50: 1–12.
7. Liu KH, Shih YH, Chen GJ, et al. Microstructural Study on Oxygen Permeated Arc Beads. *J Nanomater* 2015; 2015: 1–8.
8. Choudhary S, Sarma JVN, Pande S, et al. Oxidation mechanism of thin Cu films : A gateway towards the formation of single oxide phase. *AIP Adv*; 055114. Epub ahead of print 2018. DOI: 10.1063/1.5028407.
9. Park JH, Natesan K. Oxidation of copper and electronic transport in copper oxides. *Oxid Met* 1993; 39: 411–435.
10. Collini L. *Copper Alloys - Early Applications and Current Performance - Enhancing*

- Processes*. 2012. Epub ahead of print 2012. DOI: 10.5772/1912.
11. Izzaty RE, Astuti B, Cholimah N. *Wire Technology: Process Engineering and Metallurgy*. 1967.
 12. Black JT, Kohser RA. *DeGarmo's MATERIALS AND PROCESSES IN MANUFACTURING ELEVENTH EDITION*. 2012.
 13. Pohja R, Vestman H, Jauhiainen P. *Narrow Gap Arc Welding Experiments of Thick Copper Sections*. 2003.
 14. Singh D, Mittal V, Rana S. Estimation / Assessment of Oxygen content in copper by Metallographic method Estimation / Assessment of Oxygen content in copper by Metallographic method.
 15. Copper Wire Manufacturing Process | Annealing | Hot Dip Process, <https://www.ganpatiengineering.com/manufacturing-process.html> (accessed 17 February 2022).
 16. Manufacturing Process, <https://fast-cables.com/wp-content/uploads/2018/01/Manufacturing-Process.pdf> (accessed 17 February 2022).
 17. Copper Wire Manufacturing Process | by Grauer Weil | Medium, <https://medium.com/@growelindia1/copper-wire-manufacturing-process-9c1d88cd33af> (accessed 17 February 2022).
 18. Fellah L, Boumerzoug Z. Experimental investigation of industrial copper deformed by wire drawing process. *J Fundam Appl Sci* 2018; 10: 97.
 19. Investigations E. *Guide for Fire and Explosion Investigations 2*. NFPA 921, 2017.

20. Wang L, Yao HW, Wu ZX, et al. The application of image processing in the electrical fire physical evidence identification. *Procedia Eng* 2014; 71: 57–64.
21. Wang Y, Su X. Study on pores distribution laws in secondary short circuited melted beads of copper wires. *Procedia Eng* 2014; 84: 887–892.
22. William D. Callister J, Rethwisch DG. *Fundamentals of Materials Science and Engineering*. John Wiley & Sons, Inc., 2012.
23. Kehl GL. *Metallurgy and Metallurgical Engineering Series*. 3rd ed. McGraw Hill, 1949.
24. Neumann JP, Zhong T, Chang YA. The Cu-O (Copper-Oxygen) system. *Bull Alloy Phase Diagrams* 1984; 5: 136–140.
25. Schramm L, Behr G, Löser W, et al. Thermodynamic reassessment of the Cu-O phase diagram. *J Phase Equilibria Diffus* 2005; 26: 605–612.
26. Campbell FC. *Elements of Metallurgy and Engineering Alloys*. ASM International, 2008. Epub ahead of print 2008. DOI: 10.1097/01.sga.0000349555.12380.25.
27. Kurz W, Fisher DJ. *Fundamentals of Solidification*. 3rd ed. TRANS TECH PUBLICATIONS, 1989.
28. Russell AM, Lee KL. *STRUCTURE – PROPERTY RELATIONS IN NONFERROUS METALS*. A JOHN WILEY & SONS, INC., 2005.
29. Michael Ashby, Hugh Shercliff, David Cebon. *Materials Engineering, Science, Processing and Design*. 1st ed. Elsevier Ltd., 2007.

Chapter 2 Investigation of solidification microstructure at various cooling rates before and after heat treatments on the melted mark of copper wire

2.1 Introduction

Copper is used to make conductors in their pure form. To achieve the desired size, the copper is heated and drawn through progressively smaller dies. Such copper has no discernible crystal structure.¹ Moreover, the solidification structure of melted marks on copper wire caused by short-circuiting has received little attention. The melted mark on the copper wire is crucial evidence used by the fire investigator to determine the source of the fire because it is not severely damaged and is left after the fire. However, various melted marks are occasionally discovered in the fire, making distinguishing between primary melted mark (PMM) and secondary melted mark (SMM) difficult. A visual examination does not provide a high level of confidence in assessing the damage. More advanced examination techniques, such as cross-sectioning and polishing, metallurgical methods, and SEM/EDS examination, could support the distinction between PMM and SMM damage.¹

Lee et al.² determined the relationship between dendrite arm spacing (DAS), oxygen concentration and ambient temperature of the copper and cuprous (Cu_2O). In the oxidized structure, copper primary dendrites may be observed at an oxygen concentration of less than 0.39 wt%, and cuprous oxide (Cu_2O) primary dendrites may be observed at an oxygen concentration of 0.39 wt% or more. Both Cu primary dendrites and Cu_2O primary dendrites have increased DAS as the temperature increases because the cooling rate is slow at high temperatures. In the case of Cu primary dendrites, the lower oxygen concentration, and the case of Cu_2O primary dendrites, the higher the concentration, the farther the oxygen

concentration is from the eutectic point, the larger the DAS. When a Cu-Cu₂O binary alloy is melted and solidified, Cu crystallizes first when the oxygen concentration in the liquid phase is 0.39 wt% or less, and solidification continues while the oxygen concentration in the liquid phase increases. In contrast, Cu₂O crystallizes first when it is 0.39 wt% or higher, and solidification keeps going while the oxygen concentration in the liquid phase part decreases. When the oxygen concentration of the remaining liquid phase portion reaches 0.39 wt%, solidification is complete and a eutectic structure is formed. Consequently, the oxygen concentration is low, Cu primary dendrites appear. The oxygen concentration is high, Cu₂O primary dendrites with an oxygen concentration of 0.39% or more present. Thus, the final microstructures after solidification become either Cu-primary dendrites or Cu₂O primary dendrites surrounded by Cu-Cu₂O eutectic structure, which depends on oxygen concentration.²

Liu et al. discussed the solidification of melted mark on copper wire simulated by the short-circuiting at atmosphere. Due to the high current density of short-circuiting occurring in the atmosphere, the liquid copper at melted site adsorbs oxygen from air. The dissolved oxygen in liquid copper on the melted site obeys Sievert's law. The oxygen solubility increases in the liquid copper at high temperature due to the rapid heating from short-circuiting. According to Cu-O phase diagram, during melting, the copper liquid forms two liquids miscibility gap at the temperature below $T = 1618 \text{ K}$ ($L \rightarrow L_1 + L_2$). When the temperature of the copper liquid at the surface of an outer melted mark is decreased lower than the freezing point of cuprous oxide of $T = 1502 \text{ K}$ ($L_2 \rightarrow \text{Cu}_2\text{O}$). L_2 is then solidified into a cuprous oxide layer, which serves to protect the oxygen in the ambient atmosphere from

further dissolving into the melted mark continuously, as shown in Fig. 2.1. When the temperature of the melted mark solution is below 1496 K. ($L_1+L_2 \rightarrow L_1+Cu_2O$). The monotectic transformation thickens the cuprous oxide layer.

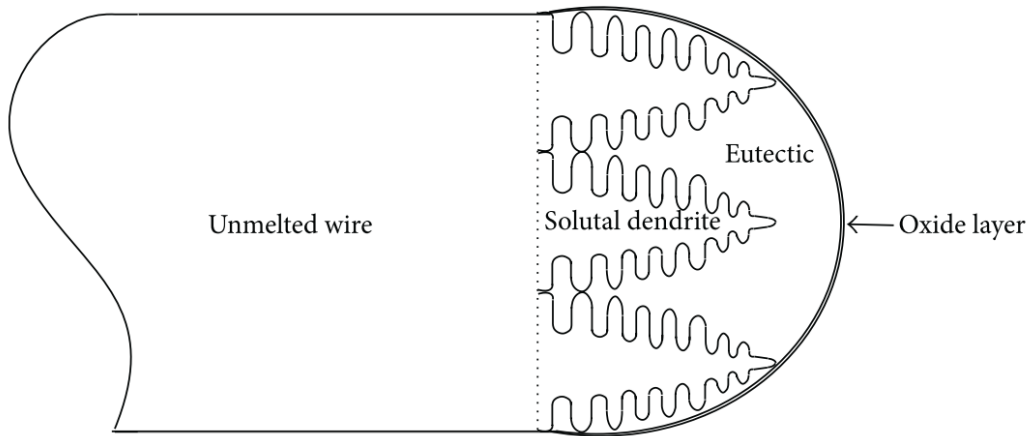


Fig. 2.1 Schematic diagram of microstructure of melted mark on copper wire³

During a rapid solidification below freezing point of copper (1358 K), copper atoms in liquid nucleate heterogeneously at the unmelted/melted interface of copper wire. Capillarity and thermal conduction cause the copper atoms on the liquid site to crystallize at the interface. The solidified Cu phase dendrites have the appearance of a nonfaceted crystal in which the growth direction of cellular dendrites is opposite to the heat flow direction. The solutal Cu dendrites develop rapidly from the unmelted site to the melted mark surface. At this stage, the solutal Cu-dendrite tips reject the oxygen into liquid and enhances the oxygen concentration in solution. As the series of events continue, the oxygen content of the solution increases, and it may eventually reach the eutectic composition of the (Cu+Cu₂O) Phase. The

residual solution repelled by Cu dendrites growth to the cuprous oxide surface of melted mark forms the eutectic composition solution. When the temperature decreases lower than the eutectic temperature of 1339 K ($L_1 \rightarrow \text{Cu} + \text{Cu}_2\text{O}$), the residual eutectic solution is finally solidified into a Cu-Cu₂O eutectic structure. Therefore, the microstructure constituents of solutal Cu-dendrites and Cu-Cu₂O eutectic structure under the cuprous oxide surface layer are the final microstructure in solidification of the melted mark on copper wire as illustrated in Fig. 2.1.³

Nevertheless, a diversity of fire behaviors is evidenced in a fire accident.⁴ The microstructure of PMM on copper caused by short-circuiting and solidifying at different cooling rates both before and after heat treatment has not been extensively researched. Besides, PMM is rapidly formed and suddenly solidified in an atmosphere at or near room temperature. SMM, on the other hand, is created and slower cooled at a high fire temperature. As a result, PMM's cooling rate should be much higher than SMM's.²

Therefore, the first goal of the research in this chapter is to investigate the characteristics of PMM solidified with various cooling types before heat treatment by observing microstructure and dendrite growth direction, as well as examining the cooling rate impact on oxygen concentration for each zone of the melted mark. The second purpose is to describe the fire behaviors from PMM cooled with different cooling rates after heat treatment by observation of surface morphology and microstructure evaluation, phase identification of the oxide layer using XRD, and investigation of the cooling rate influence on crystallite size of the oxide layer.

2.2 Materials and methods

The commercial single core copper wires (99.95 wt% Cu) of 25 mm in length and 2.6 mm in diameter have been used in the experiment. Because the short-circuiting occurs at the point where the PVC insulated copper wire is damaged, the PVC insulation was peeled off prior to simulating short-circuiting. An arc welding machine (Fig. 2.2) was used to imitate the short-circuiting on the end of copper wire with rapid melting and sudden solidifying in the air and water (Fig. 2.3(a)). The “melted mark” on copper wire obtained after melting by the arc welding machine. The air-solidified and water-solidified samples are the melted marks for without heat treatment condition.

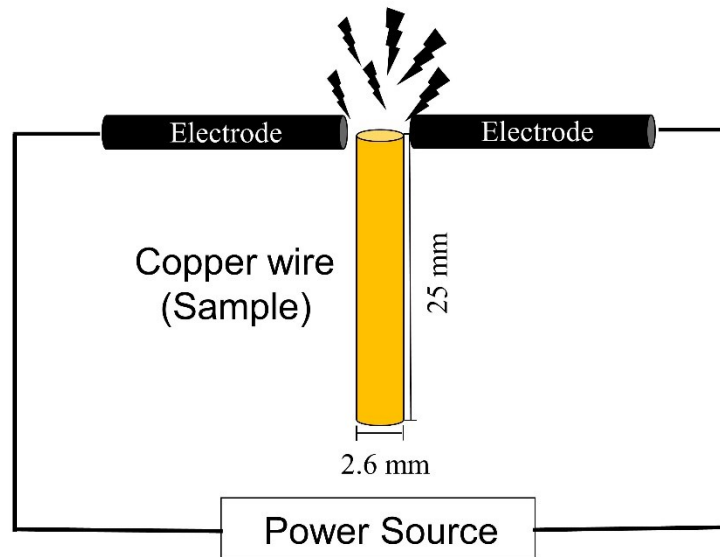


Fig. 2.2 Schematic diagram for copper wire melting by arc welding machine

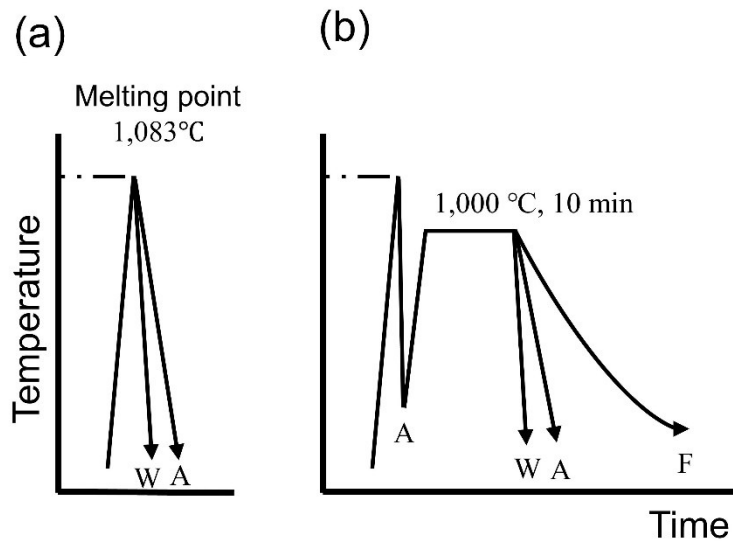


Fig. 2.3 Schematic diagram of (a) solidification process, and (b) heat treatment process

Another experimental condition is modeling the fire environment using a heat treatment process to examine the cooling rate effect after the fire. The thermocouple was placed 2 mm from the end of the copper wire under the copper wire. As shown in Fig. 2.3(b), the melted marks solidified in the air were annealed in the electric furnace for heat treatment at 1000°C for 10 minutes before being cooled to room temperature for different cooling methods (furnace, air, and water).

Both unannealed (Fig. 2.3(a)) and annealed (Fig. 2.3(b)) samples were mounted with conductive resin (Technovit) and longitudinal cut to observe the microstructure in the longitudinal section. Then, they were ground with sandpaper from #500 to #4000 and further mirror-polished by a diamond paste of 0.1 μm . The alcohol was used to clean the samples in an ultrasonic bath after grinding and polishing. Previous to using an optical microscope to

examine the microstructures, all samples were further etched for a few minutes with a solution of 10 g FeCl₃, 30 ml HCl, and 120 ml distilled water.⁵⁻⁷

The surface morphology and chemical composition of all specimens were examined by Scanning electron microscope (SEM) of HITACHI SU3500 attached Energy dispersive X-ray spectroscopy (EDS).

The phase identification of the oxide layer on melted mark was conducted by X-ray diffraction (XRD) of Rigaku, RINT-2100 under 40kV/4mA and CuK α radiation at 0.1540 nm wavelength. Data was collected in the range 2θ of 20 to 80 degrees with 0.02 degree steps.

2.3 Results and discussions

The results and discussions in this chapter are divided into two sections, including the cooling rate effect on solidification of unannealed melted marks and the cooling rate effect on microstructure formation of annealed melted marks.

2.3.1 Cooling rate effect on solidification of unannealed melted marks

The melted marks generated by arc welding machine and solidified in the air and by water were illustrated in Figs. 2.4(a) and (b), respectively. These two melted marks were examined for the following characteristics: dendrite growth, heat conduction, microstructure characterization, and oxygen concentration.

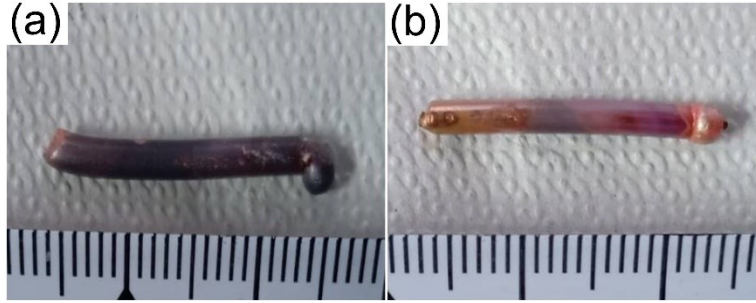


Fig. 2.4 The melted marks from simulating by arc welding machine solidified (a) in air (b) by water

2.3.1.1 Dendrite growth

Figs. 2.5(a-d) and 2.5(e-h) show the structures in the longitudinal section of melted marks on copper wire solidified in air and water, respectively. Both different solidified samples depict the microstructure of the non-melting zone, which differs from the melting zone by having a distinct boundary on the left part. The structure in the non-melting region is an annealing twin because it is like being annealed as it receives the heat transmitted from the melting area. As well known, copper has a face center cubic structure; its structure can transform into the annealing twin structure after annealing.^{8,9} In comparison, the melting region has a dendritic structure. The detail of dendritic formation will be discussed in section 2.3.1.3. Furthermore, gas porosities are only visible in the melting region; it was assumed that gas porosities were created during the solidification process when a large amount of oxygen, hydrogen, or nitrogen was dissolved into liquid copper.

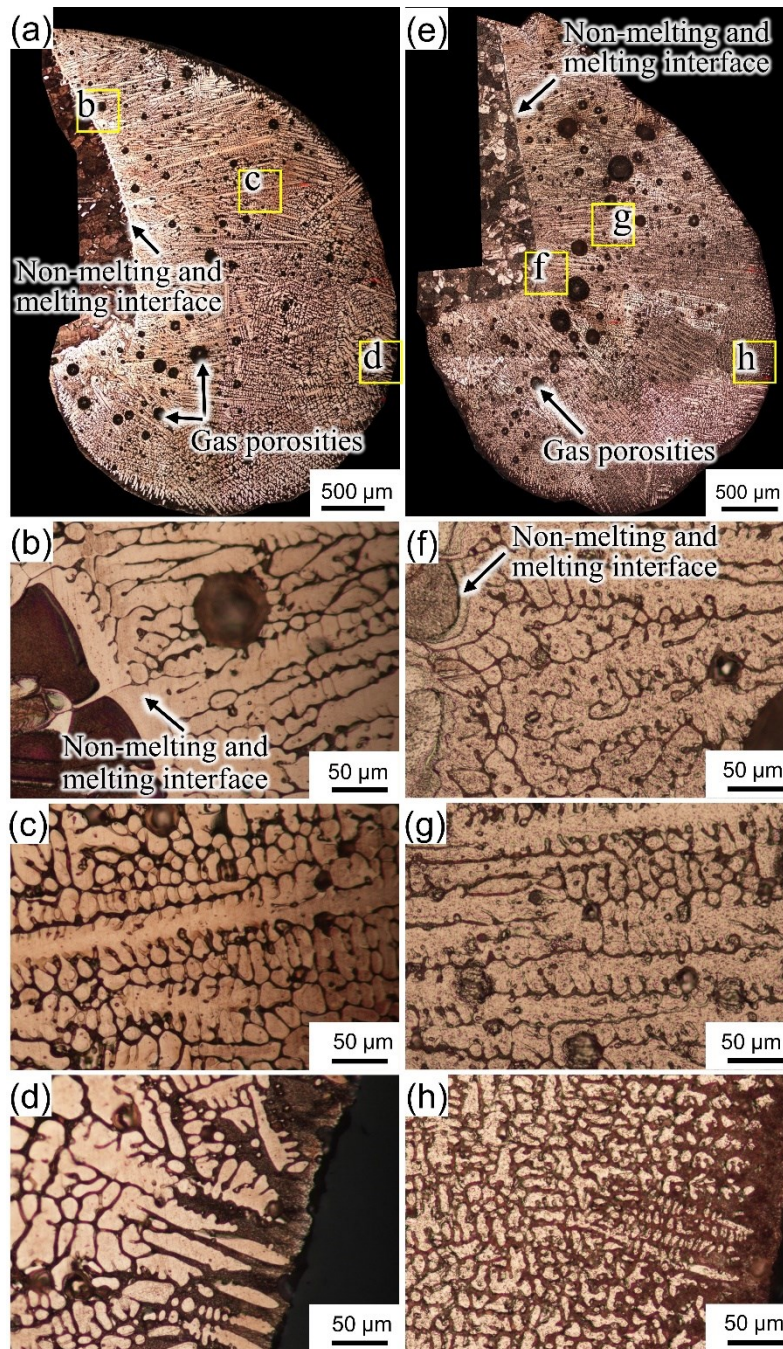


Fig. 2.5 The longitudinal section of a melted mark solidified in air (a-d) and water (e-h), with (b,f) near the non-melting zone, (c,g) in the middle, and (d,h) near the melted mark's surface.

As illustrated in Figs. 2.5(b,f), the dendrites start to develop at the non-melting/melting interface. Because during solidification, when the temperature of liquid copper is lower than the melting temperature of 1083°C,⁸ copper atoms in liquid are nucleated as crystals at the non-melting/melting interface of copper wire. Then, the crystals grow from this interface into the surface of the melted mark to form columnar crystals as exhibited in Figs. 2.5(b-d) for solidification in the air and Figs. 2.5(f-h) for solidification by water. The dendrite growth direction of both melted marks is in the same direction.

Even though the direction of dendrite growth of the water-solidified sample should be from the surface of the melted mark to the inside. Because of the very small volume of the melted mark, the liquid copper suddenly solidifies, then the dendrites progressively grow from the interface to the surface of the melted mark due to the heat propagating to the long unmelted solid copper wire. It can be seen that the growth of dendrites for both cooling types from the non-melting area to the surface of the melted mark is in the opposite direction of heat transfer which becomes the primary growth direction.

Additionally, the direction of dendrite growth and heat transfer for the air-solidified sample is compatible with the melted mark simulated from short-circuiting at 110 volts, as mentioned by Liu et al.^{4,5}

2.3.1.2 Heat conduction

Heat conduction is directly related to the dendrite growth from the non-melting zone to the surface of the melted mark for air and water-solidified samples. The random movement of atoms, molecules, or electrons in a solid causes heat to be transferred through

it.⁹ The difference in temperature drives the heat transfer. As a result, whenever a material is hotter than its surroundings, heat flows from the hotter zone to the cooler zone. The two-dimensional steady-state heat conduction problem was solved to yield the temperature distribution map and clarify the heat transfer parallel to the longitudinal copper wire.

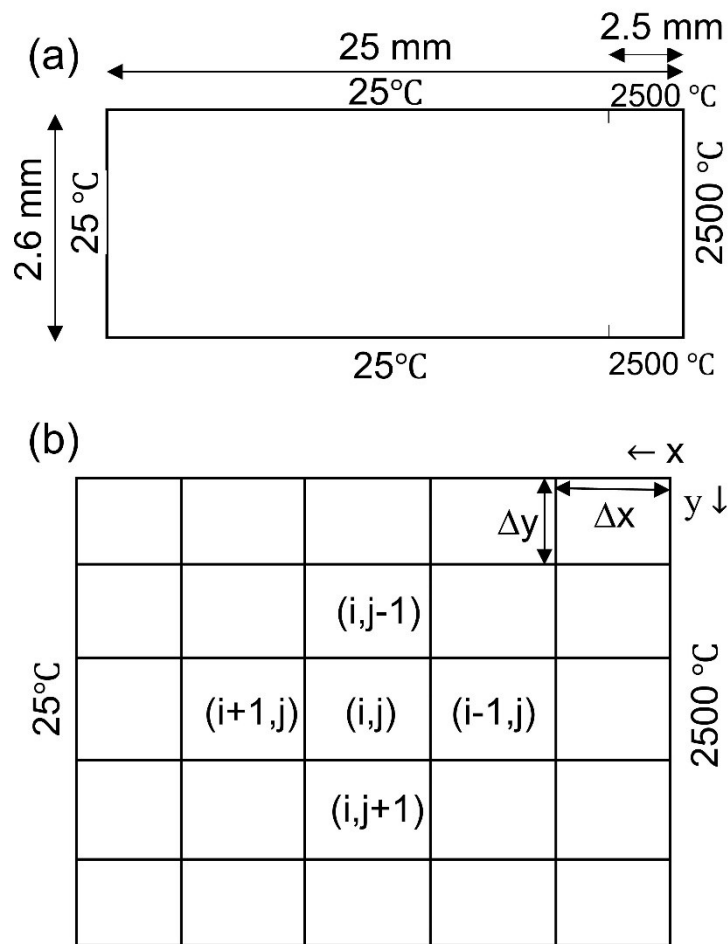


Fig. 2.6 Schematic diagram of heat conduction in two-dimension model (a) boundary conditions (b) mathematical model

Since a copper wire of 25 mm in length and 2.6 mm in diameter was carried out in this project, the melted zone is approximately 2 to 2.5 mm from the wire's end. This problem assumes steady-state heat conduction in two dimensions with a constant thermal conductivity (k) of 398 W/Km and no generation. From the schematic diagram of heat conduction in two-dimension model in Fig. 2.6, the temperature on the right side of the copper wire has been set to 2500°C as a result of optimization, while boundary conditions on the other sides have temperature of 25 °C. Thus, the x and y directions on the solid copper wire have varying temperatures.

To determine the temperature gradient, the copper wire is divided into one of the elements denoted by i and j . Let us consider the element (i, j) , as heat flows from high to low temperatures through the right boundary to the left boundary, so the energy in the x-direction comes in from the $(i-1, j)$ element and goes out to the $(i+1, j)$ element. In the same way, the temperature should be higher near the upper and lower boundaries in the y direction. Therefore, the energy balance of each element can be estimated using Fourier's law as follows:^{11,12}

$$0 = \left[-\frac{k(T_{(i,j)} - T_{(i-1,j)})}{\Delta x} + \frac{k(T_{(i+1,j)} - T_{(i,j)})}{\Delta x} - \frac{k(T_{(i,j)} - T_{(i,j-1)})}{\Delta y} + \frac{k(T_{(i,j+1)} - T_{(i,j)})}{\Delta y} \right] \quad (2.1)$$

Where $\Delta x = 2.5$ mm, $\Delta y = 0.26$ mm. The temperature distribution map solved from equation (2.1) is shown in Fig. 2.7.

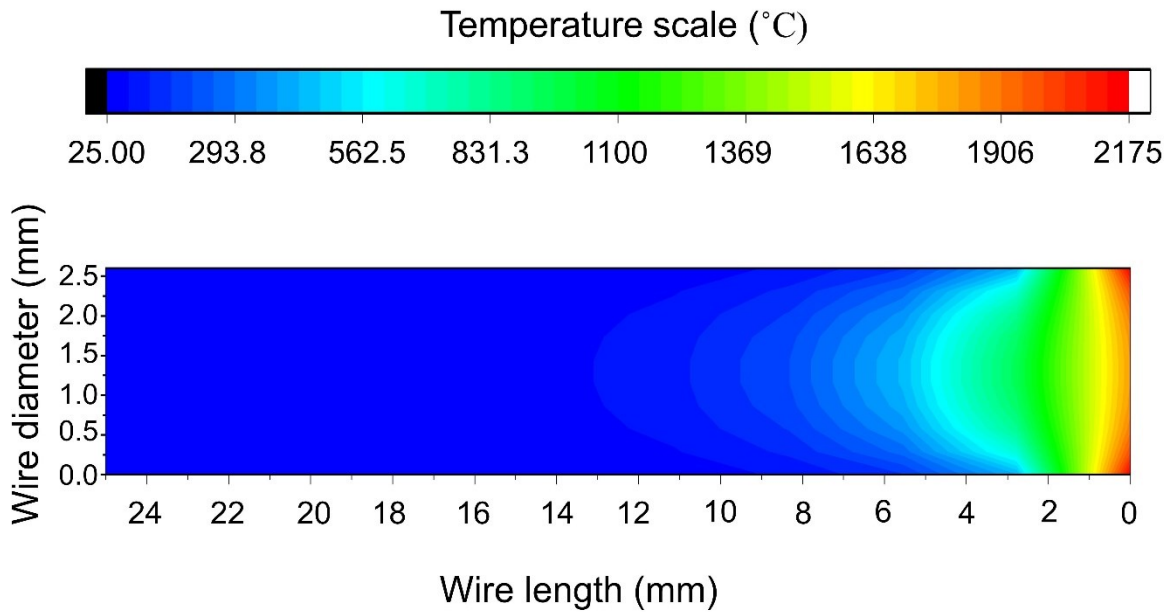


Fig 2.7. Temperature distribution map of copper wire heated at the one tip

The high-temperature zone in the temperature map appears only slightly away from the tip of the wire. The melting region should be a region with a temperature above the melting point of copper (1083 °C), positioned no more than 2.5 mm from the tip of the wire. Following the melting region, the temperature rapidly drops to a low level from the melting region. It is clear that the heat transfers from the tip of the hotter zone along the solid copper wire to the cooler zone. As the copper wire was only melted 2 to 2.5 mm from one tip, the more substantial difference in temperature between the non-melting area with a long wire and the melting area with a short wire enhances the greater heat flow. As a result, when the temperature of the liquid copper is below its melting point, whether the air-solidified sample or the water-solidified sample, nucleation is formed immediately at the non-melting/melting

interface. Then, dendrites grow rapidly from this interface to the melted mark's surface as the high heat transfer to the long copper wire.

2.3.1.3 Microstructure characterization

The microstructure characterization of the melted marks solidified in the air and water is revealed in Fig. 2.8. In most areas of both specimens, the microstructure comprises primary Cu dendrites in a bright area enclosed by a (Cu+Cu₂O) eutectic structure in a dark area.

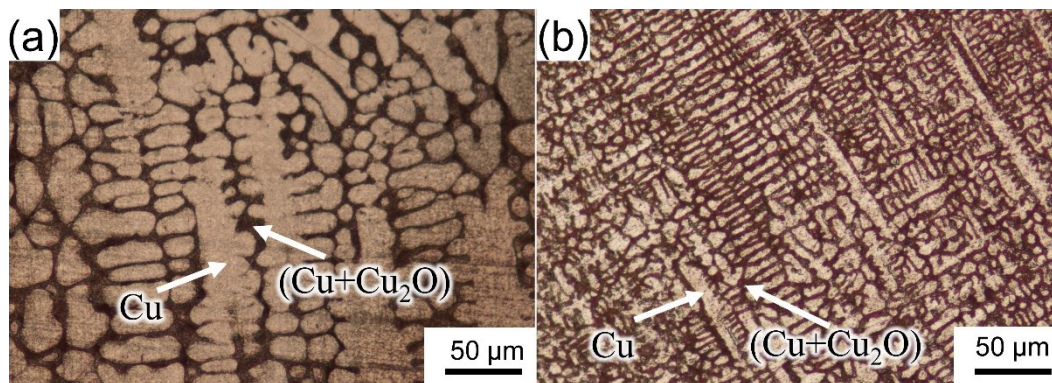


Fig. 2.8 Microstructures of the melted mark solidified in (a) air (b) water

The Cu-O phase diagram can be used to describe it.² When the temperature of liquid copper is below 1083 °C, the copper atoms initially crystallize at the non-melting/melting interface. They solidify as primary Cu dendrites and grow progressively from this interface to the melted mark's surface to shape columnar dendrites in the preferred crystallographic direction, opposite the direction of heat flow. The constitutional oxygen atoms are rejected from dendrite tips into liquid during dendrite growth, producing richer oxygen solutions in

the form of eutectic composition solutions. When the temperature is less than the eutectic temperature of 1065 °C, the eutectic solution that is repelled by dendrite tips solidifies further to form a (Cu+Cu₂O) eutectic structure. Thus, the microstructure of melted marks on the copper wire after solidifying in the air and water has two phases of primary Cu dendrites and (Cu+Cu₂O) eutectic structure. However, the EDS mapping between two different cooling rates is illustrated in Fig. 2.9. The oxide particle is visible only the water-solidified sample, as shown in oxygen mapping. It was considered that Cu₂O particles were formed as the main precipitates during cooling to room temperature. Besides, it has been also reported that a higher cooling rate accelerates more precipitation process of Cu₂O precipitates¹⁴⁻¹⁷.

Although the microstructure constituents between the air-solidified specimen and the water-solidified sample are similar, dendrite arm spacing differs noticeably. The secondary dendrite arm spacing (SDAS) of the air and water-solidified specimens is 12.0 μm and 4.7 μm, respectively. Because of the faster cooling rate in water, the SDAS of the water-solidified specimen is smaller than that of the air-solidified specimen. In detail, when the cooling rate is rapid, the undercooling to a low temperature raises the number of nuclei. As a result, the nucleation rate predominates over the growth rate, resulting in a smaller SDAS in the water-solidified sample. Therefore, the difference in SDAS due to the cooling rate effect might have valuable in clarifying the fire behaviors after short-circuiting.

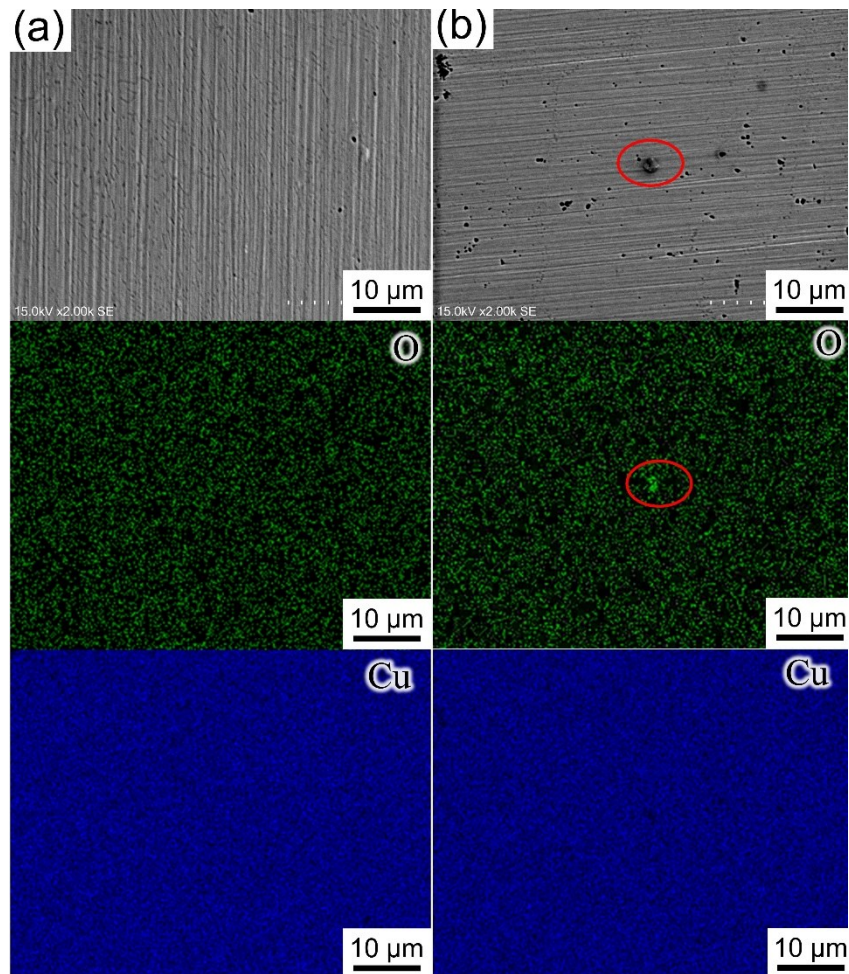


Fig. 2.9 EDS mapping of the melted mark solidified in (a) air (b) water

2.3.1.4 Oxygen concentration

According to the Cu-O phase diagram,^{13,18–20} when the oxygen content in the liquid phase of a Cu-Cu₂O binary alloy is 0.39 wt% or less, liquid copper is solidified prior, and solidification keeps going while raising the oxygen content in the liquid phase. When the remaining liquid phase's oxygen content reaches 0.39 wt%, the solidification process is finished, forming the eutectic structure. Therefore, the oxygen content in the Cu primary

dendrite part is 0.008 wt%, and the eutectic structure has 0.39 wt% oxygen.² Consequently, the oxygen concentration can be determined using the area ratio method using the following equation (2.2).

$$O(\text{wt}\%) = 0.39 \times (A - A_D) / A \quad (2.2)$$

Where O (wt%) is oxygen concentration in weight percent, A is total observed area, and A_D is area of copper dendrite.

The observed areas used to estimate the oxygen concentration are shown in Fig. 2.10. It comprises the Cu dendrites in the red parts and the eutectic structure in the dark parts. The area of the eutectic microstructure rises with the rising oxygen concentration.

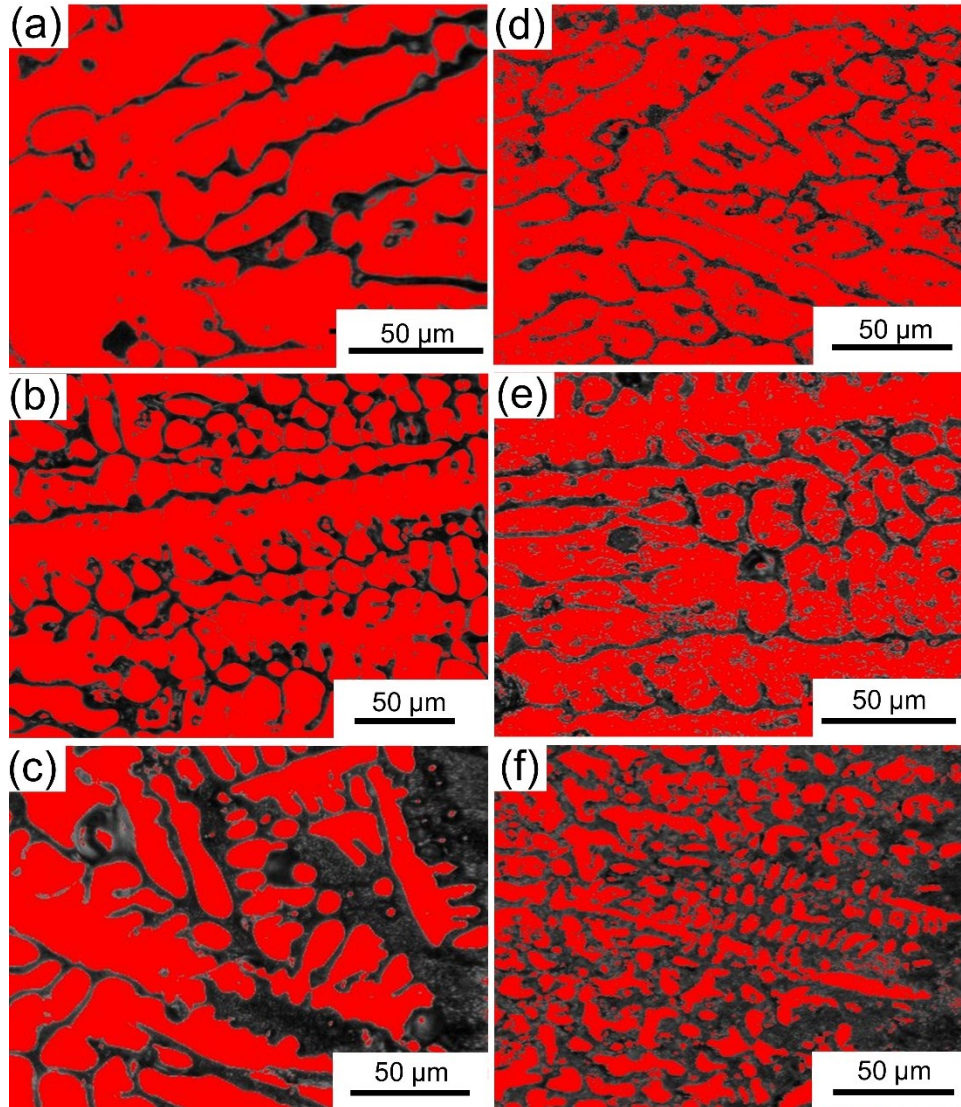


Fig. 2.10 Area ratio analysis of melted mark solidified in the air (a-c), and water (d-f) where (a,d) at close to non-melting region, (b,e) in the middle, and (c,f) at close to surface of melted mark

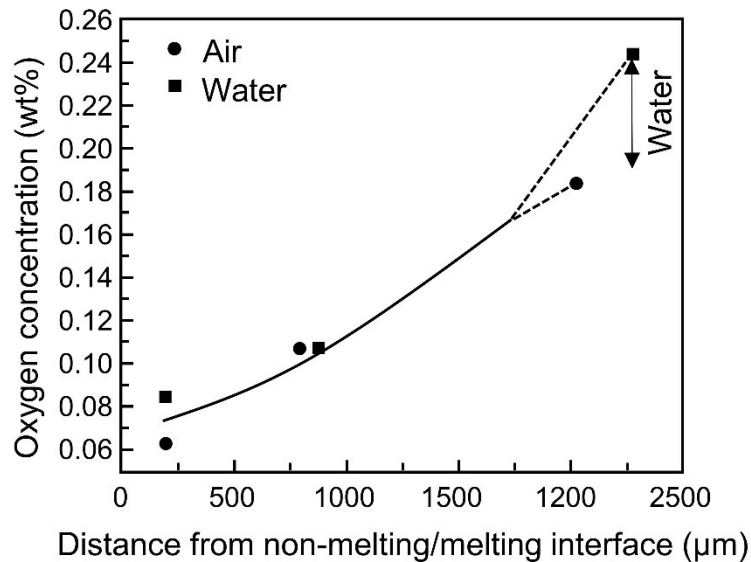


Fig 2.11. The plot of oxygen concentration versus distance to the surface of melted marks

As shown in Fig. 2.11, the oxygen content of both melted marks represents the highest content when distant from the non-melting/melting interface, which is located near the melted mark's surface and decreases with distance from the surface. During melting, it was believed that the liquid copper absorbed oxygen from the air. The oxygen content then reduced with increasing diffusion distance from the melted mark's surface.¹⁰ In addition, the change in oxygen content between air and water-solidified specimens is clearly visible near the surface and is nearly identical inside the melted mark. These could be caused by water because H₂O molecules are more easily broken up than O₂ molecules.¹¹ Another one, during the growth from the non-melting/melting interface to the surface of the melted mark, the constitutional oxygen is pushed progressively into the liquid from the dendrite tips. As a result, the region near the surface may have the highest oxygen content.⁵

In conclusion, the rapid cooling rate of the water solidified specimen results in the higher oxygen content especially at the surface. Therefore, the area ratio method for estimating oxygen concentration should be examined closer to the surface to recognize solidification and support fire investigators in interpreting the fire behaviors for fire investigation.

2.3.2 Cooling rate effect on microstructure formation of annealed melted marks

After solidifying in the air, heat treatment of melted marks on the copper wire was carried out at 1000 °C for 10 mins and cooled down with different cooling types (furnace, air, and water) to simulate the fire environment. These three samples were examined for the following characteristics: surface morphology, phase identification of oxide layer, crystallite size of oxide layer, and microstructure characterization.

2.3.2.1 Surface morphology

SEM was used to examine the surface morphology of melted marks for each cooling condition, as shown in Fig. 2.12. An almost wholly cracked oxide layer from the outer surface of the melted mark can be observed in the water-cooled sample, as revealed in Fig. 2.12(c).

In contrast, as shown in Figs. 2.12(a,b), furnace and air-cooled samples partially crack in the oxide layer. This can be referred to in terms of the difference in thermal expansion. Because of its high diffusivity and atomic mobility, the oxide layer is expected to grow strain-free during high-temperature heat treatment.¹² When the heat treatment is finished, the strain is established between the copper and copper oxide layer as the melted mark cooled down.

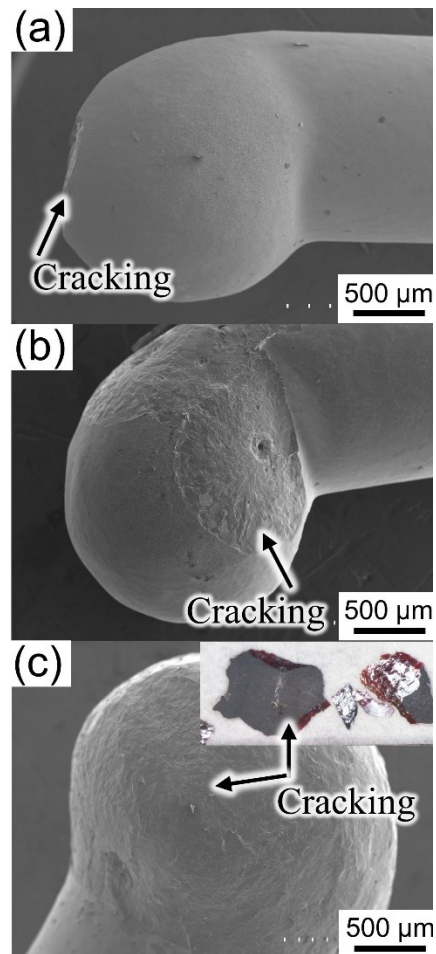


Fig. 2.12 SEM images of surface morphology of melted marks cooled in (a) furnace, (b) air, (c) water.

When the cooling rate of the water-cooled sample is speedy, the crystallites' ability to rearrange themselves cannot withstand the strain, raising the possibility of cracking the oxide layer and leaving the melted mark's outer surface.

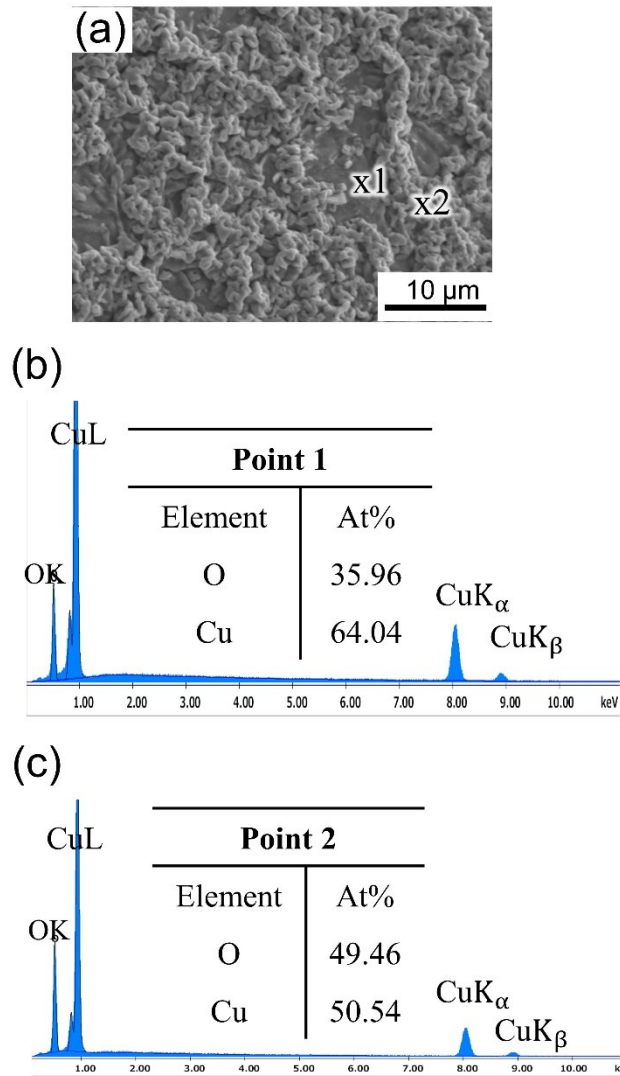


Fig 2.13. EDS results of surface morphology on melted marks cooled in the furnace

Because of a perfect oxide layer on the outer surface of melted mark cooled in the furnace, elemental analysis by EDS was performed into the oxide layer as illustrated in Fig. 2.13. The EDS spectrum on the dark depression of oxide grain at point 1 indicates the existence of copper and oxygen elements of 2:1, corresponding to the amount of copper and

oxygen in Cu₂O. In comparison, the amount of copper and oxygen at their grain boundary in the bright region (point 2) is close to the theoretical percentages of copper and oxygen elements in CuO. Therefore, the presence of Cu₂O at the inner surface covered by the CuO scale at grain boundary is the characteristic morphology of melted marks after heat treatment. Besides, phase identification of the oxide layer by XRD can be used to confirm the existence of the oxide layer, as discussed further below.

2.3.2.2 Phase identification of oxide layer

To confirm the existence of copper oxide phases, XRD analysis of copper oxide collected from the surface of the melted marks has been performed. The XRD patterns of melted marks cooled in the furnace, air and, water are illustrated in Fig. 2.14. The diffraction peaks centered at $2\theta = 29.42, 36.29, 42.16, 61.27, 73.40,$ and 77.27 degrees are attributed to the (110), (111), (200), (220), (311), and (220) reflection planes of Cu₂O, respectively. These peaks agree well with the Cu₂O powder from JCPDS file no. 00-002-1067, confirming the existence of Cu₂O for all cooling types.

The oxidation mechanism is explained by the fact that copper atoms interact with oxygen atoms to form Cu₂O, a reaction known as: $2\text{Cu} + \frac{1}{2} \text{O}_2 \rightarrow \text{Cu}_2\text{O}$.¹³ A high annealing temperature accelerates the diffusion of oxygen or copper into each other, the formation of Cu₂O is predominant, Cu₂O rapidly grows with an increase in layer thickness. There is a small amount of original Cu₂O that oxidizes to CuO via the reaction described below: $2\text{Cu}_2\text{O} + \text{O}_2 \rightarrow 4\text{CuO}$ ¹³ as demonstrated in SEM image of Figs. 2.13(a) and (c). Although, the EDS result represents the presence of CuO at grain boundary, it has not observed any XRD peaks

of CuO formation all samples. CuO growth on the Cu₂O layer is extremely limited because CuO has low atomic transport due to the lack of vacancies in CuO for quick atomic transport.¹⁴ As a result, a small amount of CuO in comparison to Cu₂O results in an undetectable amount of CuO by XRD.

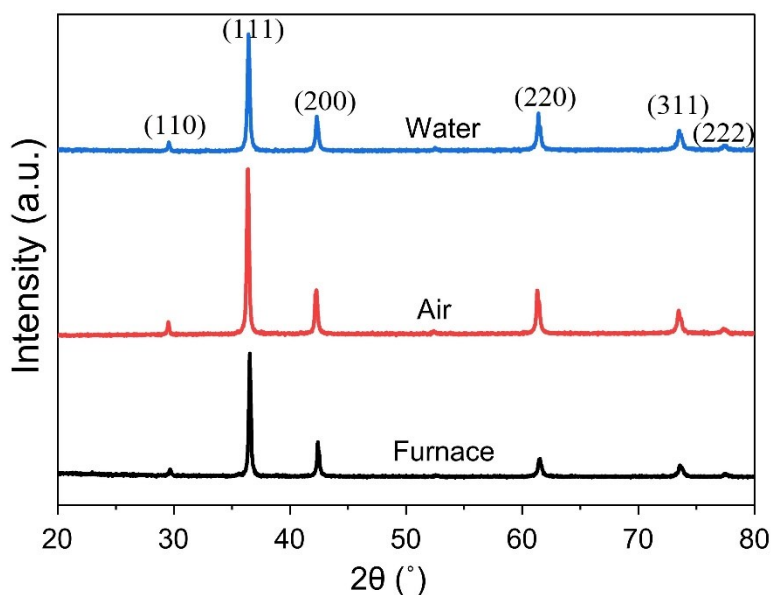


Fig. 2.14 XRD patterns of copper oxide on the melted mark of copper wire after heat treatment and cooling down with different cooling types

2.3.2.3 Crystallite size of oxide layer

Because only the Cu₂O phase can be discovered at the oxide layer covering the melted mark's surface for all cooling types, the difference in cooling rate may not affect phase transformation. However, the effect of the cooling rate on the crystallite size of Cu₂O was

still investigated. The determination of the crystallite size from the broadened peaks in the XRD patterns using the Debye-Scherrer formula in equation (2.3) is a convenient method.^{13,14}

$$D = 0.9\lambda / \beta \cos\theta \quad (2.3)$$

Where D is crystallite size of Cu_2O , λ is X-Ray wavelength of 0.1541 nm, β is Full width at half maximum (FWHM) and θ is the angle of diffraction.

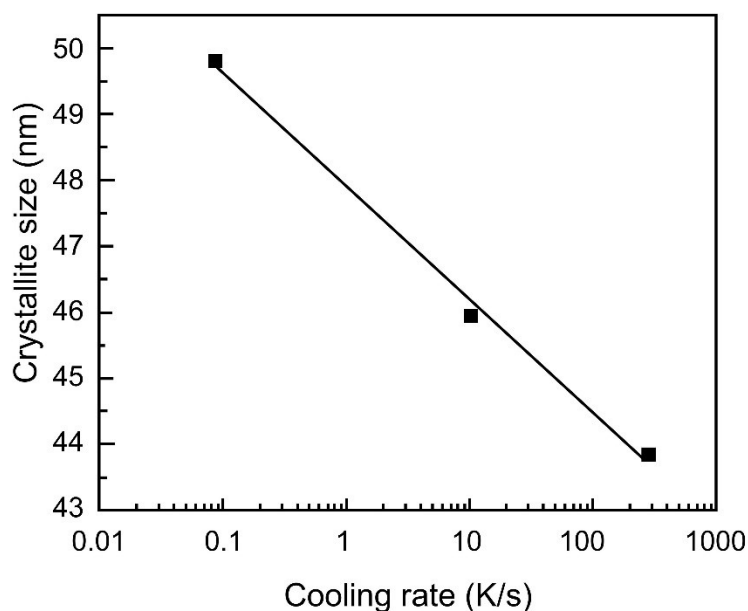


Fig. 2.15. The relationship between Cu_2O crystallite size and cooling rate

The Cu_2O crystallite sizes of all specimens were calculated from the broadened major peak centered at $2\theta = 36.29$. Fig. 2.15 depicts a logarithmic plot of cooling rate and Cu_2O crystallite size. After cooling in the furnace at a slow cooling rate, Cu_2O with a size of around 50 nm is achieved. As the cooling rate increases, the size of Cu_2O crystallites decreases rapidly to approximately 46 nm for air-cooling and 44 nm for water-cooling. From

the comparison of the Cu_2O crystallite size due to the effect of cooling on the melted mark after heat treatment, it was found that the cooling rate has a considerable impact on Cu_2O crystallite size. This indicates that the Cu_2O crystallite size forming on the melted mark's surface in the case of cooling in fire ambient may be larger than the Cu_2O size on the melted mark's surface cooled with a slower cooling rate, such as water.

2.3.2.4 Microstructure characterization

The longitudinal section of melted mark on copper wire after annealing then cooled in (a) furnace, (b) air, and (c) water are presented in Fig 2.16.

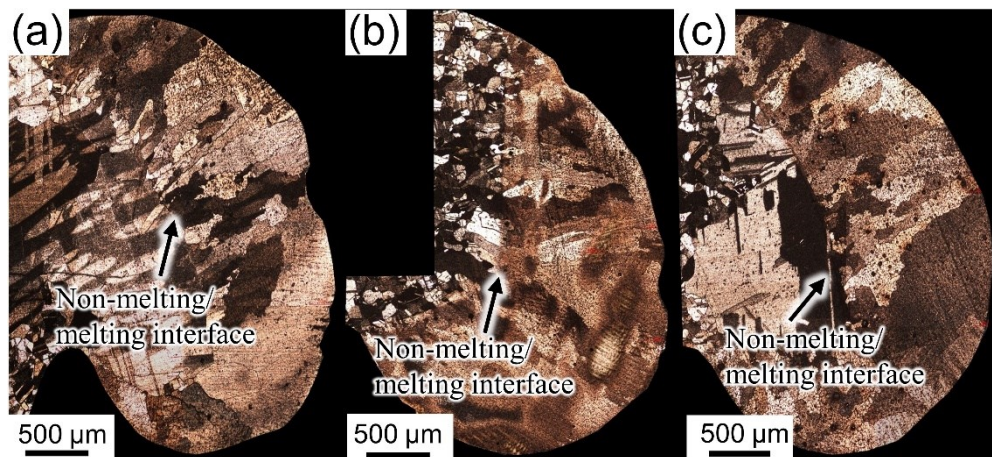


Fig. 2.16 The longitudinal section of melted mark on copper wire after annealing then cooled in (a) furnace, (b) air, and (c) water

The different cooling samples depict the structure of the non-melting zone, which differs from the melting zone by having a distinct boundary at non-melting/melting interface.

The structure in the non-melting region is an annealing twin because the original structure of copper is annealed. As well known, copper has a face center cubic structure; its structure can transform into the annealing twin structure after annealing.^{8,9,21} In comparison, the melting region has no dendrites. However, there are columnar grains arranged from the non-melting/melting interface to the melted mark's surface due to the heat transfer anti-parallel to the grain growth direction.

The optical microscope with a magnification of 200x was used to examine the microstructures of annealed samples. Fig. 2.17 demonstrates the microstructures of the melted marks (a) before annealing and (b) after annealing then cooled in furnace, (c) air, and (d) water. After annealing, there is clearly a substantial evolution in the microstructure. The microstructure prior to heat treatment consists of the following Cu dendrites in a bright part and the (Cu+Cu₂O) eutectic phase in the dark part (Fig. 2.17(a)), as explained in section 2.3.1.3. Dendrites vanish completely after heat treatment (Figs. 2.17(b-d)). Because Cu dendrites with high curvature must minimize their surface energy to achieve more thermodynamic stability, this is well known in the ripening phenomenon. The Cu dendrites are dissolved by the interdendritic liquid during heat treatment, and then they redistribute within a single grain.^{9,13,17,27,28} Simultaneously, the eutectic structure is transformed into Cu₂O particles that precipitate on the Cu matrix across the surface. EDS analysis on annealed sample was performed to determine the distribution of individual elements (Fig. 2.18). The EDS mapping shows that copper has a uniform distribution on the surface, while oxygen is concentrated at the black point. EDS identified the oxygen-richer point as the Cu₂O precipitate.

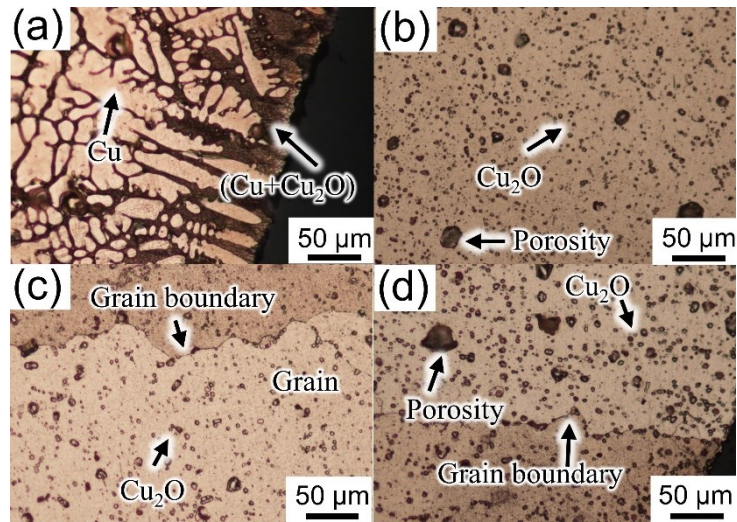


Fig. 2.17 The microstructures of melted marks: (a) before annealing, (b) after annealing then cooled in furnace, (c) air, and (d) water

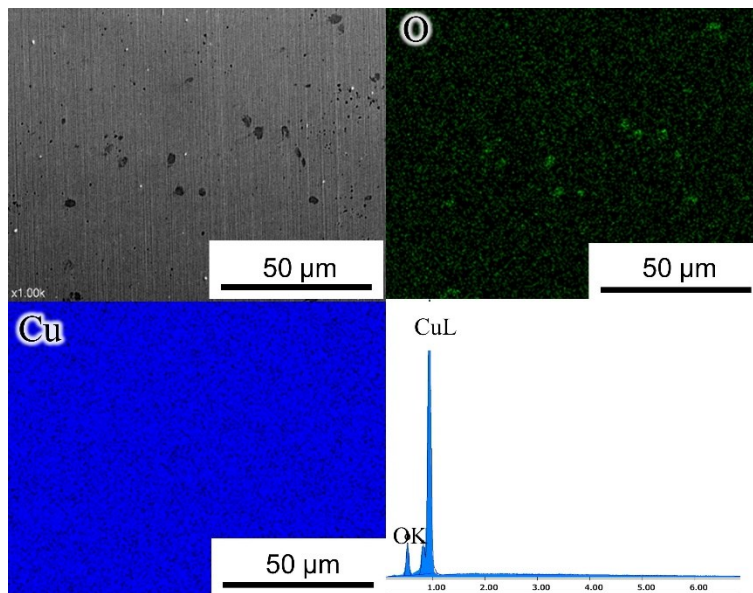


Fig. 2.18 EDS mapping of annealed sample

The microstructure of annealed specimens cooled down in the furnace, air, and water is not noticeably different. The majority of the constituents are Cu_2O particles precipitating on a copper matrix within a single grain, as seen in the tiny black spots (Figs. 2.17(b-d)). The grain boundary can also be obviously noticed. The large black points represent the gas porosities formed during the solidification process before annealing. The difference in color between the bright and dark regions of the air and water-cooled samples reflects the difference in crystal orientation for each grain. There are no dendrites observed in the microstructure after heat treatment of all samples. Even though the difference in cooling rates may not significantly impact the microstructure after annealing, as discussed in the previous section, it does affect oxide cracking and Cu_2O crystallite size. Moreover, the fading of dendrites is a specific feature of the annealed samples, suggesting that the melted mark on the copper wire was exposed to a fire for a particular time and temperature. Therefore, the appearance of Cu dendrites in the microstructure of melted mark on the copper wire may be used to explain the fire environment in the event of a fire.

In summary, the microstructures before heat treatment of melted mark on copper solidified in the air and water were illustrated in Fig. 2.19. Both different solidified samples have a $(\text{Cu}+\text{Cu}_2\text{O})$ eutectic structure, and Cu dendrites grow from the non-melting/melting interface as their significant characteristics. However, the water-solidified sample has smaller dendrite arm spacing and an oxygen-enriched area near the melted mark's surface.

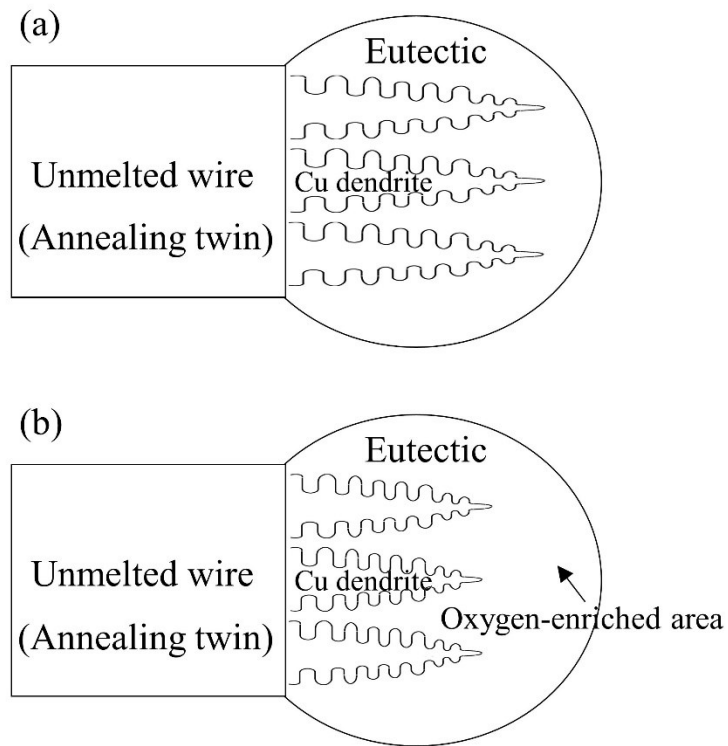


Fig. 2.19 Schematic diagram of the final microstructure of melted mark solidified in (a) air, and (b) water

In comparison, the microstructures of melted mark on copper after heat treatment at 1000 °C for 10 mins and cooled in the furnace, air, and water were shown in Fig. 2.20. All different cooled samples have no Cu dendrites, but columnar grains and Cu₂O precipitates exhibit in the microstructure as their typical features. A perfect oxide layer is found on the sample cooled in the furnace. It is damaged entirely due to the rapid cooling rate as the sample cooled in water.

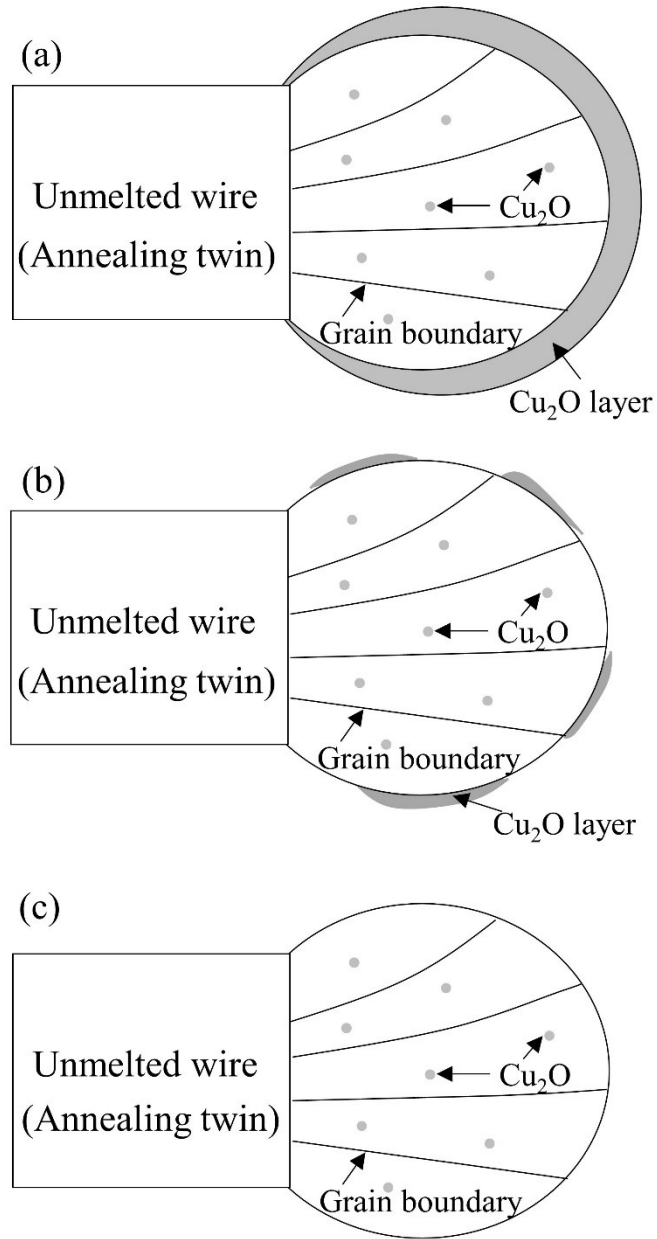


Fig. 2.20 Schematic diagram of the final microstructure of melted marks after annealing then cooled in (a) furnace, (b) air, and (c) water

2.4 Conclusions

The influence of solidification by air and water on the microstructure of the melted mark on the copper wire was examined before heat treatment. Both solidification microstructures were investigated for the following characteristics: dendrite growth, heat conduction, microstructure characterization, and oxygen concentration. The following results are achieved:

1. The cooling rate does not affect the dendrite growth for both cooling types due to the rapid heat transfer to the long wire. The direction of dendrite growth is from the non-melting/melting interface to the surface of the melted mark, and the microstructure comprises Cu dendrites and the (Cu+Cu₂O) eutectic structure.
2. The oxygen concentrations in air-solidified and water-solidified specimens differ significantly near the melted mark's surface. A higher oxygen concentration and smaller SDAS are found for a high cooling rate in the water-solidified sample.

After heat treatment at 1000 °C for 10 mins and cooled down with different cooling types (furnace, air, and water), the following characteristics were examined: surface morphology, phase identification of oxide layer, crystallite size of oxide layer, and microstructure characterization. The following outcomes are obtained:

1. The Cu₂O layer covered by the CuO scale is found on the outer surface of the melted mark, a rapid cooling rate in water causes oxide layer cracking, and the size of the Cu₂O crystallites is small.
2. The Cu dendrites on microstructure of all annealed samples disappear after annealing, and Cu₂O precipitates distribute over the copper matrix.

References

1. NFPA 921. *Guide for Fire and Explosion Investigations*. NFPA 921, 2017.
2. LEE EP, OHTANI H, SEKI T, et al. Study on discrimination between primary and secondary molten marks by DAS. *Bull Japan Assoc Fire Sci Eng* 2000; 50: 1–12.
3. Liu KH, Shih YH, Chen GJ, et al. Microstructural Study on Oxygen Permeated Arc Beads. *J Nanomater* 2015; 2015: 1–8.
4. Di M, Zhang M, Qi ZB, et al. Study of analyzing characteristic of composition on the surface of copper conductor melted marks. *Procedia Eng* 2011; 11: 68–74.
5. Scott DA. *Metallography and Microstructure of Ancient and Historic Metals*. Tien Wah Press, Ltd., 1991.
6. Rawdon HS, Lorentz MG. METALLOGRAPHIC ETCHING REAGENTS FOR COPPER. 16: 641–668.
7. Oetzow G. *Metallographic Etching*. 2nd ed. ASM International, 1999.
8. Wei MM, Mo SJ, Liang D, et al. The experiment on melted mark formed by copper wire in electrical fire and the analytic researcher on the feature parameters of metallographic structure. *Procedia Eng* 2011; 11: 504–513.
9. Collini L. *Copper Alloys - Early Applications and Current Performance - Enhancing Processes*. 2012. Epub ahead of print 2012. DOI: 10.5772/1912.
10. Jasim HR, Mohamad M, Fayyadh MM, et al. Numerical Analysis of Mass Transfer in MHD Nanoparticle Based Crude Oil Flow on a Flat Plate under Various Slip Condition. *J Phys Conf Ser*; 1366. Epub ahead of print 2019. DOI: 10.1088/1742-6596/1366/1/012042.

11. Michael Ashby, Hugh Shercliff, David Cebon. *Materials Engineering, Science, Processing and Design*. 1st ed. Elsevier Ltd., 2007.
12. William D. Callister J, Rethwisch DG. *Fundamentals of Materials Science and Engineering*. John Wiley & Sons, Inc., 2012.
13. Association CD. *Equilibrium Diagrams Selected copper alloy diagrams illustrating the major types of phase transformation*, www.cda.org.uk (1992).
14. Wan Y, Chen WQ, Wu SJ. Effect of cooling rate on the microstructure and precipitates of directional solidified 50W600 non-oriented silicon steel. *High Temp Mater Process* 2013; 32: 597–603.
15. Ritasalo R, Cura ME, Liu XW, et al. Microstructural and mechanical characteristics of Cu-Cu₂O composites compacted with pulsed electric current sintering and hot isostatic pressing. *Compos Part A Appl Sci Manuf* 2013; 45: 61–69.
16. Qin S, Bendo A, Tsuchiya T, et al. Effect of cooling rate on precipitation during homogenization cooling in balanced AlMg₂Si alloy. *Mater Trans* 2020; 61: 2115–2120.
17. Fu J, Du W, Jia L, et al. Cooling rate controlled basal precipitates and age hardening response of solid-soluted Mg–Gd–Er–Zn–Zr alloy. *J Magnes Alloy* 2021; 9: 1261–1271.
18. Neumann JP, Zhong T, Chang YA. The Cu-O (Copper-Oxygen) system. *Bull Alloy Phase Diagrams* 1984; 5: 136–140.
19. Schramm L, Behr G, Löser W, et al. Thermodynamic reassessment of the Cu-O phase diagram. *J Phase Equilibria Diffus* 2005; 26: 605–612.

20. Kehl GL. *Metallurgy and Metallurgical Engineering Series*. 3rd ed. McGraw Hill, 1949.
21. Babrauskas V. Arc beads from fires: Can ‘cause’ beads be distinguished from ‘victim’ beads by physical or chemical testing? *J Fire Prot Eng* 2004; 14: 125–147.
22. Wang JP, Cho WD. Oxidation behavior of pure copper in oxygen and/or water vapor at intermediate temperature. *ISIJ Int* 2009; 49: 1926–1931.
23. Roberts J. *Synthesis and characterisation of nanoscale oxides for energy applications*. University of Liverpool, 2014.
24. Raship NA, Sahdan MZ, Adriyanto F, et al. Effect of Annealing Temperature on the Properties of Copper Oxide Films Prepared by Dip Coating Technique. *AIP Conf Proc*; 1788. Epub ahead of print 3 January 2017. DOI: 10.1063/1.4968374.
25. Park JH, Natesan K. Oxidation of copper and electronic transport in copper oxides. *Oxid Met* 1993; 39: 411–435.
26. Suśniak M, Pałka P, Karwan-Baczewska J. Influence of milling time on the crystallite size of AlSi5Cu2/SiC composite powder. *Arch Metall Mater* 2016; 61: 977–980.
27. Scherzer O. X-Ray Diffraction Studies of Copper Nanopowder. *Zeitschrift für Phys* 1936; 101: 593–603.
28. Kurz W, Fisher DJ. *Fundamentals of Solidification*. 3rd ed. TRANS TECH PUBLICATIONS, 1989.
29. Rapp RA. The High Temperature Oxidation of Metals Forming Cation-Diffusing Scales. *Metall Trans A* 1984; 15: 765–782.

30. Flemings MC. Coarsening in solidification processing. *Mater Trans* 2005; 46: 895–900.

Chapter 3 Investigation of microstructure and oxide formations under various annealing temperatures and times on the melted mark of copper wire

3.1 Introduction

Generally, copper has two major types of oxide: cuprous oxide (Cu_2O , cuprite) and cupric oxide (CuO , tenorite). When copper is oxidized in oxygen or air at high temperatures, multiphase scales such as Cu_2O and CuO form.^{1,2} In particular, the oxide on the melted mark's surface of copper wire from short-circuiting formed in the fire ambient during fire accidents is important to describe the fire behaviors. This scientific explanation provides significant evidence that substantially impacts the reliability of fire judgments. However, the fire investigation from the oxide and microstructure of melted marks on the copper wire has received little attention. Thus, this study investigated the oxide layer and microstructure of the melted mark on copper annealed at different temperatures and times.

3.1.1 Presence of CuO

The copper oxidation in air and oxygen at temperatures between 350 °C and 1000 °C was studied by Park and Natesan.¹ CuO whiskers develop on the oxide surface at temperatures below 750 °C. It was considered that condensation/evaporation, chemical-vapor transport, and short-circuit diffusion at the whisker tips were proposed as mechanisms for whisker growth. A single-phase scale of pure Cu_2O forms when the reaction occurs at an oxygen pressure lower than the dissociation pressure of CuO . When there is an increase in

oxygen pressure greater than the dissociation pressure of CuO, a thin layer of CuO nucleates on the scale surface.¹

The presence of CuO whiskers at temperatures below 750 °C also was supported by Wang et al.³ They investigated the oxidation of pure copper in oxygen with or without water vapor at an intermediate temperature range of 500 °C to 700 °C. It was concluded that CuO whiskers were well developed and covered most of the outer oxide surface at 500 °C, whereas fewer whiskers were observed at 600 °C and almost disappeared at 700 °C. It was discovered that whiskers grown in oxygen with water vapor were longer and thinner than whiskers grown in dried oxygen, implying that water vapor may have a tendency to produce whisker growth. Moreover, it has been reported CuO whiskers develop at the tip of the whiskers due to the breakdown of oxidant molecules and the further adsorption of oxygen on the tip of the whiskers. Because H₂O molecules are easier to break up than O₂ molecules. As a result, the growth of whiskers may be accelerated in water-containing environments.³

A change in Gibbs free energy is the driving force of the oxidation process at that temperature. The Gibbs free energy (ΔG) for a chemical reaction is defined by a change in enthalpy (ΔH), entropy (ΔS), and absolute temperature (T) as follows:

$$\Delta G = \Delta H - T\Delta S \quad (3.1)$$

When the absolute temperature T increases result in a decrease in ΔG . The reaction can occur spontaneously only when the value of free energy (ΔG) becomes negative. Therefore, the formation of oxide Cu₂O at room temperature during exposure of the copper to air indicates that the value of G is negative for Cu₂O formation. However, the oxidation process is mainly

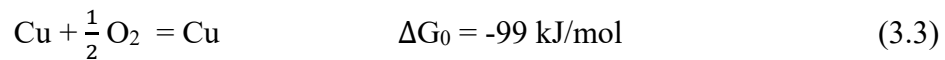
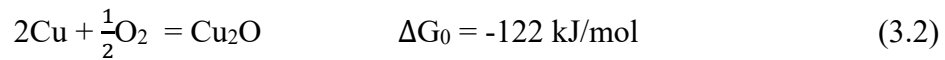
inhibited by the kinetics of oxygen diffusion through the oxide layer. As the temperature rises, thermal energy helps to overcome the diffusion barrier, allowing oxidation to proceed. Whereas the cupric oxide CuO phase begins to appear only above 320 °C reported by Choudhary *et al.*² There was no trace of CuO formation below 320 °C, even after a long oxidation period (20 hours) because diffusion kinetics play no role here. Hence, it is expected that at lower temperatures, the ΔG value becomes positive in the case of CuO formation but changes to a negative when the temperature is greater than 320 °C, allowing it to overcome the chemical reaction barrier.² Raship *et al.*⁴ also claimed that CuO phase can be observed at 450 °C annealing temperature.

According to Zhu *et al.*⁵, the CuO scale is protective, and there should be no vacancies in CuO for fast atomic transport in the temperature range of 600 °C to 1050 °C. As a result, lattice diffusion in CuO should be more difficult. For copper oxidation, the CuO scale formed on Cu₂O layer grows extremely slowly compared to the Cu₂O scale and then almost maintains a constant thickness for long periods of time.⁵

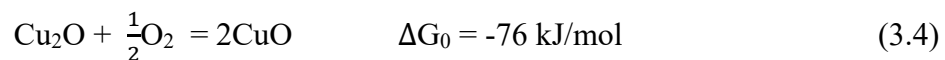
Thus, from the above literature reviews regarding the presence of CuO can be summarized that CuO phase nucleated on Cu₂O can be found at the temperature range about 320 °C to 450 °C, whereas CuO whiskers are observed at 500 °C to 750 °C. However, the limiting temperature for CuO removal from the Cu₂O layer was determined to be 1041 °C. reported by Musa *et al.*⁶

3.1.2 Presence of Cu₂O

The Cu–O phase diagram contains both CuO and Cu₂O phases which may form during oxidation.^{7–10} From thermodynamic, when the ambient oxygen partial pressure (P_{O_2}) is higher than the dissociation pressure (P_{O_2-dis}) of the oxide in equilibrium, oxides form as in following reactions.^{11,12}



Where G_0 is the Gibbs free energy change of the reaction at 400 °C. From the Gibbs free energy values, Cu₂O is probably formed initially. Further oxidation on the surface of the Cu₂O particles is possible and can be explained as



Thus, a thin layer of CuO is then form on the Cu₂O layer.^{11,12}

The copper oxidation can occur via outward diffusion of copper ions along copper vacancies in the oxide scale because the Cu vacancies are major defects in the Cu₂O. The Cu₂O grows predominantly due to the transport of Cu²⁺ ions through the cation vacant sites. While atomic transport in CuO is very slow because CuO does not have vacancies available for the fast transport of atoms.^{1,3,5}

Choudhary *et al.*² presented that at room temperature, the spontaneous formation of a very thin oxide layer on a copper is quite visible when it is exposed to air. Following that, the oxide layer becomes a barrier to further oxidation of the copper, limiting oxygen molecule diffusion through it. As a result, further oxidation of the copper at room temperature is prevented. Nevertheless, at around 150 °C, thermal energy begins to overcome the diffusion barrier, allowing further oxidation of the copper to begin. However, a well-ordered crystalline phase of Cu₂O is only noticed above 200 °C.²

The influence of annealing temperature on copper oxide films was investigated by Raship *et al.*⁴ The results found that the Cu₂O phase can be obtained at 200 °C annealing temperature. Films annealed at 300 °C had a combination phase of CuO and Cu₂O phases, while the CuO phase can be observed at an annealing temperature of 450 °C.

3.1.3 Activation energy

Several studies on the oxidation of copper at various temperatures have been conducted. A typical Arrhenius plot of the parabolic oxidation rate constants (k_p), as calculated from mass gain data gives the activation energy for the double-layer formation (Cu₂O + CuO). The activation energies reported by various researchers differ considerably, as represented in table 3.1.

Table 3.1 Activation energy of copper oxidation reported in the literatures

Reference	Type of copper	Conditions	Oxidation rate law	Temperature Range (°C)	Activation energies (kJ/mol)	Diffusion process
Park and Natesan ¹	99.999%	(1 atm O ₂ or air)	Parabolic	750 to 1040 450 to 750 350 to 450	172 84 223	Lattice Grain boundary+Whisker Whisker+surface
Zhu et al. ¹³	99.99% to >99.9999%	350 °C - 1050 °C 0.1 MPa	Parabolic	900 to 1050 600 to 850 350 to 500	98* 173 93 to 111 40 to 52	Lattice Lattice+Grain boundary Grain boundary
Sartell and Li ¹⁴	99.999%	1 atm O ₂	-	660 to 937	179	-
Valensi ¹⁵	OFHC	1 atm O ₂	-	300 to 550 550 to 900	84 158	- -
Tylecote ¹⁶	OFHC	Air	-	300 to 500 600 to 900	39 123	- -
Wang et al ³	99.99%	1 atm O ₂	Parabolic	500 to 700	90.67	Lattice

*For single layer of Cu₂O

Park and Natesan¹ proposed that the temperature dependence of the oxidation rates can be divided into three different processes for the oxidation of copper: lattice diffusion, grain boundary diffusion, and surface diffusion with whisker growth; these happen at high, intermediate, and low temperatures, respectively. The oxidation kinetic followed the parabolic rate law for all processes.

At high temperatures, the large size of Cu₂O grain grows predominantly. The calculated activation energy from the slope of the plot between log k_p and the reciprocal temperature was 172 kJ/mol. This double-layer (Cu₂O + CuO) formation was implied to rate-determining step for the lattice diffusion in Cu₂O. The activation energy at high temperatures range of 173 kJ/mol reported by Zhu et al.¹³ also is consistent with Park and Natesan. For the single-layer formation of Cu₂O, the activation governed by lattice diffusion was only 98 kJ/mol. The difference in activation energy of 75 kJ/mol governed by lattice diffusion between the double and single-layer formations supports a $(P_{O_2})^{1/4}$ -dependence of the parabolic rate constant related to the diffusion of neutral copper vacancies in Cu₂O.^{13,17}

At intermediate temperatures, a decrease in temperature occurs. The Cu₂O scale is still dominant, it obeys the parabolic rate law. The reduction in activation energy is most likely due to the contribution of grain boundary diffusion, which is the significant decrease in the Cu₂O grain mean size. The activation energy values of 84 kJ/mol at 450 °C to 750 °C from Park and Natesan¹, and 93 to 111 kJ/mol at 600 °C to 850 °C from Zhu et al.¹³ might contribute from grain boundary diffusion + whisker, and the lattice diffusion + grain boundary diffusion, respectively. Grain-boundary transport or a short-circuiting process

produces activation energy of 84 kJ/mol, and some tiny whiskers nucleate on the oxide surface.

At low temperatures, whisker formation on the surface was the rate-limiting process, and surface diffusion was responsible for this temperature range, with Park and Natesan¹ reporting a high activation energy of 223 kJ/mol. On the other hand, the calculated activation energy by Zhu et al.¹³ is significantly difference. Only 40 kJ/mol to 52 kJ/mol is the contribution from grain boundary diffusion. Moreover, Lee et al.¹² informed that diffusion along the boundaries of the Cu₂O grains was responsible for the oxidation at a temperature below 300 °C. However, the oxidation of copper at low temperature and the reasons for a change in activation energy with decreasing temperature remains unclear.

To summarize, the Cu₂O scale grows predominantly by lattice diffusion over the entire temperature range of 300 °C to 1050 °C, and the rate-determining step is implied to be the outward diffusion of copper atoms in Cu₂O. The lattice diffusion controls the copper oxidation at high temperatures. The contribution of grain boundary diffusion to copper oxidation is mainly identified at intermediate temperatures, and either surface diffusion with whisker growth or lattice diffusion. At low temperatures, copper oxidation is contributed from surface diffusion with whisker growth or grain boundary diffusion.

Furthermore, the effect of impurity on copper oxidation was investigated by Zhu et al.¹³ The high-temperature range of lattice diffusion is wider for high purity copper. However, the impurities seem not to affect high-temperature copper oxidation. The copper oxidation is enhanced in the intermediate temperature range because trace impurities impede the lateral

growth of Cu_2O grains, allowing grain boundary diffusion. The higher activation energy at low temperatures for lower-purity copper should be because grain boundary diffusion is impeded at low temperature by impurities segregated at grain boundaries.

3.1.4 Objective of the study

Because of the variety of fire behaviors discovered in the fire event,¹⁸ the evolution of the microstructure and oxide layer on the melted mark of copper wire in various fire environments is important in fire investigation. In particular, the effect of annealing temperature and annealing time on the microstructure and oxide layer of the melted mark on the copper wire after heat treatment has not been extensively researched. Therefore, this study investigated the microstructure and typical oxide layer of PMM after annealing at different annealing temperatures and times.

3.2 Materials and methods

The commercial single core copper wires (99.95 wt% Cu) of 25 mm in length and 2.6 mm in diameter have been used in the experiment. Because the short-circuiting occurs at the point where the PVC insulated copper wire is damaged, the PVC insulation was peeled off prior to simulating short-circuiting. An arc welding machine was used to imitate the short-circuiting on the tip of copper wire with rapid melting and sudden solidifying in the air (Fig. 3.1). The “melted mark” on copper wire obtained after melting by the arc welding machine.

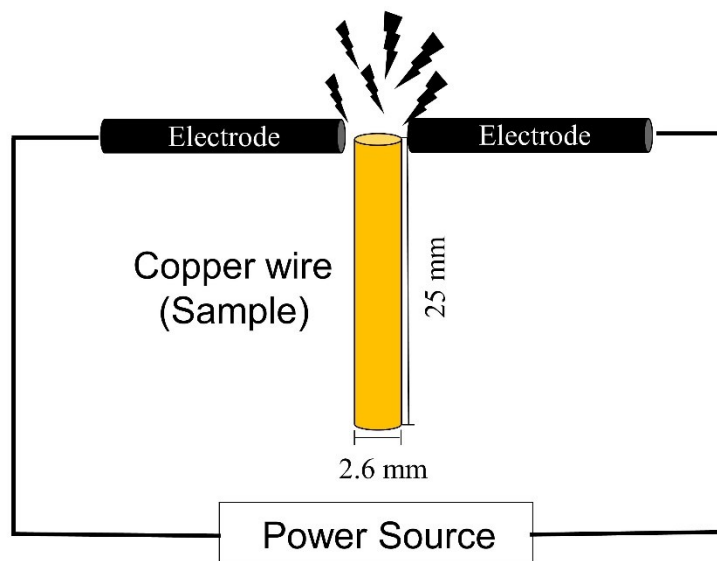


Fig. 3.1 Schematic diagram for copper wire melting by arc welding machine

In order to simulate the fire ambient, the melted mark on copper wire was annealed in the furnace under various heat treatment parameters as shown in table 3.2 and cooled down in the furnace to room temperature.

Table 3.2 Heat treatment conditions on melted mark of copper wire

Temperature (°C)	Annealing time			
	0 min	20 mins	60 mins	120 mins
1000	0 min	20 mins	60 mins	120 mins
800	0 hr	1 hr	2 hrs	4 hrs
600	0 hr	1 hr	2 hrs	4 hrs
400	0 hr	2 hrs	4 hrs	8 hrs
220	0 hr	2 hrs	4 hrs	8 hrs

All unannealed specimens were mounted with conductive resin (Technovit) and longitudinal cut to observe the microstructure in the longitudinal section. Then, they were ground with sandpaper from #500 to #4000 and further mirror-polished by a diamond paste of 0.1 μm . The alcohol was used to clean the samples in an ultrasonic bath after grinding and polishing. Previous to using an optical microscope to examine the microstructures, all samples were further etched for a few minutes with a solution of 10 g FeCl_3 , 30 ml HCl , and 120 ml distilled water.¹⁹⁻²¹

The surface morphology and chemical composition of all specimens were examined by Scanning electron microscope (SEM) of HITACHI SU3500 attached Energy dispersive X-ray spectroscopy (EDS).

The phase identification of the oxide layer on melted mark was conducted by X-ray diffraction (XRD) of Rigaku, RINT-2100 under 40kV/4mA and $\text{CuK}\alpha$ radiation at 0.1540

nm wavelength. Data was collected in the range 2θ of 20 to 80 degrees with 0.02 degree steps.

3.3 Results and discussions

The results and discussions in this chapter are divided into four main sections, including temperature dependence, change in oxide layer thickness, calculation of activation energy, and observations on microstructure characterization.

3.3.1 Temperature dependence

The melted marks generated by arc welding machine and annealed in the furnace at 400 °C, 600 °C, 800 °C, 1000 °C for 2 hours were examined temperature dependence for the following characteristics: evolution of surface morphology, phase transformation of oxide layer, and temperature effect on Cu₂O crystallite size.

3.3.1.1 Evolution of surface morphology

At first, the influence of the annealing temperature on the evolution of the surface morphology of the melted mark on the copper wire was studied. The surface micrographs of melted marks on copper wire annealed at temperatures of (a) 1000 °C, (b) 800 °C, (c) 600 °C, and (d) 400 °C for two hours were taken by SEM, as illustrated in Fig.3.2.

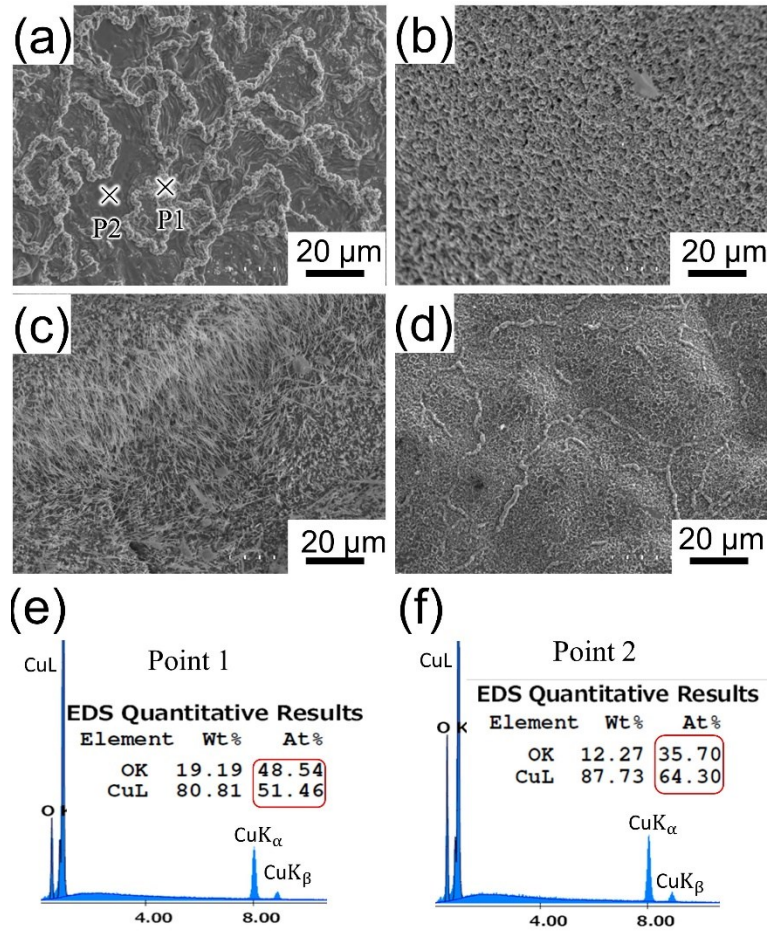


Fig. 3.2 Oxide evolution on melted mark of copper wire at annealing temperature of (a) 1000 °C (b) 800 °C (c) 600 °C (d) 400 °C. (e) and (f) show EDS spectrum of (a)

At 1000 °C, the dark depression can be observed inside grains surrounded by strong boundaries at their grain boundaries with a bright tone. Both inside grain (point1) and grain boundary (point2) were elementally analyzed by EDS (Fig. 3.2(e) and (f)). The amount of copper and oxygen elements at a ratio of 1:1 was identified by EDS as shown in the EDS quantitative results of point 1, matching the quantity of copper and oxygen in CuO. Meanwhile, in the grains themselves (point 2), the copper and oxygen concentrations at the grain boundary are equivalent to the percentages of copper and oxygen in Cu₂O. As a result, the characteristic surface morphology of melted marks after annealing at 1000 °C is the Cu₂O grains encompassed by the CuO at the grain boundary.

At 800 °C, there is a smaller oxide grain size than 1000 °C, along with a uniform covering of the CuO scale on the Cu₂O layer at the outer surface.

At 600 °C, the presence of Cu₂O at the inner oxide (point 2) and CuO whiskers (point 1) randomly formed on the Cu₂O surface were indicated by the EDS, as revealed in Fig. 3.3. It has been published that CuO whiskers form on Cu₂O and grow primarily by surface diffusion caused by the breakup of adsorbed oxygen, which is attributed to the presence of water vapor.⁵⁻⁹

At 400 °C, the surface is not flat with slightly covered by CuO and whiskers cannot observe at this temperature.

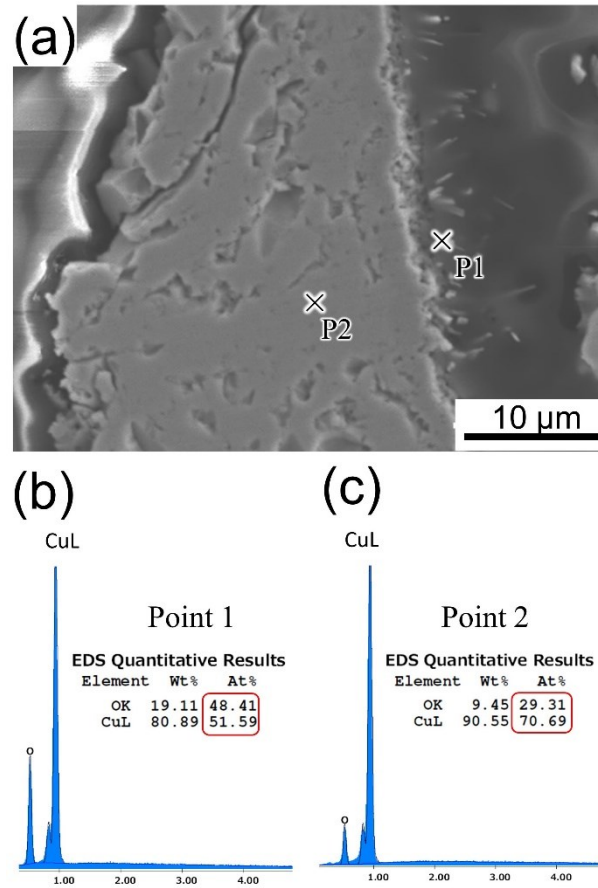


Fig. 3.3 Analysis of element on the surface of melted mark annealed at 600 °C (a).

(b) and (c) are the EDS spectrums at point 1 and 2, respectively.

The above results can be described in the following profound way. The surface of the melted mark annealed at 1000 °C exhibits the larger oxide grain because there is sufficient diffusion activation energy to transport atoms at a high temperature; the crystal lattices are occupied by the transported atoms and encourage the small grains by grain boundary diffusion, which is caused in larger grains.⁴ The CuO whiskers form at random on the Cu₂O

layer for the melted mark annealed at 600 °C. The surface diffusion through the overgrowth at their tips from screw dislocation arising on the metal surface due to the breaking of the absorbed oxygen was identified as the development of whiskers on Cu₂O.¹

It can be seen that the surface morphology of copper oxide on the melted mark of copper wire evolved with distinct characteristics depending on the annealing temperature. Therefore, each typical morphology under different annealing temperatures is expected to assist in clarifying fire behaviors and determining the origin of the fire accident.

In addition, the phase transformation of copper oxide on the melted mark of copper wire was identified by XRD to confirm the presence of the copper oxides, as discussed further below.

3.3.1.2 Phase transformation of oxide layer

To confirm the existence of copper oxide phases, XRD analysis of copper oxide collected from the surface of the melted marks has been performed. The XRD patterns of melted marks annealed in the furnace at 1000 °C, 800 °C, 600 °C, and 400 °C for 2 hours are illustrated in Fig. 3.4. The diffraction peaks centered at $2\theta = 29.42, 36.29, 42.16, 61.27, 73.40,$ and 77.27 degrees are attributed to the (110), (111), (200), (220), (311), and (220) reflection planes of Cu₂O, respectively. These peaks agree well with the Cu₂O powder from JCPDS file no. 00-002-1067, confirming the existence of Cu₂O for all heat treatment temperatures.

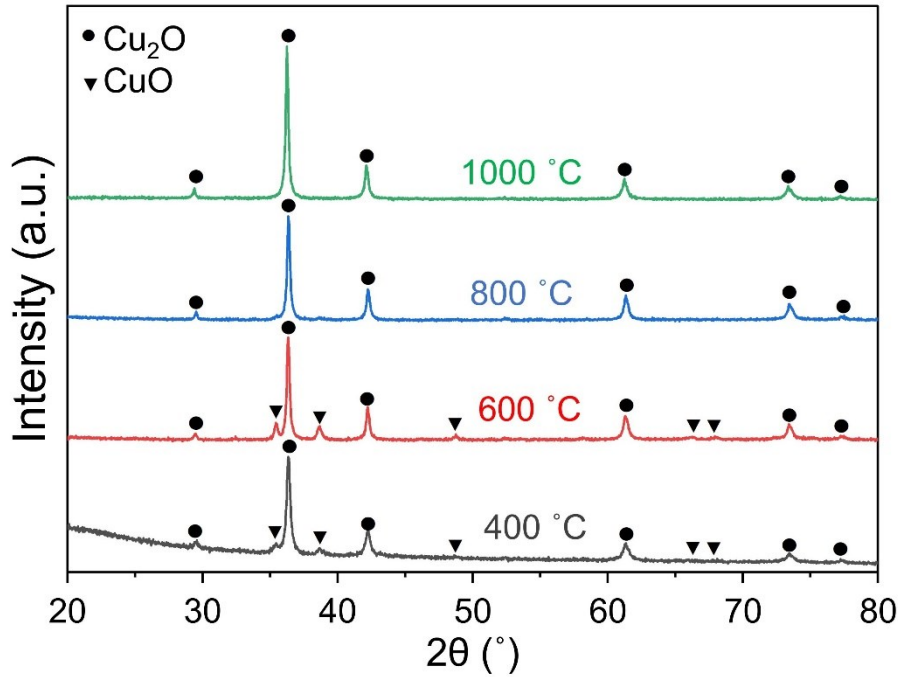


Fig. 3.4 XRD patterns of copper oxide on melted mark of copper wire annealed at different temperatures for 2 hrs.

The oxidation mechanism is explained by the fact that copper atoms interact with oxygen atoms to form Cu_2O , a reaction known as: $2\text{Cu} + \frac{1}{2} \text{O}_2 \rightarrow \text{Cu}_2\text{O}$.⁴ A high annealing temperature accelerates the diffusion of oxygen or copper into each other, the formation of Cu_2O is predominant, Cu_2O rapidly grows with an increase in layer thickness.

At low temperatures of 400 °C and 600 °C, the additional peaks centered at $2\theta = 35.44, 38.58, 48.74, 58.21, 66.36,$ and 68.08 degrees start to appear. These diffraction peak positions can be attributed to (002), (111), (-202), (202), (022), and (113) CuO planes (JCPDS file no. 00-002-1040) which indicating the existence of of CuO. Because there is a

small amount of original Cu_2O that oxidizes to CuO via the reaction: $2\text{Cu}_2\text{O} + \text{O}_2 \rightarrow 4\text{CuO}$.⁴ On the other hand, at high temperature of 1000 °C, CuO growth on the Cu_2O layer is extremely limited because CuO has low atomic transport due to the lack of vacancies in CuO for quick atomic transport.¹ Accordingly, a small amount of CuO in comparison to Cu_2O results in an unnoticeable amount of CuO by XRD. As annealing temperature decreases to 800 °C, CuO phase begins to occur and the XRD pattern shows an additional small peak at $2\theta = 35.44$ and 38.58 which agree well with (002) and (111) planes of CuO , respectively because of the small original Cu_2O oxidizing into CuO due to instability at this temperature.

According to the XRD patterns at 600 °C and 400 °C, a mixture of Cu_2O and CuO phases were discovered on the oxide surface of the melted marks. Because of the low temperature, the Cu_2O is not completely oxidized; it becomes unstable and eventually oxidizes into the CuO phase.^{10,11}

In summary, the oxide layer on the melted mark of copper after heat treatment at 1000 °C and 800 °C predominantly consists of the Cu_2O phase. In contrast, a mixture of Cu_2O and few amounts of CuO phase appear at annealing temperatures of 600 °C and 400 °C.

3.3.1.3 Temperature effect on Cu₂O crystallite size

Moreover, the crystallite size of Cu₂O can be estimated from the broadened peaks in the XRD patterns by using the Debye-Scherrer formula: ^{1,4,24}

$$D = 0.9\lambda / \beta \cos\theta \quad (3.5)$$

Here, D is crystallite diameter dimension, λ is X-Ray wavelength (0.1541 nm), β is FWHM (Full width at half maximum) and θ is the diffraction angle. The broadened major peak located at $2\theta = 36.29$ was used to determine the crystallite sizes of all samples.

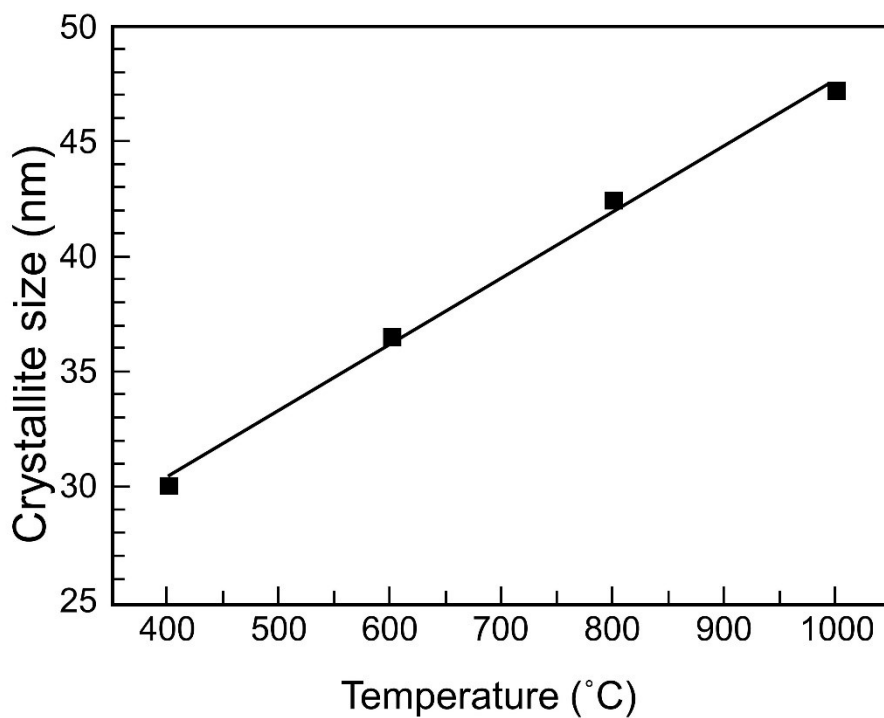


Fig. 3.5 The relationship between Cu₂O crystallite size and annealing temperature

The relationship between Cu₂O crystallite size and annealing temperature is depicted in Fig. 3.5. There is an increase in Cu₂O crystallite from 30 nm to 47 nm at heat treatment temperatures between 400 °C to 1000 °C. As the temperature increases, the plane of atoms is distanced, resulting in the Cu₂O crystallite being formed larger. It can be seen that the determination of the Cu₂O crystallite size from the broadened peaks in the XRD patterns using the Debye-Scherrer formula might help fire investigators evaluate the fire temperature during a fire accident to find the source of the fire.

3.3.2 Change in oxide layer thickness

The thickness of the copper oxide layer was measured on the melted mark's surface after heat treatment at different times and temperatures, as shown in Fig. 3.6. As discussed previously, CuO is slightly nucleated on the Cu₂O layer and thus cannot be seen after mounting and polishing with an optical microscope. Hence, the measurement of the CuO thickness for each sample is impossible, while the Cu₂O layer is obviously visible on the copper melted mark. Accordingly, Cu₂O layers were determined on the melted mark's surface for all annealing conditions.

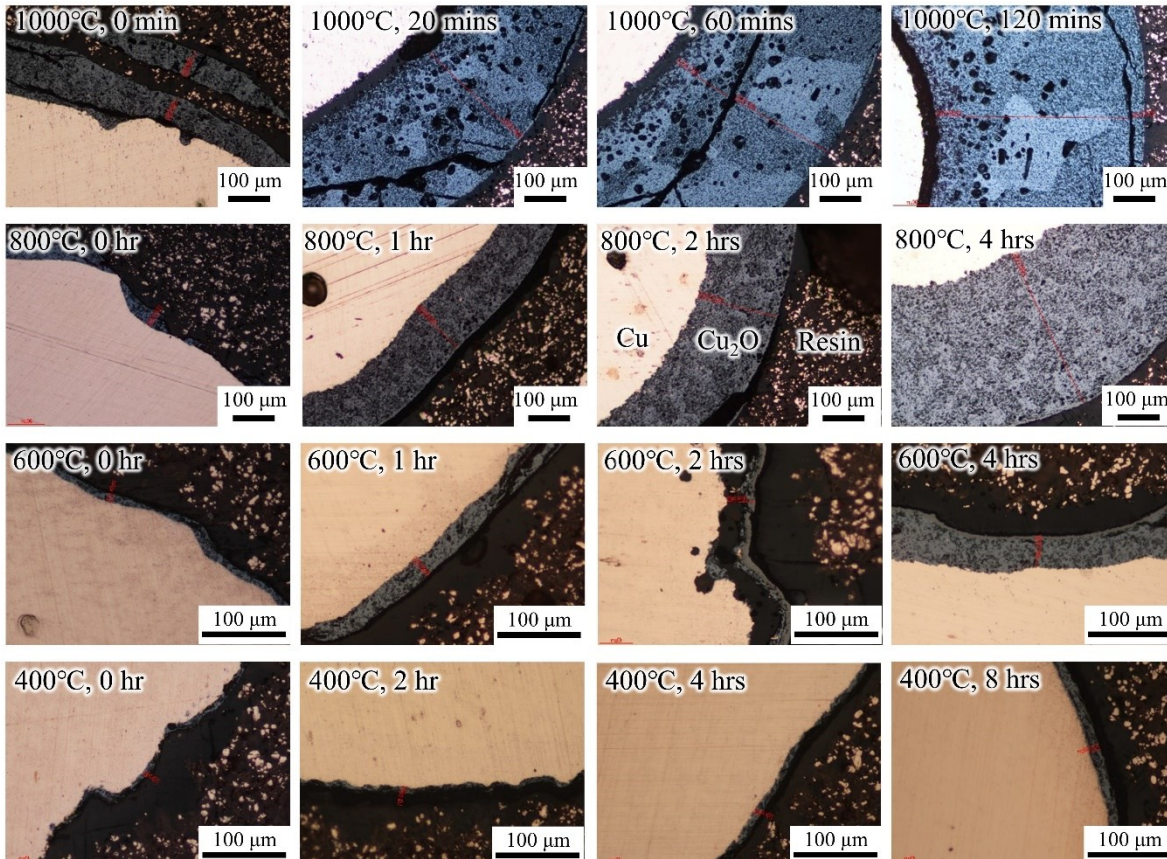


Fig. 3.6 The Cu_2O layer thickness at various annealing times and temperatures

The plot of Cu_2O layer thickness and annealing time at various annealing temperatures is displayed in Fig. 3.7. At low temperatures of 220°C and 400°C , the Cu_2O thickness almost remains unchanged at around $8.8\ \mu\text{m}$ with annealing time, whereas at 600°C , the thickness moderately increases.

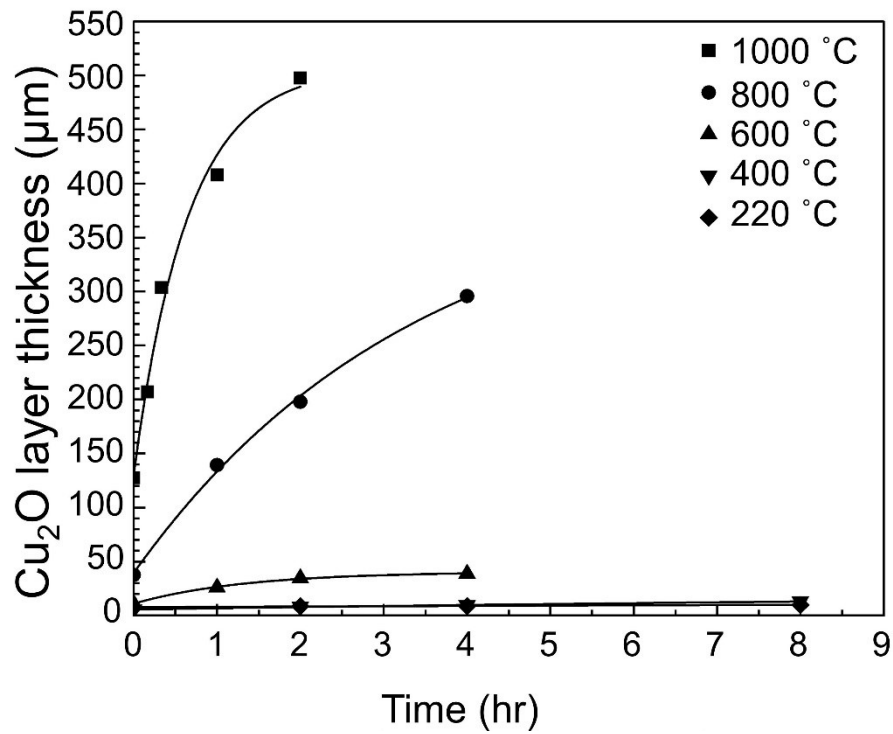


Fig. 3.7 The plot of Cu_2O layer thickness and annealing time

At high temperatures of 800°C and 1000°C , there is a substantial change. The thickness increases rapidly in an early phase of oxidation and then slowly in a later phase. The diffusion-controlling process can be used to describe this phenomenon. At the early phase of oxidation, the oxide layer is extremely thin. Accordingly, the required time for either outward copper diffusion or inward oxygen diffusion is much shorter than the

required timeframe for the chemical reaction that produces Cu_2O . As a result, a faster growth rate in the Cu_2O is expected to be a reaction-limited growth regime in this early phase. As the oxide Cu_2O layer becomes thickened, the diffusion timeframe through the thick oxide layer outpaces the reaction timeframe. Hence, the rate of oxidation slows down and is predicted to be a diffusion-limited growth regime at the later phase.²

Besides, the annealing temperature represents a greater influence than the annealing time. An increase in annealing temperature mainly increases the Cu_2O thickness; there is a rapid increase in Cu_2O thickness with temperature. At 220 °C and 400 °C, the Cu_2O layer is extremely thin because the formation of Cu_2O is limited due to the low temperature. Then, Cu_2O gradually grows and slowly oxidizes into CuO . At intermediate temperatures, the Cu_2O thickness rises, and either copper or oxygen cannot easily diffuse to react with each other at the copper/oxygen interface. Then, Cu_2O turns unstable and fully oxidizes into CuO , as indicated in SEM and XRD results. At 1000 °C, the Cu_2O grows predominantly due to stability in thermodynamics and rarely oxidizes into CuO .²

Additionally, the linear relationships are obtained from the plot of the Cu_2O thickness and the square root of annealing time, as shown in Fig. 3.8, indicating that a diffusional process controls the oxidations at 1000 °C, 800 °C, 600 °C, 400 °C, and 220 °C.¹² Furthermore, Cu_2O growth from 220 °C to 1000 °C follows the parabolic rate law, which agrees with the finding of Zhu et al.¹³

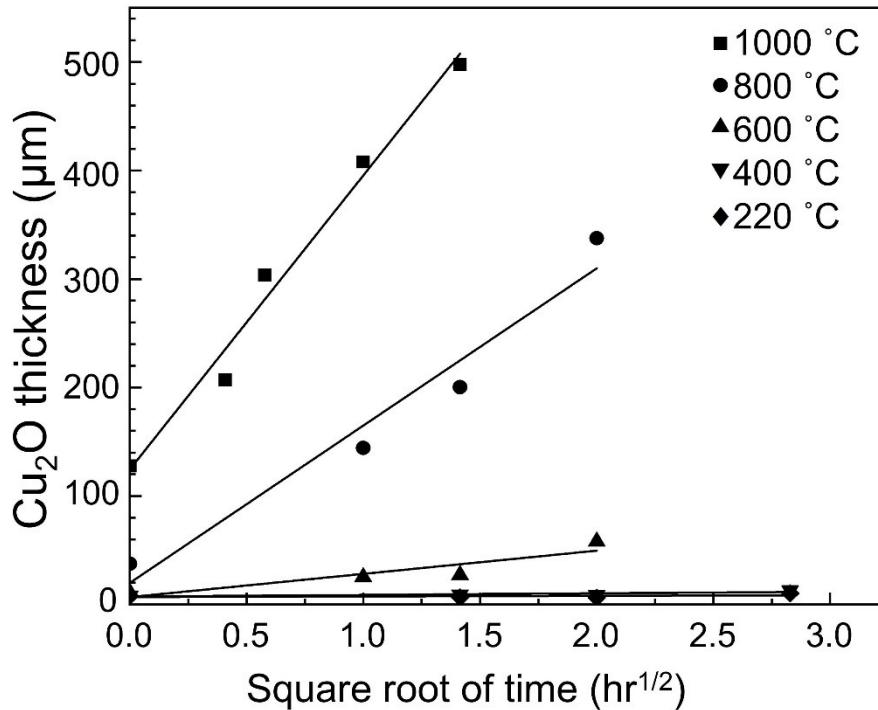


Fig. 3.8 The variation of Cu₂O layer thickness with the square root of annealing time at different temperatures

The slope of the parabolic plot can be used to calculate the parabolic rate constant (k_p) or diffusion rate constant. The calculated parabolic rate constant values are 20.4 $\mu\text{m}^2/\text{s}$, 5.8 $\mu\text{m}^2/\text{s}$, 0.13 $\mu\text{m}^2/\text{s}$, $6.12 \times 10^{-4} \mu\text{m}^2/\text{s}$, and $1 \times 10^{-4} \mu\text{m}^2/\text{s}$ at 1000 °C, 800 °C, 600 °C, 400 °C, and 220 °C, respectively. The ability of the oxygen and copper atoms to diffuse through the copper oxide layer and meet each other is controlled by these rates. Because it takes more time for the copper and oxygen atoms to migrate through as the thickness increases, the oxidation rate is controlled by the diffusion rate. Besides that, the parabolic rate constant at 220 °C is equivalent to a rate of $1 \times 10^{-4} \mu\text{m}^2/\text{s}$, as published by Lee et al.¹² Therefore, a

significant change in Cu₂O layer thickness of melted marks on the copper wire is expected to describe fire behaviors in order to identify the origin of the fire accident.

3.3.3 Calculation of activation energy

As described previously, increased Cu₂O thickness and oxidation rate are mainly caused by increasing the annealing temperature. Consequently, the calculated parabolic rate constant (k_p) must be adjustable for temperature influences to explain the oxidation mechanism. Accordingly, the influence of annealing temperature on the parabolic rate constant may reasonably be described by the Arrhenius expression in equation (3.6)²⁵

$$k_p = Ae^{-\left(\frac{Q}{RT}\right)} \quad (3.6)$$

Where, k_p is parabolic rate constant (um²/s), Q is the activation energy (J), T is temperature (K), R is the gas constant (8.314 J/mol K), and A is pre-exponential constant (um²/s).

Arrhenius plot of the parabolic rate constants from 220 °C to 1000 °C for copper oxidation in the air is presented in Fig. 3.9. The plot is roughly classified into two zones: a high-temperature zone (400 °C to 1000 °C), and a low-temperature zone (220 °C to 400 °C). The activation energy can be calculated from the slope of log k_p vs. reciprocal-temperature plot. From the calculation, the activation energy of 127 kJ is gained at high-temperature range. At low-temperature range, the calculated activation energy is 28 kJ. Surprisingly, the temperature dependence closely resembles the outcomes presented in the literature.^{5,7-9} At temperatures ranging from 600 °C to 900 °C and 300 °C to 500 °C, Tylecote¹⁶ reported Q values of 123 kJ and 39 kJ, respectively. According to the correspondence of the oxidation

activation energy with other literature, it might be claimed that diffusion in the Cu_2O over a wide temperature range is the rate-determining step which is implied as to the movement of copper atoms outward in Cu_2O .^{1,13,26}

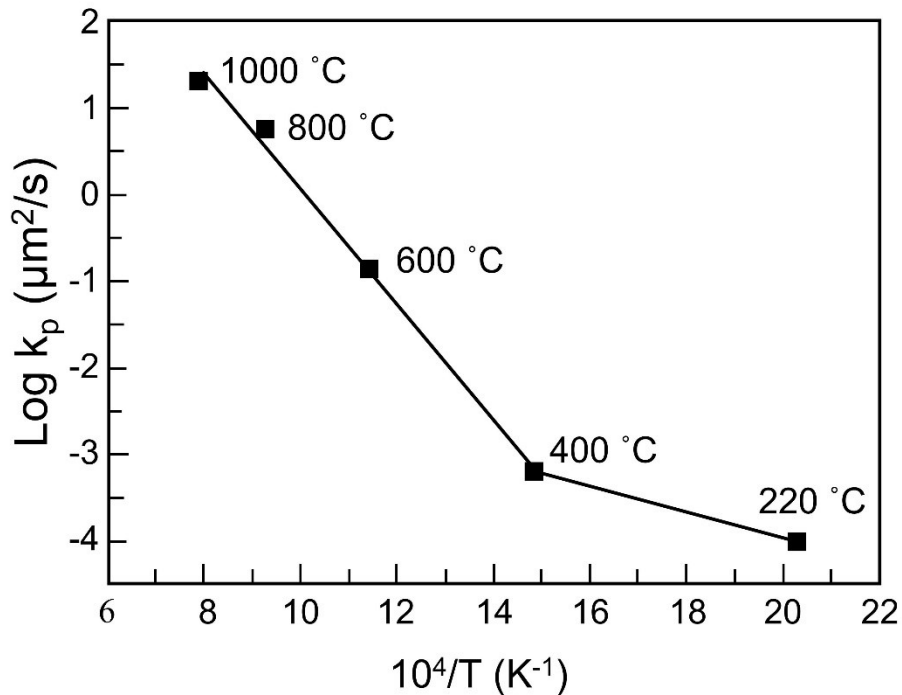


Fig. 3.9 Arrhenius plot of the logarithmic parabolic rate constants from 220 °C to 1000 °C for copper oxidation in the air.

For further understanding, the diffusion rates of the lattice, grain boundary, and the surface are classified by the diffusion coefficients accompanying activation energy Q_l , Q_{gb} , and Q_s , where $Q_l > Q_{gb} > Q_s$.²⁷ It was believed that lattice diffusion might contribute to the oxidation of Cu_2O over the broader temperature range of 400 °C to 1000 °C because of higher activation energy. In contrast, copper oxidation at a low-temperature range between 220 °C and 400 °C may result from grain boundary diffusion due to lower activation energy.^{1,13}

Additionally, surface diffusion has lower activation energy than lattice diffusion, so growth related to screw dislocation might result in whisker growth by surface diffusion at 600 °C. Alternatively, the development of lateral lattice diffusion is enhanced as the temperature rises, and oxide growth produces flatter morphologies such as pyramids.²⁷

3.3.4 Observation on microstructure characterization

The microstructure characterization of melted marks on copper wire after annealing under various annealing temperatures and times are demonstrated in Fig. 3.10. It can be clearly seen that the microstructures evolve from low to high temperatures. At low temperatures (400 °C to 600 °C), a dendritic structure can be observed, but it gradually fades at high temperatures of 800 °C and 1000 °C. The mechanism behind this microstructural evolution is discussed following. As the melted mark was rapidly melted by arc welding machine and suddenly solidified in the atmosphere before heat treatment. During solidification, when the temperature of liquid copper is less than the melting point of 1083 °C, copper atoms nucleate at the interface between the non-melting and melting zones on copper wire. Then, they grow from the interface to surface of the melted mark to form copper dendrites. At the same time, oxygen atoms are pushed away from dendrite tips to liquid, creating oxygen richer solutions that eventually form eutectic composition solutions. Then, the eutectic composition solution rejected by dendrite tips solidifies into a (Cu+Cu₂O) eutectic structure when the temperature falls below the eutectic temperature (1065 °C). Therefore, the final microstructure of melted mark on copper wire before heat treatment comprises copper dendrites surrounded by (Cu+Cu₂O) eutectic structure.^{8,9,7}

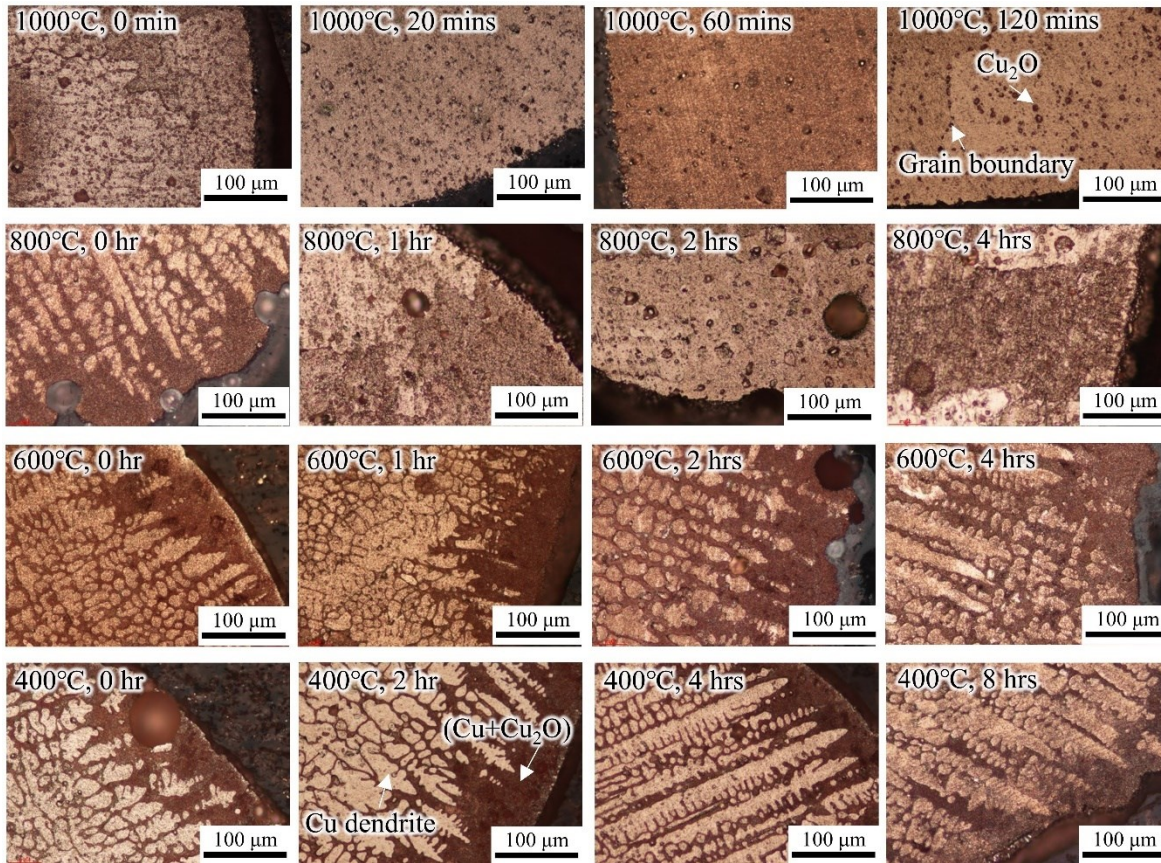


Fig. 3.10 Microstructure characterization of melted marks on copper wire after annealing under various heat treatment conditions

After annealing at 400°C with various annealing times, the microstructure remains similar to the microstructure before heat treatment, in which Cu dendrites and (Cu+Cu₂O) eutectic can be observed at all annealing times. Regardless, the darker tone on the Cu dendrites begins to occur after heat treatment at 4 and 8 hours. It was believed that small Cu₂O particles start to precipitate on the Cu dendrites for a longer period during the annealing process. After increasing the annealing temperature to 600°C, the Cu dendrites are still noticeable for all annealing times, but Cu₂O is more precipitated on the Cu dendrites. Interestingly, the Cu dendrites fade away after annealing at 800 °C for more than one hour and at 1000 °C for all annealing times. It can still observe the Cu dendrites for an unannealed microstructure at 800 °C because the annealing time is insufficient to dissolve the Cu dendrites completely, but they disappear after.

After annealing at high temperature, Cu dendrites fade away entirely due to Cu dendrites with high curvature must minimize their surface energy to achieve more thermodynamic stability, this is well known in the ripening phenomenon. The Cu dendrites are dissolved by the interdendritic liquid during heat treatment, and then they redistribute within a single grain.²⁸⁻³¹ Simultaneously, the eutectic structure is transformed into Cu₂O particles that precipitate on the Cu matrix across the surface. Moreover, the grain boundary can also be obviously noticed. The different colors split by the grain boundary on the microstructure after annealing, such as at 1000 °C, 120 minutes, reflect the difference in crystal orientation for each grain.

Consequently, the final microstructure of melted mark annealed at 800 °C to 1000 °C is the columnar grain structure with Cu_2O precipitates.

To summarize, Cu dendrites surrounded by (Cu+ Cu_2O) eutectic structure under both Cu_2O and CuO is the characteristic microstructure of the melted mark on the copper wire after annealing at 400 °C to 600 °C, as demonstrated in Fig. 3.11(a). The fingerprint feature of the melted mark after heat treatment at 800 °C to 1000 °C is columnar grain structure with Cu_2O precipitates and no dendrites beneath Cu_2O layer (Fig. 3.11(b)).

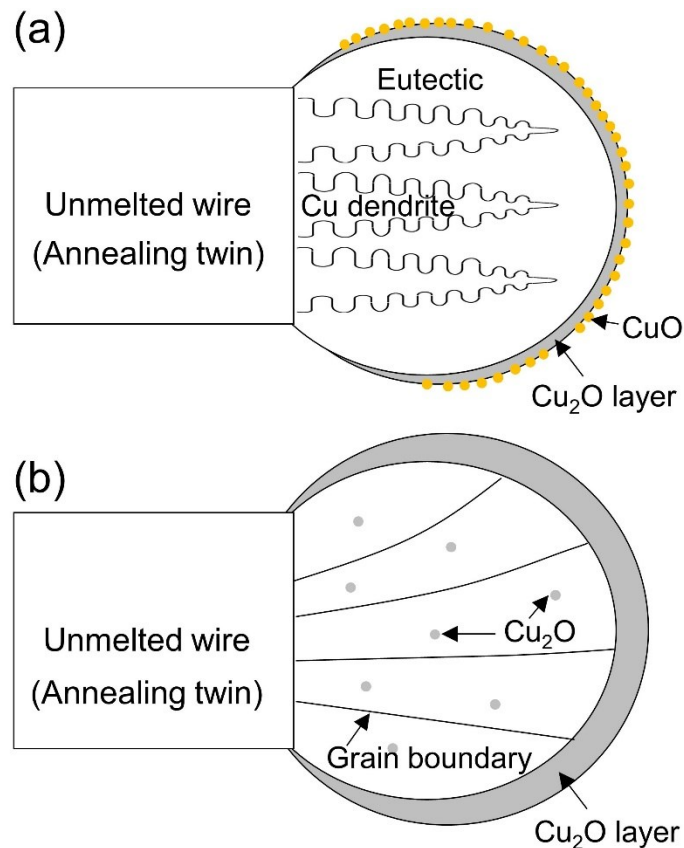


Fig. 3.11 The final microstructure of melted mark on copper wire after heat treatment at (a) 400 °C to 600 °C and (b) 800 °C to 1000 °C.

As a result, the copper oxide and microstructural evolution at various annealing conditions may be used to explain the fire behaviours. It is a fact that the PMM should be in more prolonged fire surroundings as well as have a higher fire temperature than other melted marks due to its being created before a fire. Therefore, the last structure should be similar to the microstructure of the high heat treatment temperature: a grain structure with Cu_2O precipitates and no dendrites beneath Cu_2O layer. However, the copper oxide and microstructural evolution on the melted mark of copper wire at different heat treatment conditions are inadequate to discriminate PMM from other melted marks. This is because the melted mark at high temperatures may be caused by the most fuels in the most damaged area.

3.4 Conclusions

The effect of annealing temperatures and times on the copper oxide and microstructural evolution of the melted mark on the copper wire was examined for the following characteristics: temperature dependence, change in oxide layer thickness, calculation of activation energy, and observations on microstructure characterization. The following results are achieved:

1. The surface morphology evolves with the annealing temperature. At 1000 °C, the large Cu₂O grains are encircled by the slight CuO scale at their grain boundary and reduce in grain size at 800 °C, while at 600 °C, the CuO whiskers are formed.
2. A mixture of Cu₂O and CuO phases is found at 400 °C and 600 °C, whereas only the Cu₂O phase is discovered at 800°C and 1000°C.
3. The thickness of the Cu₂O layer becomes thicker by increasing annealing temperature and time, which follows the parabolic rate law. The diffusion processes accountable for Cu₂O growth are lattice diffusion at 220 °C to 400 °C and grain boundary diffusion at 400 °C to 1000 °C.
4. The microstructure of melted mark annealed at 400 °C and 600 °C is a dendritic structure, while at 800 °C to 1000 °C is a columnar grain structure with Cu₂O precipitates.

References

1. Park JH, Natesan K. Oxidation of copper and electronic transport in copper oxides. *Oxid Met* 1993; 39: 411–435.
2. Choudhary S, Sarma JVN, Pande S, et al. Oxidation mechanism of thin Cu films : A gateway towards the formation of single oxide phase. *AIP Adv*; 055114. Epub ahead of print 2018. DOI: 10.1063/1.5028407.
3. Wang JP, Cho WD. Oxidation behavior of pure copper in oxygen and/or water vapor at intermediate temperature. *ISIJ Int* 2009; 49: 1926–1931.
4. Raship NA, Sahdan MZ, Adriyanto F, et al. Effect of Annealing Temperature on the Properties of Copper Oxide Films Prepared by Dip Coating Technique. *AIP Conf Proc*; 1788. Epub ahead of print 3 January 2017. DOI: 10.1063/1.4968374.
5. Zhu Y, Mimura K, Isshiki M. Oxidation mechanism of Cu₂O to CuO at 600-1050 °C. *Oxid Met* 2004; 62: 207–222.
6. Musa AO, Akomolafe T, Carter MJ. Production of cuprous oxide, a solar cell material, by thermal oxidation and a study of its physical and electrical properties. *Sol Energy Mater Sol Cells* 1998; 51: 305–316.
7. Association CD. *Equilibrium Diagrams Selected copper alloy diagrams illustrating the major types of phase transformation*, www.cda.org.uk (1992).
8. Neumann JP, Zhong T, Chang YA. The Cu-O (Copper-Oxygen) system. *Bull Alloy Phase Diagrams* 1984; 5: 136–140.

9. Schramm L, Behr G, Löser W, et al. Thermodynamic reassessment of the Cu-O phase diagram. *J Phase Equilibria Diffus* 2005; 26: 605–612.
10. Kehl GL. *Metallurgy and Metallurgical Engineering Series*. 3rd ed. McGraw Hill, 1949.
11. Xu CH, Woo CH, Shi SQ. The effects of oxidative environments on the synthesis of CuO nanowires on Cu substrates. *Superlattices Microstruct* 2004; 36: 31–38.
12. Lee SK, Hsu HC, Tuan WH. Oxidation behavior of copper at a temperature below 300°C and the methodology for passivation. *Mater Res* 2016; 19: 51–56.
13. Zhu Y, Mimura K, Lim J-W, et al. Brief Review of Oxidation Kinetics of Copper at 350 °C to 1050 °C. *Metall Mater Trans A* 2006; 37A: 1231–1237.
14. Sartell JA, Li CH. The oxidation of high-purity copper-nickel alloys. *Trans Am Soc Met* 1962; 55: 158–168.
15. Valensi G. Pittsburgh International Conference on Surface Reactions. 1948; 156–159.
16. Tylecote RF. The oxidation of copper at 350°C – 900°C in air. *J Inst Met* 1950; 78: 327–350.
17. Shuyonfu. *Influence of purity on copper oxidation*. Tohoku University, 2002.
18. Wang Y, Su X. Study on pores distribution laws in secondary short circuited melted beads of copper wires. *Procedia Eng* 2014; 84: 887–892.

19. Di M, Zhang M, Qi ZB, et al. Study of analyzing characteristic of composition on the surface of copper conductor melted marks. *Procedia Eng* 2011; 11: 68–74.
20. Rawdon HS, Lorentz MG. METALLOGRAPHIC ETCHING REAGENTS FOR COPPER. 16: 641–668.
21. Scott DA. *Metallography and Microstructure of Ancient and Historic Metals*. Tien Wah Press, Ltd., 1991.
22. Zhu Y, Mimura K, Isshiki M. Oxidation mechanism of copper at 623-1073 K. *Mater Trans* 2002; 43: 2173–2176.
23. S.J.Mo, L.Wang CQ. Research on oxidation characteristics of electrical contact melted mark in short circuited fire. *An indian J* 2014; 10: 407–412.
24. Caballero-Briones F, Palacios-Padrós A, Calzadilla O, et al. Evidence and analysis of parallel growth mechanisms in Cu₂O films prepared by Cu anodization. *Electrochim Acta* 2010; 55: 4353–4358.
25. Michael Ashby, Hugh Shercliff, David Cebon. *Materials Engineering, Science, Processing and Design*. 1st ed. Elsevier Ltd., 2007.
26. Bridges DW, Baur JP, Baur G, et al. Oxidation of Copper to Cu₂O and CuO (600°–1000°C and 0.026–20.4 atm Oxygen). *J Electrochem Soc* 1956; 103: 475–478.
27. Raynaud GM, Rapp RA. In Situ Observation of Whiskers, Pyramids and Pits During the High-Temperature Oxidation of Metals. *Oxid Met*; 21.

28. Flemings MC. Coarsening in solidification processing. *Mater Trans* 2005; 46: 895–900.
29. Rappaz JAD and M. *Solidification*. 2nd ed. EPFL Press,
http://solidification.mechanical.illinois.edu/Figures/chap13/Fig_13_17.pdf (2016).
30. Glicksman ME, Voorhees PW. Ostwald Ripening and Relaxation in Dendritic Structures. *Metall Trans A, Phys Metall Mater Sci* 1984; 15 A: 995–1001.
31. Rappaz M, Grasso PD, Mathier V, et al. How does coalescence of dendrite arms or grains influence hot tearing? *Solidif Alum Alloy* 2004; 179–190.

Chapter 4 Establishing the metallurgical examination method and method validating by using the melted mark from real fire scenes

4.1 Introduction

At present, fire investigation from the melted mark on the copper wire by the metallurgical examination method has rarely been published. This may be because research on the melted mark of copper wire cannot be comprehensive enough to understand all the fire behaviors due to the complexity and diversity of fire behaviors that have been discovered in fire accidents.¹ In Japan, the National Institute of Technology and Evaluation (NITE) was disclosed the Manual for investigating the cause of fire accidents in home appliances 2010.² They discriminated PMM and SMM by estimating the surrounding temperature during short-circuiting from the “dendrite arm spacing” (DAS) method and the “cell size” (CS) method, as presented in Fig. 1.12.

The estimation of surrounding temperature during short-circuiting by comparing the oxygen concentration in the oxidized structure with the reference dendrite arm spacing (DAS) table was reported by Lee et al.³ It became clear that the atmospheric temperature at the time of melted mark formation can discriminate between primary melted mark (PMM) and secondary melted mark (SMM). Because the PMM can be formed at about 400 °C or less, the oxygen concentration in the oxidized structure ranges from 0.05 wt% to 0.16 wt%, while the SMM can be made at about 600 °C or more, and the oxygen concentration of 0.05 wt% to 0.26 wt% contains in the oxidized structure, as depicted in Fig. 4.1.

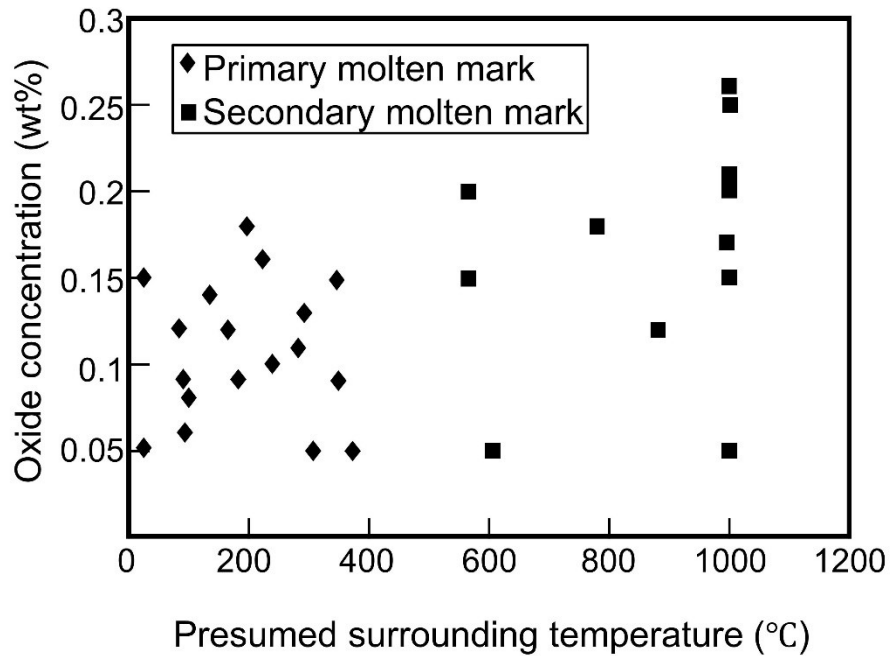


Fig. 4.1 Relationship between presumed surrounding temperature and oxygen concentration³

Moreover, they prepared the experimental PMM and SMM to verify the matching of surrounding temperature between the experiment and the reference DAS table. The estimated temperature values by DAS and oxygen concentration measuring were all below 400 °C, but most are higher than the reference temperature (25 °C).³

The non-melting solid copper wire under different heat treatment and cooling conditions was carried out by Wei et al.^{4,5} The image processing software was used to evaluate the grain size. They found that the average grain size of copper after annealing increases with increasing temperature and time. Additionally, when the copper wires were cooled by water, in the air, and in the furnace, the particle size increased by followed.^{4,5}

M. Di et al.⁶ studied the contents of elements on melted marks of the copper conductor formed by short-circuiting in a normal atmosphere and fire environment by using SEM/EDS and Auger electron spectrometer (AES). The results represented that the composition of melted mark on the copper wire between in normal atmosphere and a fire environment is obviously different such as copper, carbon, and oxygen. It is possible to distinguish the melted marks generated before the fire or after the fire.

Liu et al. explored the relationships of primary spacing of dendrites (λ) and various wire diameters (D) on the melted mark of solid copper wire simulated by the short-circuiting at ambient atmosphere. The primary spacing of dendrites which is proportional to the wire diameter was obtained. Moreover, the microstructure of the melted mark was investigated. One of their investigations is the dendrite growth direction. The primary dendrites of copper grow parallel to another one and opposite to heat flow. The characteristic microstructure of melted mark consists of the cuprous oxide surface layer covering constituents of Cu-dendrites and Cu-Cu₂O eutectic structure.^{7,8}

Lee et al.⁹ researched the differences of properties in external characteristic, cavities and metallographic structures of the primary melted mark (PMM) and secondary melted mark (SMM) performed under the several different conditions. They concluded the followings. 1. There is no relationship between grain size and the cooling condition, but the grain size only depends on the temperature. Thus, it is pointless to use the grain size to characterize PMM from SMM. 2. PMM and SMM cannot discriminate by external features

and cavity distribution. 3. The oxidation structure is not only formed before short-circuiting but also after short-circuiting by absorption of ambient oxygen.

From literature reviews, the actual surrounding temperature during short-circuiting seems impossible to obtain because the estimated temperature is very different from the reality. Besides, if the estimated ambient temperature ranges between 400 °C to 600 °C, it may not distinguish between PMM and SMM.

4.2 Objectives of this chapter

The fire investigation method on the melted mark of copper wire by metallurgical technique remains unclear. Thus, the objectives of the research presented in this chapter are: the first aim is to establish a metallurgical examination method for melted marks on the copper wire formed in a fire accident by referring to the solidification microstructure and oxide evolution in chapters 2 and 3 to describe the fire behavior. The second objective is to validate the method by examining real melted marks on copper wires collected from an actual fire scene in Thailand using our established metallurgical examination method.

4.3 Establishing the metallurgical examination method

The experimental results in Chapters 2 and 3 were summarized to establish a metallurgical examination method for the melted marks on the copper wire formed in a fire accident to describe the fire behavior. Because the melted marks on copper wires created by the arc welding machine in Chapters 2 and 3 have rapid heating and rapid solidification in the air, they were assumed to be PMMs. The SMM could not be created in this research because of the limitation of the experiment. It is difficult to simulate the SMM by the arc welding machine inside the electric furnace while the furnace is operating simultaneously. Moreover, the fire melted mark (FMM), which is thermal damage along a conductor wire resulting from a flame burning, may not validate with this method. Thus, this method validates for PMM only. As stated in Chapter 1, PMM is a primary melted mark created from the first short circuiting that caused the fire. As a result, in addition to explaining the behavior of fire, it may also identify the origin of fire by examining the PMM. Indeed, we do not know which of the melted marks collected from the actual fire scene is the PMM, SMM, or FMM, but we need to know which is the PMM in order to identify the origin of the fire. Therefore, this method was established according to the microstructure and oxide investigation of PMM in the two previous chapters.

The analysis procedure was divided into many stages depending on the observed structure. The main stages are surface morphology observation by SEM/EDS, oxide layer investigation, and microstructure observation, as shown in Fig. 4.2.

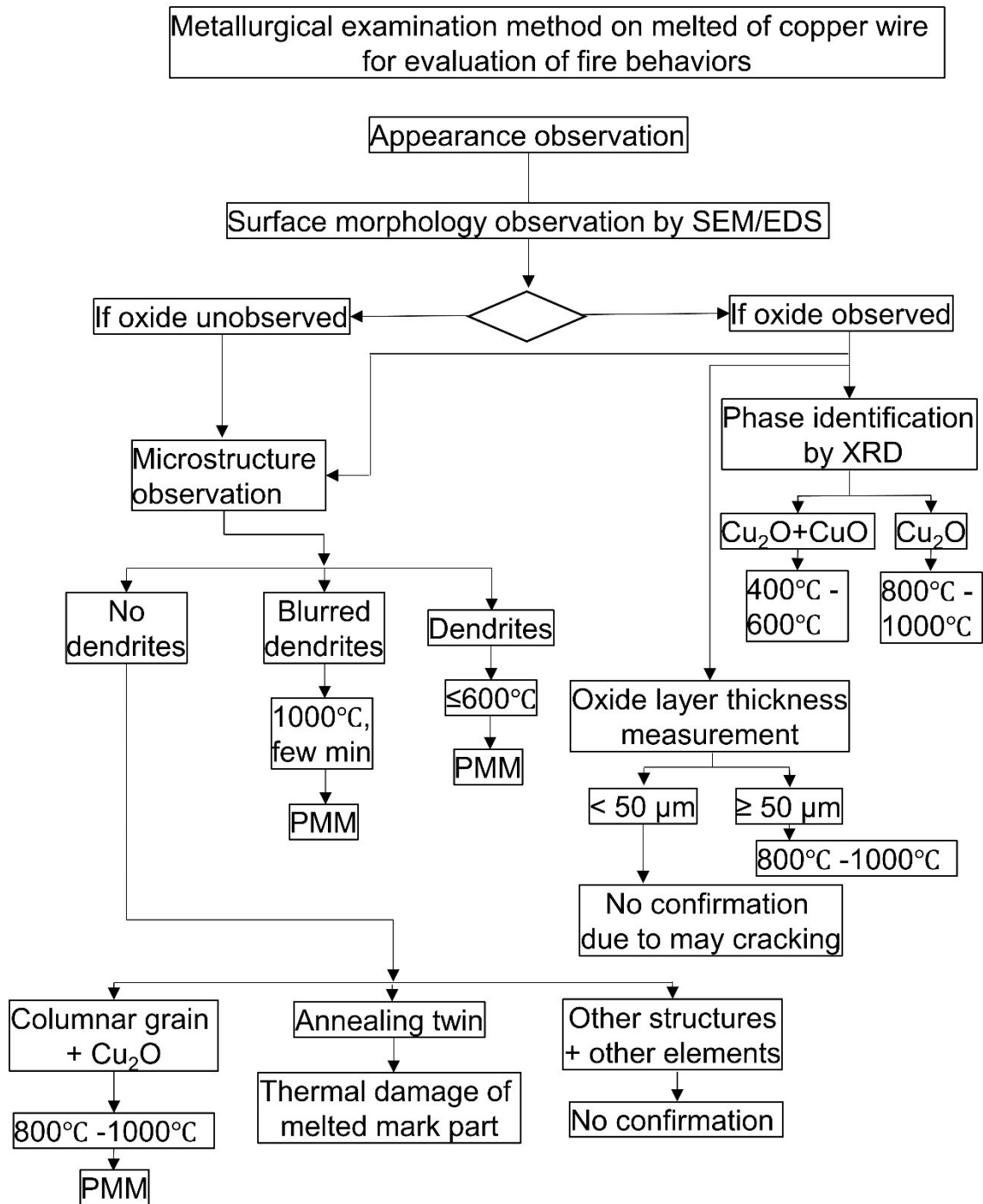


Fig. 4.2 Flow chart of the metallurgical examination method on melted of copper wire for evaluation of fire behaviors.

The following is a method description for metallurgical examination of the melted marks on the copper wire at each stage.

1. Appearance observation

The general exterior appearance of a melted mark on the copper wire should be inspected first, including wire types, wire diameter, the boundary between unmelted/melted interface, localized point of contact, round shape or visible effect from gravity, etc. The sharp boundary between the unmelted/melted interface with a round shape and a localized point of contact are the typical characteristic of EMM.¹⁰

2. Surface morphology observation by SEM/EDS (From chapters 2 and 3)

After appearance observation, the surface morphology of the melted mark on the copper wire should be examined by SEM/EDS. As discussed in Chapter 2, the oxide layer covering the melted mark was broken when it was cooled down with a high cooling rate, such as water, because of the difference in thermal expansion. Nevertheless, it remained at the melted mark for the furnace cooling case. Moreover, Cu_2O grains surrounded by CuO scale at their grain boundary as well as CuO whiskers were observed after heat treatment, as discussed in Chapter 3. However, the samples from real fire scenes may not show the perfect oxide morphology due to the damage from fire events and contamination. Thus, this stage is the initial examination to determine which elements are on the surface of the melted mark. Two major elements have to know elemental content: copper and oxygen. The oxygen content should be highest on the copper oxide layer covering the outer surface and least inside the melted mark. In comparison, the copper content is the opposite. Therefore, the EDS

analysis should be performed from the inside layer to the outer layer of the melted mark. Furthermore, the other elements from the contamination should also be reported to know that each melted mark is collected from the same area or the same surrounding material or not.

3. Oxide layer investigation (From chapter 3)

When copper is oxidized in oxygen or air at high temperatures, multiphase scales such as Cu_2O and CuO form.^{11,12} However, the oxide layer may completely cracked and leaving the melted mark's outer surface or that sample has no oxide. Thus, if oxide cannot be observed, the microstructure observation is the next stage. On the other hand, if oxide can be observed, the examination should be performed following steps.

3.1 Phase identification by XRD (From chapter 3)

To know the oxide phase, the trace of oxide leaving from melted mark's outer surface is crushed to be a powder before XRD testing. Please noted that, the melted mark will be measured oxide layer thickness after longitudinal cutting and polishing. Thus, oxide collected for phase identification by XRD should be carried out carefully. From the experimental results about phase appearance of copper oxide in chapter 3, it can suggest the annealing temperature, which is helpful to point out what fire temperature the melted mark had been before. The copper oxide detected by XRD is classified into two categories following.

3.1.1 If Cu_2O and CuO are detected \rightarrow fire temperature is 400 °C to 600 °C

If a mixture of Cu_2O and CuO is observed in the XRD pattern, it means the copper oxide was annealed at temperatures of $400\text{ }^\circ\text{C}$ - $600\text{ }^\circ\text{C}$. This indicates that the fire temperature of the melted mark on copper is between $400\text{ }^\circ\text{C}$ and $600\text{ }^\circ\text{C}$.

3.1.2 If Cu_2O is detected \rightarrow fire temperature is $800\text{ }^\circ\text{C}$ to $1000\text{ }^\circ\text{C}$

If only Cu_2O is observed in the XRD pattern, it means the copper oxide was annealed at temperatures of $800\text{ }^\circ\text{C}$ to $1000\text{ }^\circ\text{C}$. This indicates that the fire temperature of the melted mark on copper is between $800\text{ }^\circ\text{C}$ and $1000\text{ }^\circ\text{C}$.

3.2 Oxide layer thickness measurement (From chapter 3)

The measurement of copper oxide layer thickness is performed after longitudinal cutting and mirror-polishing. The copper oxide layer can be observed at the outer surface of the melted mark. The optical microscope is used to measure the thickness. The measured oxide layer thickness can be evaluated following.

3.2.1 If the oxide thickness $\geq 50\text{ }\mu\text{m}$ \rightarrow fire temperature is $800\text{ }^\circ\text{C}$ to $1000\text{ }^\circ\text{C}$

The value of $50\text{ }\mu\text{m}$ in oxide thickness is significant value to identify the fire temperature. From chapter 3, no matter how long it is annealed at $400\text{ }^\circ\text{C}$ to $600\text{ }^\circ\text{C}$, it will not oxidize to a thickness greater than $50\text{ }\mu\text{m}$. Conversely, if the measured thickness is more than $50\text{ }\mu\text{m}$, it means the oxidation occurs at $800\text{ }^\circ\text{C}$ to $1000\text{ }^\circ\text{C}$.

3.2.2 If the oxide thickness $< 50\text{ }\mu\text{m}$ \rightarrow No confirmation due to possible cracking

The higher temperature has a thicker oxide which is to crack. Therefore, the measured thickness will be less than the actual thickness. Thus, a thin layer thickness does not always

indicate a low fire temperature, so the temperature cannot be confirmed if the thickness is less than 50 μm .

4. Microstructure observation (From chapters 2 and 3)

4.1 If dendrites are observed \rightarrow fire temperature $\leq 600\text{ }^{\circ}\text{C}$ \rightarrow PMM (From chapters 2 and 3)

The Cu dendrites growing within the columnar grain and the (Cu+Cu₂O) eutectic structure are the characteristics of the melted mark on copper rapidly solidified, which is PMM, as revealed in Fig. 4.3(a). The presence of columnar Cu dendrites in columnar grains is referred to high heat transfer from the melted mark's surface to the non-melting/melting interface due to rapid solidification in the atmosphere, as discussed in Chapter 2. The Cu dendrites can still be observed even in a heat treatment environment at a temperature of less than or equal to 600 $^{\circ}\text{C}$. Thus, the appearance of columnar Cu dendrites in columnar grains indicates the fire temperature less than or equal to 600 $^{\circ}\text{C}$. This characteristic can be identified as a PMM, the primary melted mark on the copper wire at the origin of the fire.

4.2 If blurred dendrites are observed \rightarrow fire temperature is 1000 $^{\circ}\text{C}$ for a few minutes \rightarrow PMM (From chapter 3)

From Chapter 3, when PMM, which has a dendritic structure, is annealed in an atmosphere of fire, the Cu dendrites are dissolved by the interdendritic liquid during heat treatment. Then they redistribute within a single columnar grain.¹³⁻¹⁶ If the annealing time is insufficient to dissolve the Cu dendrites completely, they remain in their grains as blurred

dendrites. This phenomenon occurs at a fire temperature of 1000 °C for a few minutes, pointing to PMM.

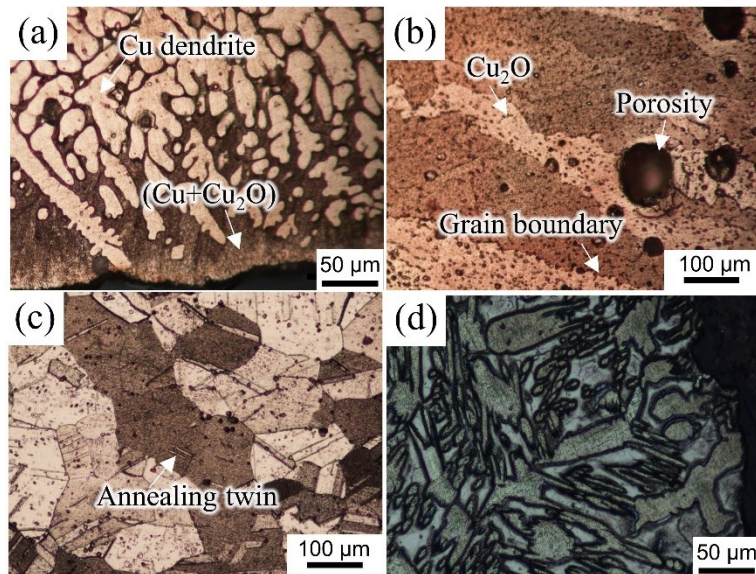


Fig. 4.3 Micrograph of (a) dendritic structure, (b) grain structure, (c) annealing twin, (d) other structure

4.3 If dendrites are unobserved (From chapter 3)

Cu dendrites fade away entirely due to Cu dendrites with high curvature must minimize their surface energy to achieve more thermodynamic stability at high annealing temperatures of 800 °C after 1 hr and at 1000 °C after 10 mins. Simultaneously, the eutectic structure is transformed into Cu₂O particles that precipitate on the Cu matrix across the surface. Therefore, elemental analysis by EDS should be carried out to examine Cu₂O precipitates and other residual elements. As a result, if dendrites are unobserved, the

following features should be classified to investigate the fire temperature, describe the melted mark forming, and identify the origin of the fire.

4.3.1 Grain structure with Cu_2O → fire temperature is 800 °C to 1000 °C → PMM

If different colored areas split by the grain boundary are observed in the microstructure, it reflects the difference in crystal orientation for each grain, as depicted in Fig. 4.3(b). It can be seen in the microstructure along with Cu_2O precipitates. This is the characteristic microstructure of PMM annealed at 800 °C after 1 hr and at 1000 °C after 10 mins.

4.3.2 Annealing twin → thermal damage of melted mark part

Because copper has a face center cubic structure; its structure can transform into the equiaxed grains with annealing twin after annealing.^{4,5,17} When the copper wire is heated below its melting point, its deformation direction due to drawing disappears. The final structure becomes equiaxed grains with an annealing twin, as shown in Fig. 4.3(c). If the annealing twin is observed, the copper wire is unmelted but heated below the melting point. It can imply that it resulted from a fire burning (FMM). It is not the melted mark from the electrical short circuit (EMM).

4.3.3 Other structures with other elements → No confirmation due to no information

The melted marks on copper wire collected from real fire accidents are highly contaminated. Various foreign elements might be detected in the microstructure. Hence, the microstructural composition might not have contained only copper and oxygen, but other

foreign elements resulting in various structures may be observed in addition to the discussed structure above, as illustrated in Fig. 4.3(d). In this case, the fire temperature cannot be evaluated because of a lack of information. However, it has been published that other metal elements can form alloys in the melted mark structure due to dropping onto copper wire during a fire and cooling. They lightly stick to the copper wire as a spot. If that spot is heated further by fire, it can penetrate the inside of the copper wire and form an alloy with copper. The presence of alloys can be confirmed by elemental analysis. An alloy spot may exhibit a shiny grey area. As a result, the presence of alloys is referred to as the melting by fire (FMM),¹⁰ which is not primary melted mark.

4.4 Method validation on melted marks of copper wire collected from real fire scenes

To validate the established metallurgical examination method, the melted marks on copper wire collected from the real fire scene were examined to describe the fire behavior and identify the origin of the fire.

4.4.1 Materials and Methods

The examined materials in this chapter are the melted marks on copper wire of six samples collected from real fire sites in Thailand between 2019 and 2021. These samples were collected from four different fire scenes, denoted by case numbers 138, 141, 272, and 335. The case numbers 138 and 141 have two melted marks in each fire site, defined by 138-1, 138-2, and 141-1, 141-2, respectively, as revealed in Fig. 4.4. As depicted in table 4.1, the wire type and wire diameter of all samples were determined.

Table 4.1 Wire type and wire diameter of melted marks on copper wire from real fire scenes

Case number	Wire type	Diameter (mm)
138-1	Stranded wire	4.65
138-2	Stranded wire	4.65
141-1	Single wire	1.7
141-2	Stranded wire	1
272	Stranded wire	1
335	Stranded wire	1

To describe the fire behaviors from the melted mark on copper wire, the microstructure and oxide layer of all specimens were investigated by the metallurgical examination method established in the previous section.

The surface morphology and chemical composition of all specimens were examined by Scanning electron microscope (SEM) of HITACHI SU3500 attached Energy dispersive X-ray spectroscopy (EDS).

The phase identification of the oxide layer on melted mark was conducted by X-ray diffraction (XRD) of Rigaku, RINT-2100 under 40kV/4mA and CuK α radiation at 0.1540 nm wavelength. Data was collected in the range 2θ of 20 to 80 degrees with 0.02 degree steps. The oxide was crushed into a powder for XRD testing.



Fig. 4.4 The melted marks on copper wire collected from the real fire sites

The measurement of oxide layer thickness and microstructure observation were examined by an optical microscope. All melted marks from real fire sites were mounted with conductive resin (Technovit) and longitudinal cut. Then, they were ground with sandpaper from #500 to #4000 and further mirror-polished by a diamond paste of 0.1 μm . The alcohol was used to clean the samples in an ultrasonic bath after grinding and polishing. The thickness of the oxide layer was measured in this step, and SEM/EDS identified the chemical composition in the longitudinal section of the melted mark. Previous to using an optical

microscope to examine the microstructures, all samples were further etched for a few minutes with a solution of 10 g FeCl₃, 30 ml HCl, and 120 ml distilled water.¹⁸⁻²⁰

4.4.2 Examination of typical appearance

The general exterior appearances of a melted mark on the copper wire from real fire accidents were inspected first. In Fig. 4.4, the stranded wires in cases 138-1 and 138-2 were melted together across the wires. In case 141-1, there was irregular melting on the melted mark, and the surface was rough. The two strands of wire in case 141-2 were melted together at the end of the wire. In case 272, the stranded wire was melted on another wire at a localized point of contact, and its shape was round. In case 335, the melted mark shape was round, and the boundary between the unmelted/melted interface was observed. These typical appearances will be interpreted with other examinations and concluded later.

4.4.3 Examination of surface morphology

The surface morphology of the samples from real fire scenes was greatly damaged and contaminated due to fire events and evidence collection, as depicted in Fig. 4.5. They were not in perfect condition enough to inspect the surface morphology. However, elemental analysis on the surface by EDS is an initial examination to determine which elements are on the surface of the melted mark. The EDS analysis were performed from the inner layer to the outer layer of the melted mark.

The results of elemental analysis on surface of melted marks from real fire scenes are illustrated in Fig. 4.6. All melted marks consist of copper and oxygen elements as major elements. It can be clearly seen that the oxygen content of most samples is highest at the outer surface, and it gradually decreases from there, while copper content is the opposite. This is the phenomenon of oxygen absorption from the air into the melted mark. The minor elements are carbon, chlorine, and calcium. As shown in Fig. 4.7, elemental mapping represents Cl and Ca concentrating on the oxide layer. It has been reported that Cl was released from the combustion of PVC insulation, whereas Ca was an element from ash-forming such as wood combustion.^{10,21,22} Most of the C comes from the ambient CO₂ during the fire and the residual C on the wire's surface as a result of wire burning.²³ In addition, various foreign elements were detected on the outer surface of the melted mark from real fire accidents, such as Si, Al, S, Fe, P, and Sn. The melted marks collected from the same fire sites (138-1 and 138-2) and (141-1 and 141-2) present the same elements.

In summary, the major elements on surface of the melted mark from real fire accident are Cu and O. The minor elements are C, Cl, and Ca. The foreign elements have various elements depending on their environment. The melted marks from the same fire sites contain the same elements.

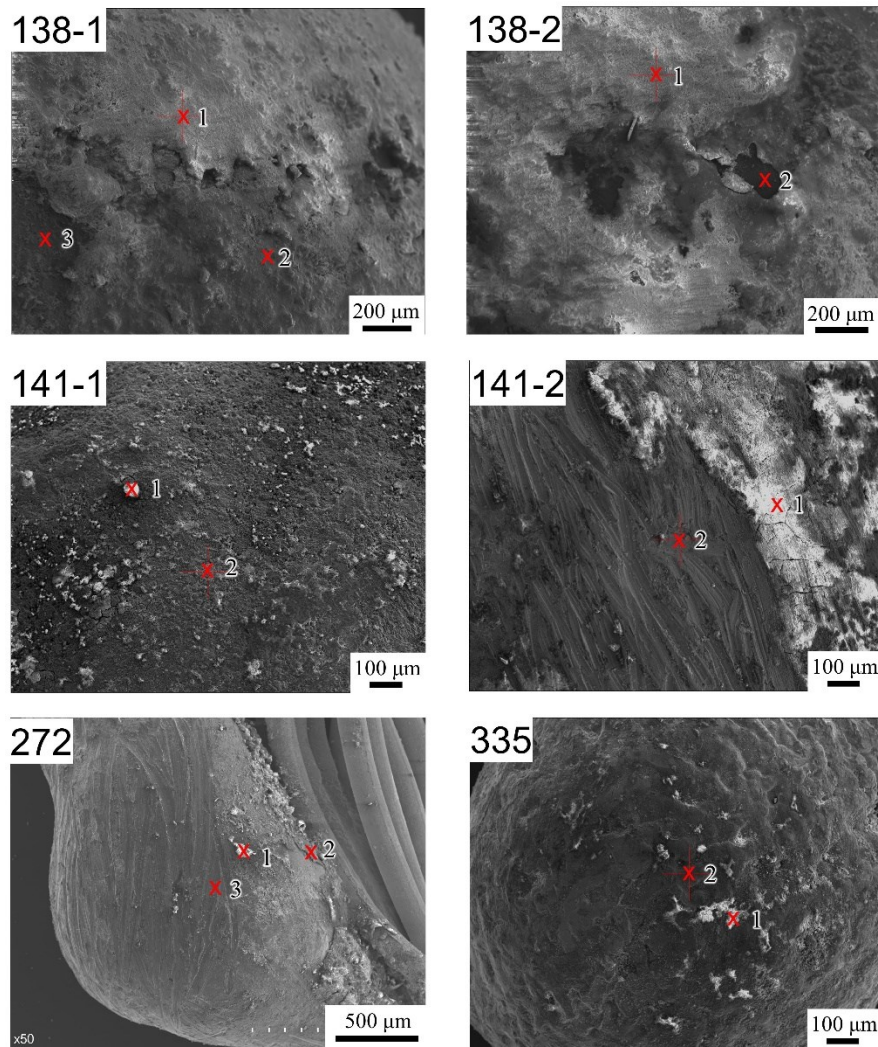


Fig. 4.5 Surface morphology of melted marks on copper wire from four fire accidents

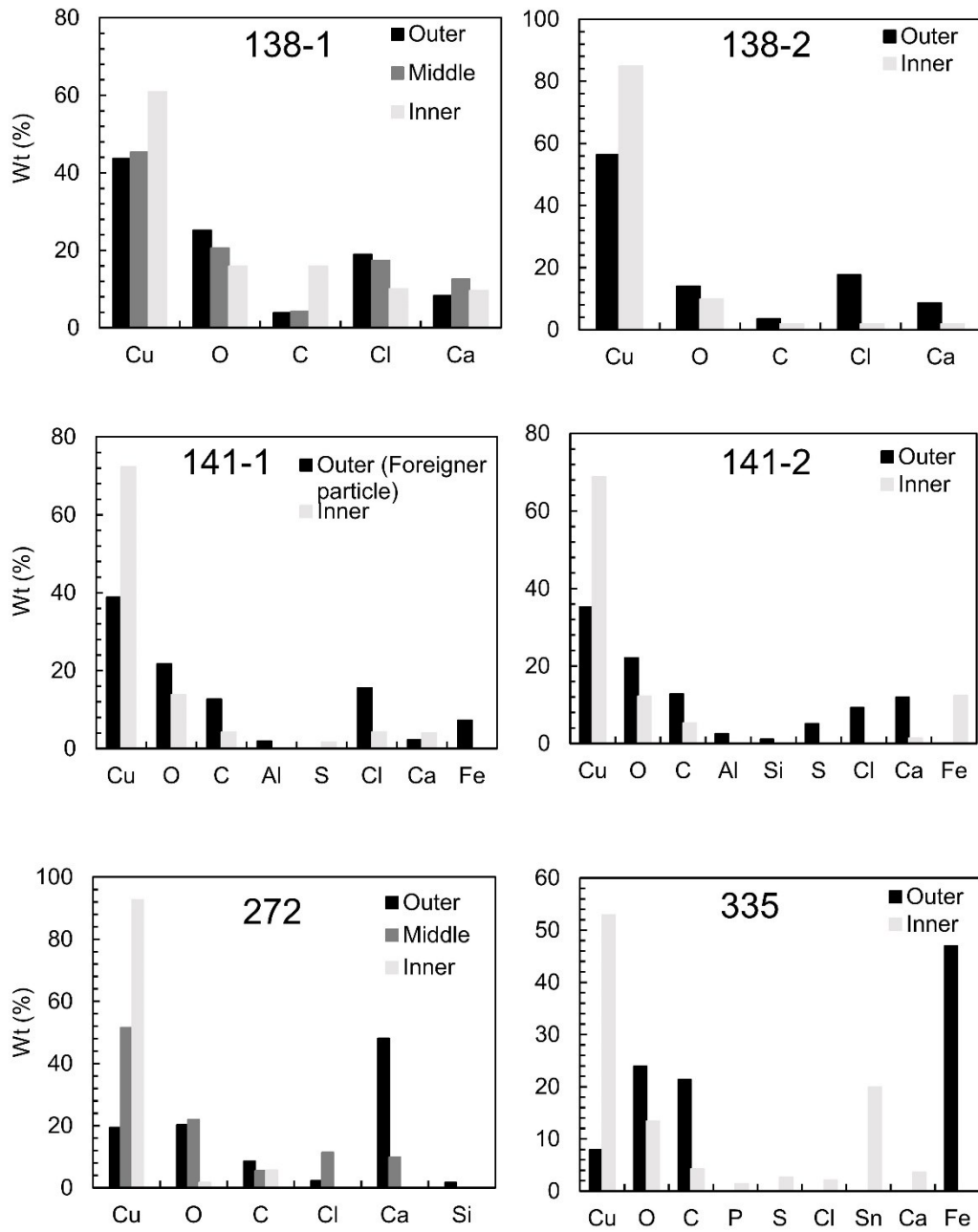


Fig. 4.6 Elemental analysis on surface of melted marks from real fire scenes

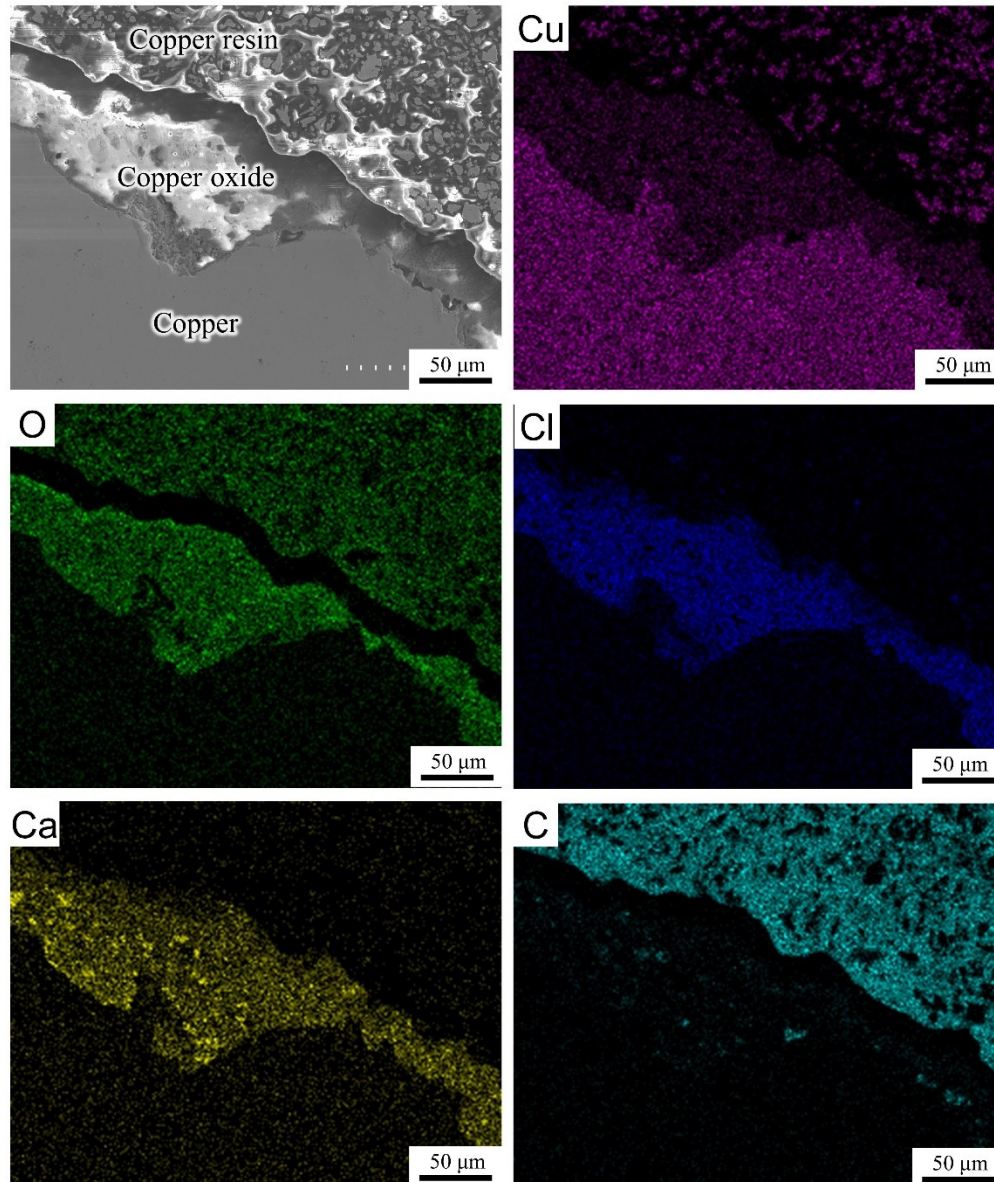


Fig. 4.7 Elemental mapping on microstructure in longitudinal section of the melted mark case number 138-1

4.4.4 Examination of oxide layer

There are four melted marks for copper oxide examination because they present some trace oxide on their melted marks' surfaces, including case numbers 138-1, 138-2, 141-1, and 141-2.

4.4.4.1 Evaluation of fire temperature from copper oxide

The estimation of fire temperature from copper oxide was conducted by phase identification of the oxide layer by XRD according to the established method in the previous section. Fig. 4.8 demonstrates XRD patterns of oxide layer from real fire scenes. The types of copper oxide and fire temperature evaluation are presented following.

Case 138-1: Copper oxide type is Cu_2O and CuO

Evaluated fire temperature is 400 °C to 600 °C

Case 138-2: Copper oxide type is Cu_2O and CuO

Evaluated fire temperature is 400 °C to 600 °C

Case 141-1: Copper oxide type is Cu_2O

Evaluated fire temperature is 800 °C to 1000 °C

Case 141-2: Copper oxide type is Cu_2O

Evaluated fire temperature is 800 °C to 1000 °C

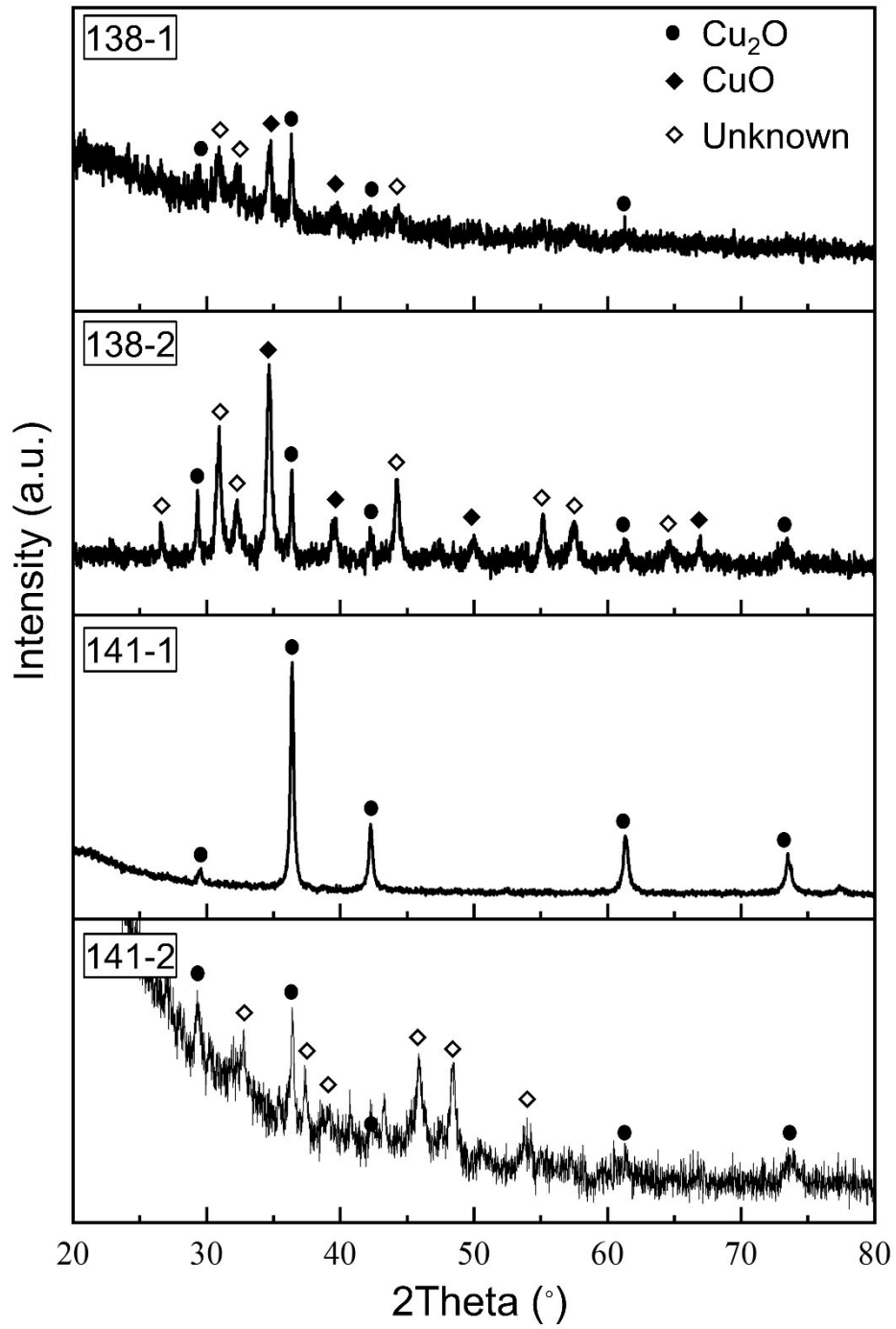


Fig. 4.8 XRD patterns of oxide layer on melted mark on copper wire from real fire scenes

4.4.4.2 Investigation of Cu₂O crystallite size

Although the established method does not include estimating fire temperature from Cu₂O crystallite size, this section desires to present crystallite size differences between simulation and real fire sites and invalidate estimating fire temperature from Cu₂O crystallite size.

The comparison of Cu₂O crystallite size at (111) plane between real fire scene samples and reference plot from simulated samples is shown in Fig. 4.9. The crystallite size distribution of simulated samples used as reference is no distinguishable relationship with temperatures and times. At a certain size, various temperatures and times are obtained. For example, 138-1 and 141-1 have a crystallite size of 36.4 nm and 35.3 nm, respectively. When their size is compared with the reference plot, a wide temperature range from 400 °C to 1000 °C is achieved. Furthermore, some Cu₂O crystallite sizes from real fire scenes are out of scope from the reference plot. Because the reference plot was created from the limitation of heat treatment temperatures of 1000 °C, it is not comprehensive whenever the melted mark collected has a higher fire temperature than 1000 °C. The cooling rate also has effect on crystallite sizes as discussed in chapter 2. Although they have the same fire temperature if they are cooled with different cooling rates, such as in the fire environment and by water, resulting in different crystallite sizes. As a result, estimating fire temperature from Cu₂O crystallite size might be impossible.

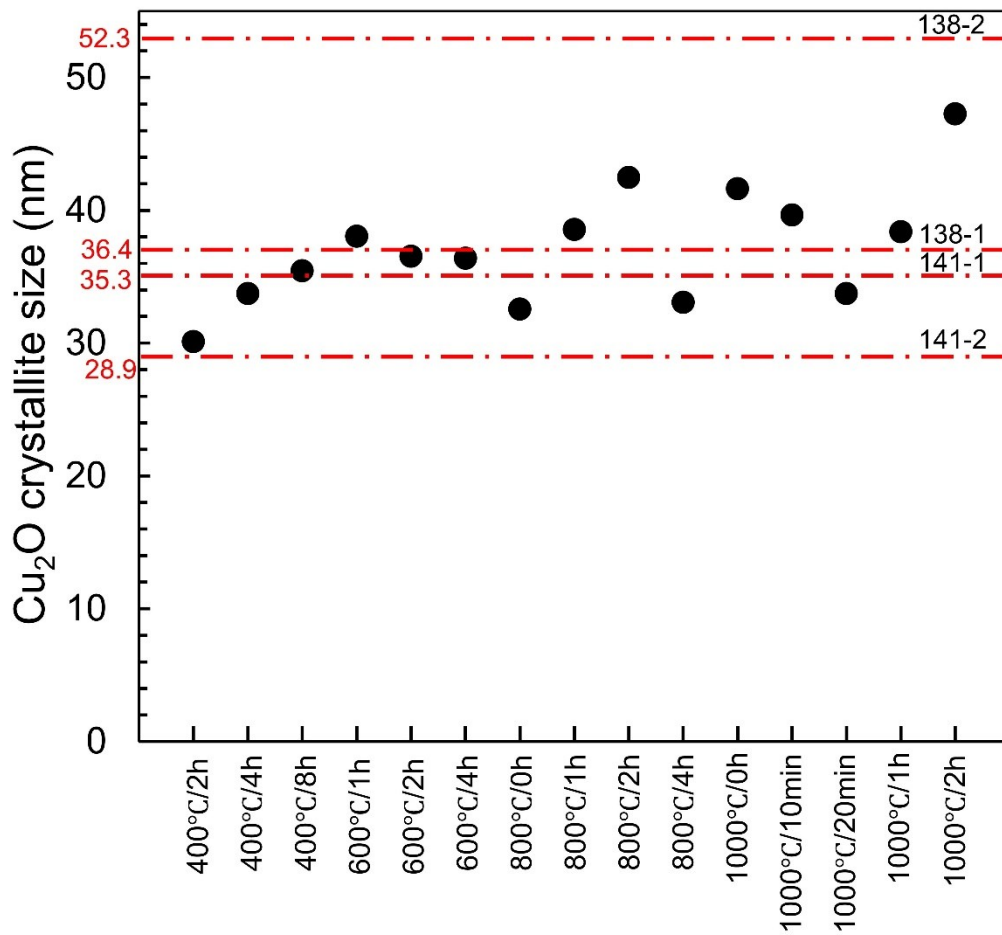


Fig. 4.9 Comparison of Cu₂O crystallite size at (111) plane between real fire scene samples and reference plot from simulated samples

4.4.4.3 Evaluation of fire temperature from copper oxide layer thickness

There are four melted marks for estimating fire temperature from copper oxide layer thickness because they present some trace oxide on the melted mark's surface, including case numbers 138-1, 138-2, 141-1, and 141-2, as revealed in Fig. 4.10. The thickness of copper oxide and fire temperature evaluation are presented following.

Case 138-1: Copper oxide layer thickness is 80 μm

Evaluated fire temperature is 800 °C to 1000 °C

Case 138-2: Copper oxide layer thickness is 53 μm

Evaluated fire temperature is 800 °C to 1000 °C

Case 141-1: Copper oxide layer thickness is 23 μm

Evaluated fire temperature is no confirmation due to possible cracking

Case 141-2: Copper oxide layer thickness is 35 μm

Evaluated fire temperature is no confirmation due to possible cracking

The evaluated fire temperature of cases 138-1 and 138-2 is similar at 800 °C to 1000 °C because they were collected from the same fire sites as well as cases 141-1 and 141-2.

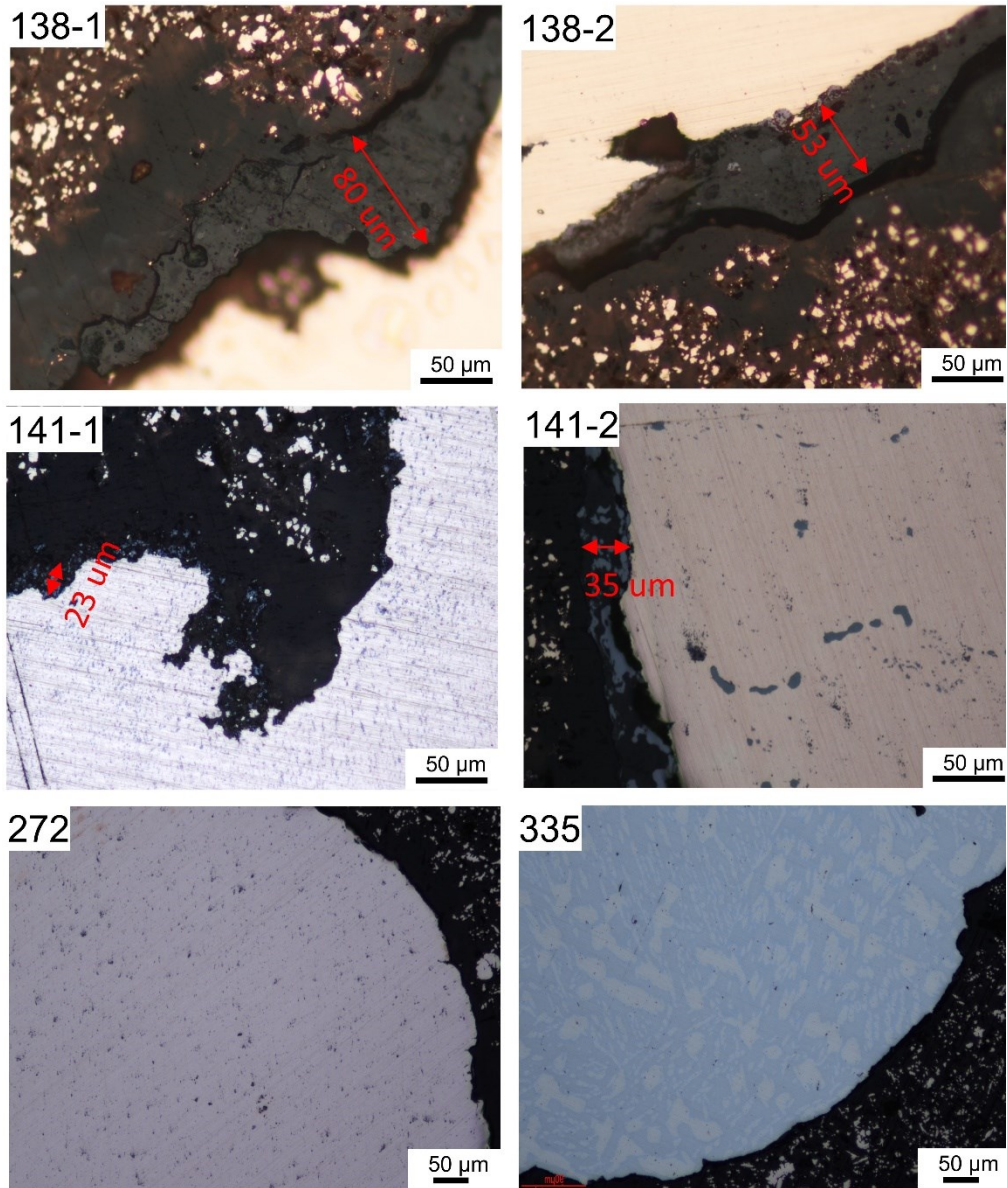


Fig. 4.10 Oxide layer thickness measurement of melted marks from real fire scenes

4.4.5 Describing melted mark forming from microstructure

The microstructures of all melted marks from real fire accidents were examined using the metallurgical examination method. The etched and unetched surfaces were prepared for microstructure observation and composition investigation by EDS, respectively. Fig. 4.11 and 4.12 illustrate etched microstructure of melted marks on copper wire from real fire scenes. There is a difference in the structure of all the samples following.

Case 138-1: No dendrite, Grain structure with grain size of 1.56 mm

Case 138-2: No dendrite, Grain structure with grain size of 2.63 mm

Case 141-1: No dendrite, Grain structure with grain size of 0.18 mm, oxygen richer grains

Case 141-2: No dendrite, Grain structure with grain size of 0.28 mm

Case 272: Blurred dendrite in columnar grain with grain size of 0.22 mm

Case 335: No dendrite, other structures

Case 138-1, 138-2, and 141-2 present similar grain structures due to annealing in fire temperature, but different grain sizes may be due to different fire conditions and different wire diameters. The oxygen-richer grains are observed in case 141-1, which may indicate the powerful ambient oxygen in the fire site. Interestingly, the microstructure of case 272 appears blurred dendrite in columnar grain. This structure is similar to the rapidly solidified structure of a simulated sample. The heat treatment effect causes the blurred dendrite. It remains in the structure because of incomplete dissolution.

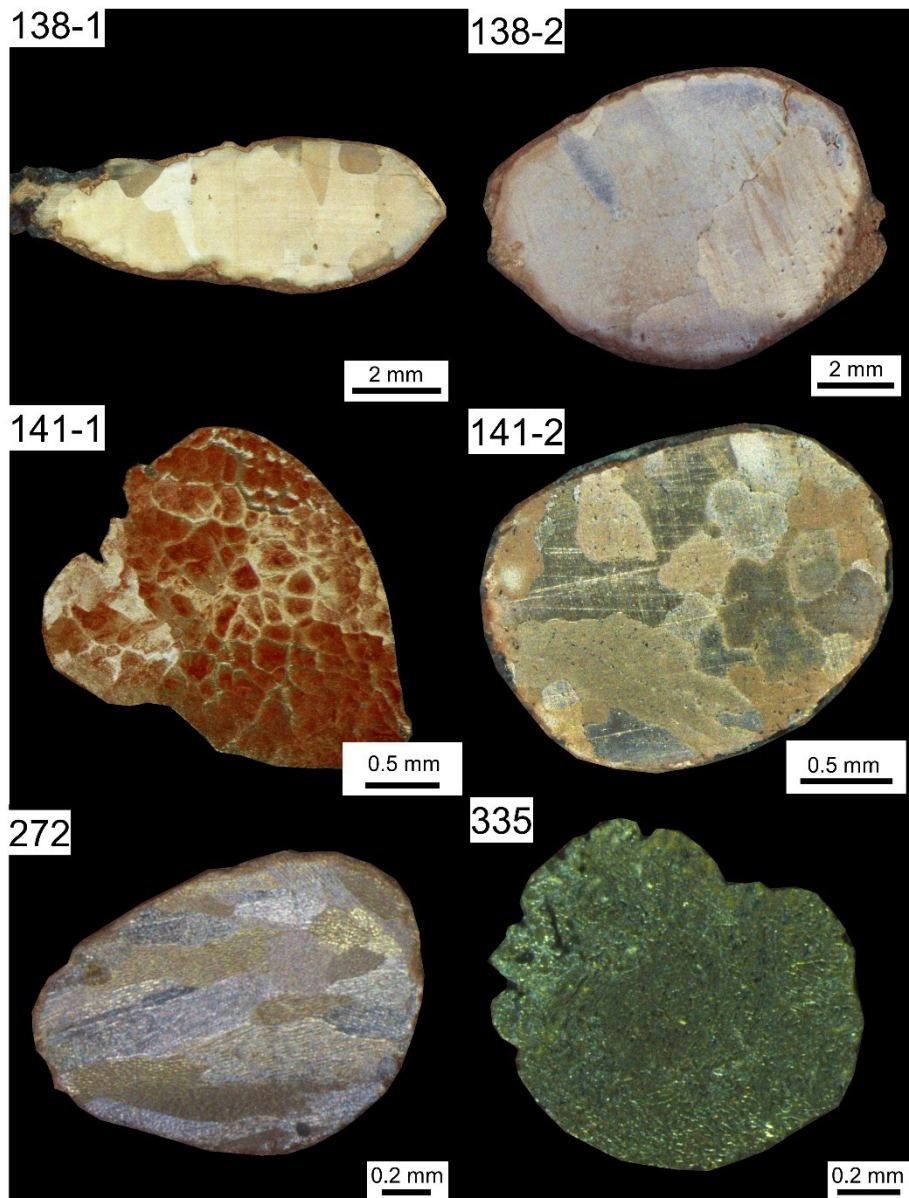


Fig. 4.11 Etched microstructure of melted marks on copper wire from real fire scenes

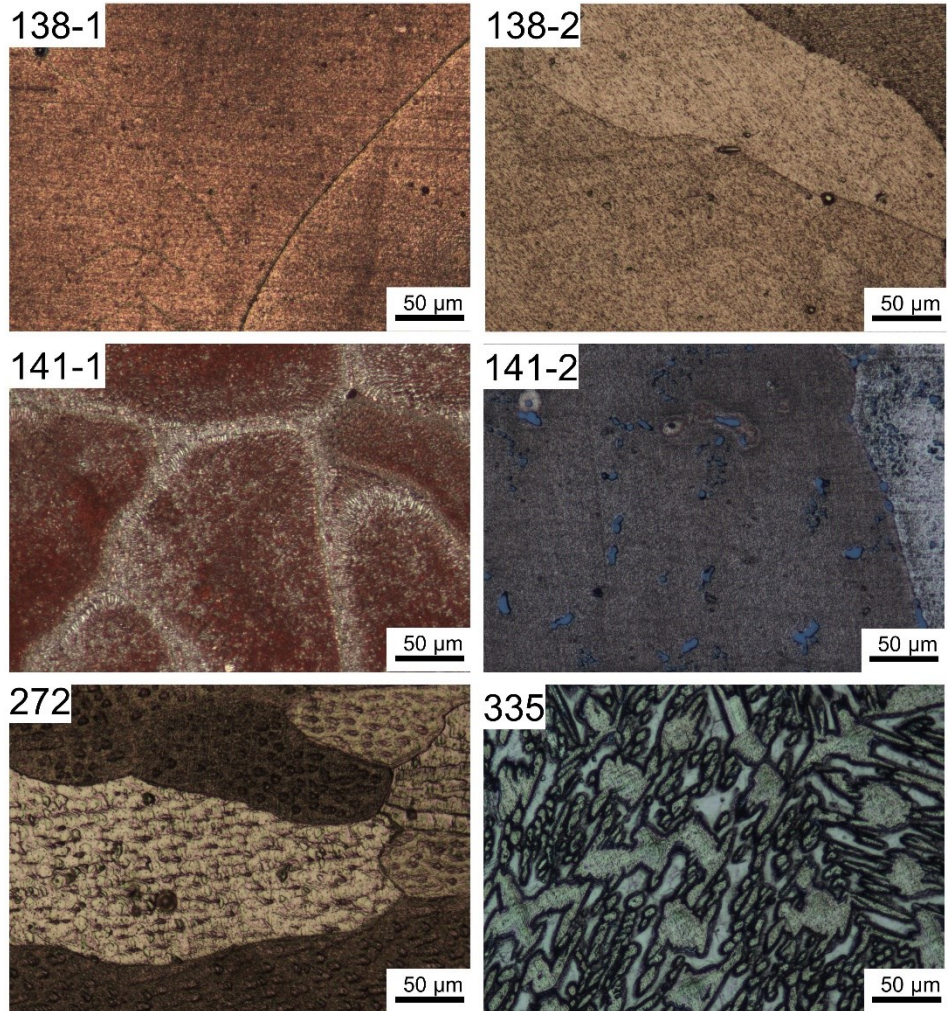


Fig. 4.12 Microstructure of melted marks on copper wire from real fire scenes under magnification 200x

Moreover, the columnar grain formed in the longitudinal section indicates a rapid heat transfer from one side to the other. As a result, this melted mark may be generated from short-circuiting. From the established method, this kind of microstructure is classified as PMM, which means being at a fire temperature of 1000 °C for a few minutes. Additionally, the structure of case 335 is not familiar, and grain boundaries cannot be observed. If the melted mark comprises major elements of copper and oxygen, the grain boundary appears after etching with FeCl₃ solution. Therefore, the microstructural compositions are necessary to examine. The microstructural compositions of melted marks on copper wire from real fire scenes are depicted in Fig. 4.13. The following outcomes are observed.

Case 138-1: Cu, porosities and no Cu₂O

Case 138-2: Cu, porosities and no Cu₂O

Case 141-1: Cu, Cu₂O, Pb and porosities

Case 141-2: Cu, Pb, S, porosities and no Cu₂O

Case 272: Cu, porosities and no Cu₂O

Case 335: Cu and Cu+Sn

Cases 138-1 and 138-2 present similar composition because they were collected from the same real fire scenes. The Cu₂O precipitate and Pb were found in case 141-1. Pb has been used as an electronic component.^{21,24-27} This Pb exhibits a distinctly different metallic color in the microstructure. It can imply that copper wire might be directly below the material, including Pb, that melted and dropped onto copper wire during a fire and cooling.¹⁰

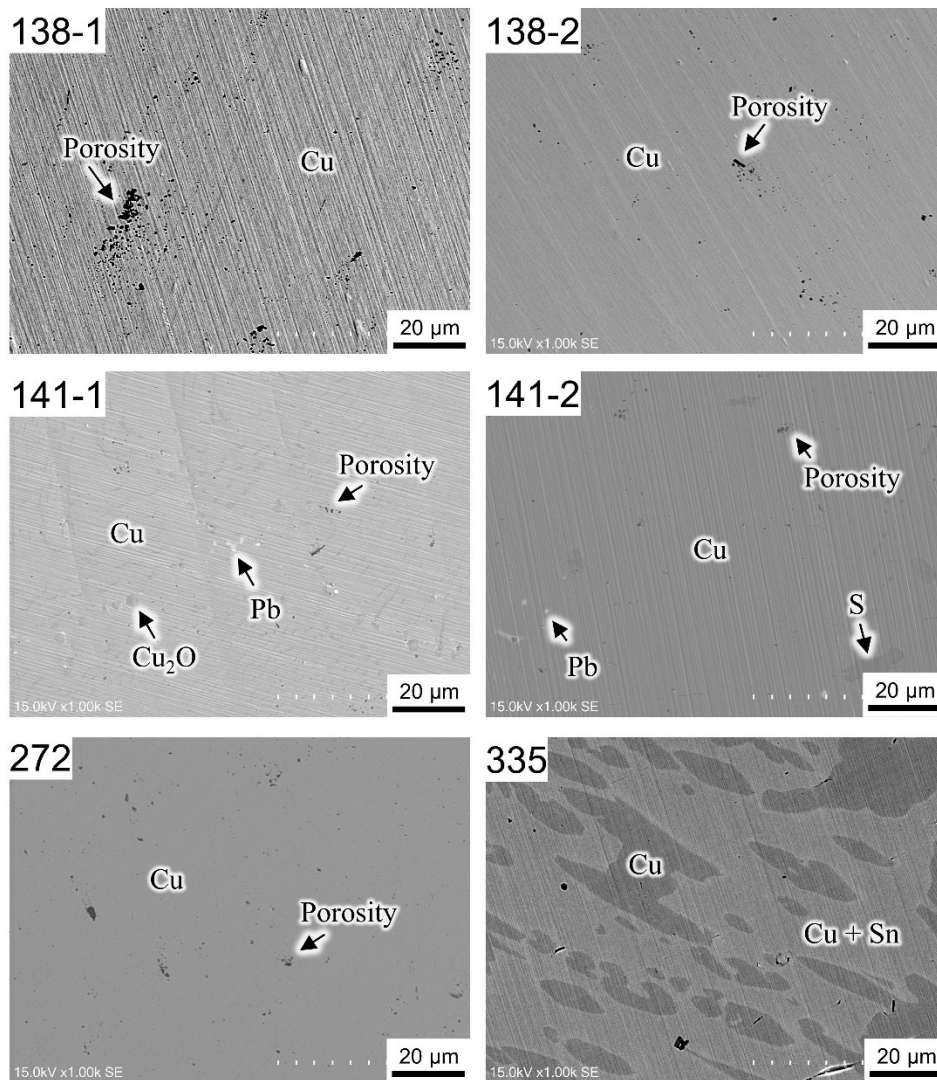


Fig. 4.13 Microstructural compositions of melted marks on copper wire from real fire scenes

The melted mark in case 141-2, which was collected from the same fire accident as case 141-1 shows different alloying elements, including S and no Cu_2O . They might be gathered from different area in same fire accident. The presence of different residual elements in the microstructure could indicate the surrounding materials during a fire. In case 242, there are no other residual elements in the microstructure. It is similar to the microstructure of the simulated PMM. The unetched microstructure in case 335 differs from the others, with Cu in the bright region and Cu+Sn in the dark region. Generally, Sn-Pb has been used as a solder for joining two electronic components.^{21,24-27} Thus, copper wire containing solder may have alloying area and rounded end. These effects result from the interaction of the copper and the solder.¹⁰ Accordingly, this melted mark is not both EMM and FMM.

4.4.6 Explaining fire behaviors and identifying fire's origin

From oxide and microstructure investigations, all results were interpreted together to identify the origin of the fire. The fire behaviors and the formation of the melted mark on copper wire collected from real fire scenes are explained following.

In case 138-1 and 138-2

1. Because a mixture of Cu_2O + CuO was found at the oxide layer, it indicates that the surrounding fire temperature is 400 °C to 600 °C. However, the estimated fire temperature from the thickness measurement is 800 °C to 1000 °C, which is inconsistent. This is because the established method has no data in the 600 °C to 800 °C range if the melted mark has been in that temperature range. This will result

in inconsistent temperatures estimated from the oxide type and oxide thickness measurements.

2. These two melted marks were melted at a temperature over the melting point and solidified. There were no dendrites, no Cu_2O precipitates, and no residual elements in the grain structure. Because there is no Cu_2O precipitate, these two melted marks are not the melted marks that are the cause of the fire accident.

In case 141-1

1. Because only Cu_2O phase was found at the oxide layer, it indicates that the surrounding fire temperature is 800 °C to 1000 °C.
2. This melted mark was melted at a temperature over the melting point in the powerful oxygen ambient and solidified because the oxygen-richer grains were observed. There were no dendrites, but the residual element (Pb) was found in the microstructure. It implies that the fire accident occurs before generating this melted mark on copper, then surrounding materials are melted and dropped onto that copper wire. Thus, this melted mark is not the melted mark that is the cause of the fire accident.

In case 141-2

1. Because a mixture of $\text{Cu}_2\text{O} + \text{CuO}$ was found at the oxide layer, it indicates that the surrounding fire temperature is 400 °C to 600 °C.

2. This melted mark was melted at a temperature over the melting point and solidified. The oxygen-rich grains were not observed, indicating collection from a different area from case 141-1, but in the same fire accident. There were no dendrites, but the residual elements (Pb, S) were found in the microstructure. It implies that the fire accident occurs before generating this melted mark on copper, then surrounding materials are melted and dropped onto that copper wire. Thus, this melted mark is not the melted mark that is the cause of the fire accident.

In case 272

1. Because the melted mark has no oxide layer, evaluating the surrounding fire temperature from the oxide layer is impossible. However, it can be evaluated by the microstructure observation described below.
2. This melted mark was generated from short-circuiting because the blurred dendrites in columnar grains were observed. The columnar grain formed in the longitudinal section indicates a rapid heat transfer from one side to the other. The heat treatment effect causes the blurred dendrite. However, it remains in the structure because of incomplete dissolution. There were no residual elements in the microstructure. This structure is comparable to the rapidly solidified structure of a simulated sample. Therefore, this melted mark is a primary melted mark (PMM) which is a cause of the fire accident and had been in a fire temperature of 1000 °C for a few minutes.

In case 335

1. Because the melted mark has no oxide layer, evaluating the surrounding fire temperature from the oxide layer is impossible.
2. The microstructure of this melted mark comprises Cu and Cu + Sn. Sn comes mostly from solder, which is used to join two electronic components. Thus, Cu and Sn might be melted during metal interconnection. As a result, this melted mark is not the melted mark that is the cause of the fire accident, and the surrounding temperature cannot be evaluated due to a lack of information. However, the external morphology has a rounded shape similar to PMM as in case 272. If it is inspected only through a visual examination without a metallurgical examination, the evaluation of that damage may be inaccurate.

4.5 Conclusions

We have succeeded in establishing metallurgical examination method for melted marks on the copper wire by using the solidification microstructure and oxide evolution of PMM in chapters 2 and 3. This method provides precious fire investigation information following.

1. The surrounding fire temperature can be evaluated by investigating the oxide layer.
2. The formation of melted mark can be described by elemental analysis and microstructure observation in the longitudinal section.
3. The origin of the fire accident can be identified from microstructure examination.

This method was created using the solidification microstructure and oxide layer of the primary melted mark, which is a melted mark that represents the cause of the fire at the origin of the fire. Thus, if the examined sample has different features from the characteristics in this method or is incomparable to this method, it is not the primary melted mark and is not the cause of the fire accident.

Furthermore, this established method was validated by examining real melted marks on copper wires collected from an actual fire scene in Thailand. The following valuable results are achieved.

1. The melted mark identified as the cause of the fire accident is case 272, the surrounding temperature is 1000 °C.

2. The melted marks generated after a fire are cases 138-1, 138-2, 141-1, and 141-2, which indicate that they are not the cause of a fire due to the presence of alloy elements in their microstructures.
3. The melted mark that is not formed in a fire accident is case 335. It was created from the joining of copper wire with another electronic component by Sn solder.

References

1. Wang Y, Su X. Study on pores distribution laws in secondary short circuited melted beads of copper wires. *Procedia Eng* 2014; 84: 887–892.
2. NITE. 家電製品の発火事故原因究明 マニュアル2010. 2010.
3. LEE EP, OHTANI H, SEKI T, et al. Study on discrimination between primary and secondary molten marks by DAS. *Bull Japan Assoc Fire Sci Eng* 2000; 50: 1–12.
4. Wei MM, Zhao Z, Liang D. Experiment of electrical fire burned copper wire and parameters analysis on metallographic test of melted mark. *Procedia Eng* 2011; 11: 496–503.
5. Wei MM, Mo SJ, Liang D, et al. The experiment on melted mark formed by copper wire in electrical fire and the analytic researcher on the feature parameters of metallographic structure. *Procedia Eng* 2011; 11: 504–513.
6. Di M, Zhang M, Qi ZB, et al. Study of analyzing characteristic of composition on the surface of copper conductor melted marks. *Procedia Eng* 2011; 11: 68–74.
7. Liu KH, Shih YH, Chen GJ, et al. Microstructural Study on Molten Marks of Fire-Causing Copper Wires. *Materials (Basel)* 2015; 8: 3776–3790.
8. Liu KH, Shih YH, Chen GJ, et al. Microstructural Study on Oxygen Permeated Arc Beads. *J Nanomater* 2015; 2015: 1–8.
9. Lee EP, Ohtani H, Seki T, et al. A Fundamental Study on Electrical Molten Marks.

Bull Japan Assoc Fire Sci Eng 2001; 51: 1–10.

10. NFPA 921. *Guide for Fire and Explosion Investigations*. NFPA 921, 2017.
11. Choudhary S, Sarma JVN, Pande S, et al. Oxidation mechanism of thin Cu films : A gateway towards the formation of single oxide phase. *AIP Adv*; 055114. Epub ahead of print 2018. DOI: 10.1063/1.5028407.
12. Park JH, Natesan K. Oxidation of copper and electronic transport in copper oxides. *Oxid Met* 1993; 39: 411–435.
13. Flemings MC. Coarsening in solidification processing. *Mater Trans* 2005; 46: 895–900.
14. Rappaz JAD and M. *Solidification*. 2nd ed. EPFL Press, http://solidification.mechanical.illinois.edu/Figures/chap13/Fig_13_17.pdf (2016).
15. Glicksman ME, Voorhees PW. Ostwald Ripening and Relaxation in Dendritic Structures. *Metall Trans A, Phys Metall Mater Sci* 1984; 15 A: 995–1001.
16. Rappaz M, Grasso PD, Mathier V, et al. How does coalescence of dendrite arms or grains influence hot tearing? *Solidif Alum Alloy* 2004; 179–190.
17. Collini L. *Copper Alloys - Early Applications and Current Performance - Enhancing Processes*. 2012. Epub ahead of print 2012. DOI: 10.5772/1912.
18. Scott DA. *Metallography and Microstructure of Ancient and Historic Metals*. Tien Wah Press, Ltd., 1991.

19. Rawdon HS, Lorentz MG. METALLOGRAPHIC ETCHING REAGENTS FOR COPPER. 16: 641–668.
20. Oetzw G. *Metallographic Etching*. 2nd ed. ASM International, 1999.
21. Gramatyka P, Nowosielski R, Sakiewicz P. WEEE Recycling of Waste Electrical and Electronic Equipment. 2020; 20: 535–538.
22. Vasconcelos de Carvalho A, Manuel Gonçalves da Costa M, Estefânia Rodrigues Fernandes Rabaçal M, et al. *Effects of potassium and calcium on the combustion behaviour of biomass Mechanical Engineering Examination Committee*. 2017.
23. Wu Y, Zhao CZ, Di M, et al. The Surface Analysis of Melted Arc Copper Beads. *Mater Sci Forum* 2007; 561–565: 2455–2458.
24. Multicores Solder. Properties of Solders. 2007; 1–4.
25. ชำรงวัฒนา ธ. วัสดุต่างๆ ที่เป็นอันตรายพบได้ในขยะอิเล็กทรอนิกส์. *thaigoodview.com*, <http://www.thaigoodview.com/node/51719> (2009, accessed 16 April 2022).
26. Howell K, Sweatman K, Miyaoka M, et al. MICROALLOYED Sn-Cu Pb-FREE SOLDER FOR HIGH TEMPERATURE APPLICATIONS. SMTA Proceedings, 2011.
27. N.M Mohd Nan, M.Z Bukhari J. S and MN. A. EFFECT OF TEMPERATURE TO THE MICROSTRUCTURE OF Sn-Pb SOLDER ALLOY. NMC2006, 2006, pp. 10–12.

Chapter 5 Conclusions

The characteristic microstructures and copper oxide phases of the primary melted mark on the copper wire were investigated to describe the fire behaviors and identify the origin of the fire accident. The experiments were simulated to resemble the real fire accidents as much as possible under various parameter conditions, including cooling rates, annealing temperatures, and annealing times. The characteristic features investigated under different conditions were used to establish the metallurgical examination method of melted mark on copper wire. To validate the method, real melted marks on copper wires collected from different actual fire scenes were examined using this method. From all investigations, a summary in each chapter is represented following.

In **chapter 2**, the influence of solidification by air and water on the microstructure of the melted mark on the copper wire was examined before heat treatment. After heat treatment at 1000 °C for 10 mins and cooled down with different cooling types (furnace, air, and water), the effect of cooling rate after heat treatment on PMM also was examined. It can be concluded that the microstructures before heat treatment of PMM solidified in the air and water are different. Both different solidified samples have a (Cu+Cu₂O) eutectic structure, and Cu dendrites grow from the non-melting/melting interface as their significant characteristics. However, the water-solidified sample has smaller dendrite arm spacing and an oxygen-enriched area near the melted mark's surface. In comparison, the microstructures of PMM after heat treatment at 1000 °C for 10 mins and cool in the furnace, air, and water are significantly different from before heat treatment. All different cooled samples have no Cu

dendrites, but columnar grains and Cu_2O precipitates exhibit in the microstructure as their typical features. A perfect oxide layer is found on the sample cooled in the furnace. It is damaged entirely due to the rapid cooling rate as the sample cooled in water.

In **chapter 3**, the effect of annealing temperatures and times on the copper oxide and microstructural evolution of the PMM was examined. It can be summarized that the surface morphology evolves with the annealing temperature. At 1000 °C, the large Cu_2O grains are encircled by the slight CuO scale at their grain boundary and reduce in grain size at 800 °C, while at 600 °C, the CuO whiskers are formed. A mixture of Cu_2O and CuO phases is found at 400 °C and 600 °C, whereas only the Cu_2O phase is discovered at 800°C and 1000°C. The thickness of the Cu_2O layer becomes thicker by increasing annealing temperature and time, which follows the parabolic rate law. The diffusion processes accountable for Cu_2O growth are lattice diffusion at 220 °C to 400 °C and grain boundary diffusion at 400 °C to 1000 °C. Moreover, the microstructure of melted mark annealed at 400 °C and 600 °C is a dendritic structure, while at 800 °C to 1000 °C is a grain structure with Cu_2O precipitates.

In **chapter 4**, we have succeeded in establishing metallurgical examination method for melted marks on the copper wire by using the solidification microstructure and oxide evolution of PMM in chapters 2 and 3. This method provides precious fire investigation information following.

1. The surrounding fire temperature can be evaluated by investigating the oxide layer.

2. The formation of melted mark can be described by elemental analysis and microstructure observation in the longitudinal section.
3. The origin of the fire accident can be identified from microstructure examination.

Furthermore, this established method was validated by examining real melted marks on copper wires collected from an actual fire scene in Thailand. The following valuable results are achieved.

1. The melted mark identified as the cause of the fire accident is case 272, the surrounding temperature is 1000 °C.
2. The melted marks generated after a fire are cases 138-1, 138-2, 141-1, and 141-2, which indicate that they are not the cause of a fire due to the presence of alloy elements in their microstructure.
3. The melted mark that is not formed in a fire accident is case 335. It was created from the joining of copper wire with another electronic component by Sn solder.

Suggestions

1. This method was created using the solidification microstructure and oxide layer of the primary melted mark, which is a melted mark that represents the cause of the fire at the origin of the fire. Thus, if the examined sample has different features from the characteristics in this method or is incomparable to this method, it is not the primary melted mark and is not the cause of the fire accident.

2. This method cannot identify whether SMM or FMM because the formations of these melted marks are different from PMM, so it is incomprehensive. To identify SMM and FMM, the simulation of SMM and FMM under different fire conditions must be carried out. However, the most important for fire investigation is to identify the origin of the fire which is determining the origin of the fire, which is the location of PMM.

3. The heat treatment process was conducted in the air. It was assumed that the oxygen pressure is constant at room oxygen pressure. The oxygen content in a real fire accident may be reduced during a fire. It may result in copper oxide phase transformation. The evaluation of fire temperature from the oxide layer is invalidated at an intermediate fire temperature between 600 °C and 800 °C.

Acknowledgments

First of all, I would like to express my special gratitude to Prof. Hirofumi Miyahara, for giving me the opportunity of being a member of the Miyahara Laboratory. All research results presented in this dissertation are impossible for me without the precious suggestions and real support of Prof. Miyahara.

I would also like to appreciate Assoc. Prof. Kohei Morishita for his valuable advice when I presented my experimental results and to thank him for supporting me during my research activity.

I would like to thank my colleagues, Police Major Satina Polyiam and Police Major Sunattha Tunplouk, for collecting the melted marks on copper wires from real fire accidents in Thailand and sending them to me.

I also want to thank Mr. Juhuai Ma and Mr. Takeru Yamanouchi, as well as all the staff and students in Miyahara Laboratory, who kindly guided using the facilities in Miyahara Lab and provided assistance in many situations regarding the Japanese language.

I would like to express my gratitude to my father, my mother, and my younger brother for their love, moral support, and pushing me forward.

I have to thank Police Lieutenant Colonel Yuppharat Pinkaew and Miss Pichamon Aiemsard for their support and kind encouragement.

Finally, I extend my sincere thanks to The Thai Government and The Royal Thai Police for providing me the scholarship and this educational opportunity.

Supattra SACHANA

April 20, 2022